

AD-A134 850

A CATALOGUE OF SPREADING MODULATION SPECTRA(U)
MASSACHUSETTS INST OF TECH LEXINGTON LINCOLN LAB
E J KELLY 20 SEP 83 TR-596 ESD-TR-83-053
F19628-80-C-0002

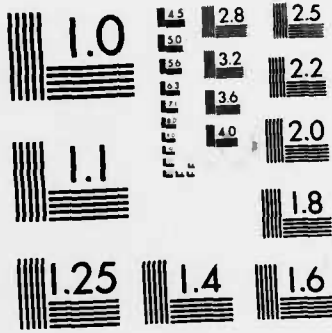
1/2

UNCLASSIFIED

F/G 17/4

NL





MICROCOPY RESOLUTION TEST CHART
NATIONAL BUREAU OF STANDARDS-1963-A

AEI (12)

AD-A134850

Technical Report

596

A Catalogue of Spreading Modulation Spectra

E.J. Kelly

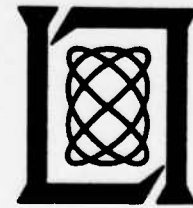
20 September 1983

Prepared for the Department of Defense under Electronic Systems Division Contract F19628-80-C-0002 by

Lincoln Laboratory

MASSACHUSETTS INSTITUTE OF TECHNOLOGY

LEXINGTON, MASSACHUSETTS



Approved for public release; distribution unlimited.

DTIC FILE COPY

DTIC
NOV 21 1983
A

83 11 18 061

The work reported in this document was performed at Lincoln Laboratory, a center for research operated by Massachusetts Institute of Technology, with the support of the Department of the Air Force under Contract F19628-80-C-0002.

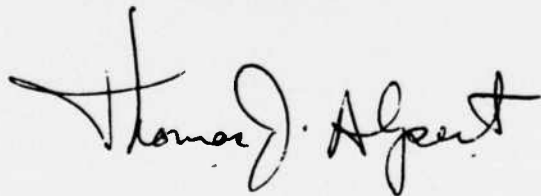
This report may be reproduced to satisfy needs of U.S. Government agencies.

The views and conclusions contained in this document are those of the contractor and should not be interpreted as necessarily representing the official policies, either expressed or implied, of the United States Government.

The Public Affairs Office has reviewed this report, and it is releasable to the National Technical Information Service, where it will be available to the general public, including foreign nationals.

This technical report has been reviewed and is approved for publication.

FOR THE COMMANDER

A handwritten signature in black ink that reads "Thomas J. Alpert". The signature is written in a cursive style with a large initial 'T' and 'A'.

Thomas J. Alpert, Major, USAF
Chief, ESD Lincoln Laboratory Project Office

Non-Lincoln Recipients

PLEASE DO NOT RETURN

Permission is given to destroy this document
when it is no longer needed.

MASSACHUSETTS INSTITUTE OF TECHNOLOGY
LINCOLN LABORATORY

A CATALOGUE OF
SPREADING MODULATION SPECTRA

E.J. KELLY

Group 41

TECHNICAL REPORT 596

20 SEPTEMBER 1983

Approved for public release; distribution unlimited.

LEXINGTON

MASSACHUSETTS

ABSTRACT

Spreading modulation waveforms are discussed in general terms, and a classification system is described. Several well-known examples are given, and a new, standard set of spreading modulations is introduced. Spectra of all the waveforms are given, and spectral properties are discussed in relation to system performance. It is shown that these properties are essentially determined by three waveform parameters, for a large class of spreading modulations.

Accession For	
NIS GRAI	<input checked="" type="checkbox"/>
DTIC TAB	<input type="checkbox"/>
Unannounced	<input type="checkbox"/>
Justification	
By	
Distribution/	
Availability Codes	
Dist	Avail and/or Special
A-1	



CONTENTS

ABSTRACT	iii
I. INTRODUCTION	1
II. WAVEFORM CLASSES AND METHOD OF COMPUTATION OF SPECTRA	5
III. CONSTANT-PHASE WAVEFORMS	8
IV. BINARY FM WAVEFORMS	21
V. TYPICAL BINARY FM WAVEFORMS	32
VI. POLYNOMIAL FM WAVEFORMS	53
VII. WAVEFORM COMPARISONS	78
VIII. SUMMARY AND CONCLUSIONS	100
REFERENCES	102
APPENDIX A - MEASURES OF SPREADING PERFORMANCE	103

I. INTRODUCTION

A random spreading modulation is, basically, a means of complicating the signal of a communications system in order to make that system more difficult to jam. Like any other electronic counter-counter measure tactic, it is a game, whose object is to maximize the cost to the jammer of achieving a given degradation to one's system. Absolute immunity to jamming generally cannot be achieved, except possibly temporarily, until the opponent figures out what you are doing. The tactic of spreading is approached here from the point of view that the adversary knows exactly what you are doing, and is free to do his best to degrade your performance.

The complication introduced by random spreading has two essential features: a randomness in the waveform modulation which greatly reduces the effectiveness of repeat jamming, and a spreading of the instantaneous spectrum, which increases the available processing gain against a given level of total jamming power. Simple frequency hopping, which increases the system bandwidth without changing the width of the instantaneous spectrum, is a related, and complementary technique, which is not discussed further in this study.

A simple example will illustrate the application of a random spreading modulation. Suppose a communications link, designed for a friendly environment, makes use of a signal which consists entirely of simple pulses, organized in a way which permits both synchronization and data transmission. The pulses all have the same shape (say rectangular) and the same carrier frequency, and occur in a burst of some fixed pattern for synchronization. Data may be transmitted by a systematic alteration of some pulse parameter, such as its transmission time, as in pulse-position modulation. To add some anti-jam capability to such a system, the simple pulse may be divided into N equal sub-pulses, or chips, with the carrier phase in each chip either reversed (i.e., changed by 180°) or unaltered in accordance with an N -bit pseudorandom binary sequence. This is binary phase-shift keying, BPSK, one of the simplest of the spreading modulation techniques. By the use of BPSK, the pulse bandwidth is increased by a factor of N , which is one of the objectives of the spreading technique.

When BPSK is used in this way, the pseudorandom bit sequence must be known to the receiver, where a filter matched to the spread pulse is implemented. It is a major feature of systems utilizing random spreading modulations that the spreading bit-sequence is known to the receiver, although any modulation technique normally used for the transmission of information bits could, in principle, be used as a spreading modulation. Thus random spreading implies a different receiver structure than data demodulation of the same waveform, and, most important, a different criterion for performance.

It is not intended that the bit sequence, or code, used in one pulse be used for all, but rather that this code be continually changed from pulse to pulse. In effect, both sender and receiver must have the ability to generate the same, unlimited sequence of bits in time synchronism, successive groups of N bits being used to "code" successive signal pulses. Of course, the sender must be able to modulate his pulses with these ever-changing code sequences, and more significantly, the receiver must be able to configure a filter, matched according to some criterion, to each expected coded pulse. For the spreading modulations studied here, this last requirement presents difficulties of widely varying degree. Such implementation issues will have a decisive effect as the choice of modulation in practice, but hardware techniques change rapidly, and no attempt is made here to assess the value of a modulation scheme from a hardware point of view.

The example just given is perhaps the simplest scheme that has the requisite properties of a random spreading modulation. A very general definition would consider any scheme which mapped a finite sequence of bits into a finite segment of waveform to be a possible spreading modulation technique. We restrict this definition by the application of two constraints, one of practical importance, and one of a simplifying nature, in order to define a workable class of waveforms for analysis.

The first constraint is to limit ourselves to constant-envelope waveforms. The major reasons for this requirement are practical, allowing the use of simple power amplifiers in transmitters and repeaters. Constant envelope also allows the maximum signal energy, in a given signal duration, in the face of a peak power limitation. These reasons are often compelling in

real system design, and many effective spreading modulations have been devised within the constant-envelope constraint. Other waveforms may be converted to constant-envelope form by clipping, either deliberate or inadvertent, but the original waveform's spectral properties are usually not improved in this way. Subsequent filtering will restore some amplitude modulation, hence it is desirable to study constant-envelope modulations which meet the spectral occupancy limitations within which the system must be designed in the first place. Spectral occupancy restrictions play a key role in spreading modulation performance evaluation, and the general goal is to maximize anti-jam processing gain while operating within a given bandwidth or spectral window.

Since the waveform is to have constant envelope, it can be described by its phase or frequency modulation. Our second constraint requires that the waveform be segmented into equal chips, that the phase or frequency modulation imposed within a given chip be one of a small number of possibilities, and that the choices made in the successive chips depend in a simple way on a pseudo-random bit sequence of a non-repeating nature.

We tend to think of the waveform as built of pulses, as in our simple example, each pulse requiring N input bits for its specification. But, in the analysis of spectral properties, we treat N as large, and it is not important that the waveform actually be segmented into separate pulses, hence our results will be valid for continuous waveforms as well. Our second constraint will be made more specific in Section II, where a classification system is introduced and the method of spectral analysis described.

If a signal structure is indeed built out of pulses, each of which is modulated by a random spreading modulation, then other anti-jam techniques can still be used as well. For example, pulse-to-pulse frequency hopping can widen the system bandwidth still further, and randomization of the timing of pulses according to a scheme available to the receiver can also be employed.

Quantitative measures of spreading performance have been discussed elsewhere⁽¹⁾, in terms of efficiency parameters which measure the loss in processing gain (from the ideal value of time-bandwidth product) which results from operating in a fixed band against an optimizing noise jammer. These parameters depend only on the average power spectrum of the modulation, and

they favor spectra which are flat within an allotted band and fall off rapidly outside that band. A brief derivation of these performance measures is given in Appendix A. Interference with other systems, or other users of the same system, will place more specific requirements on the spectral density of the spreading modulation, in terms of sidelobe levels and spectral decay beyond the nominal band. These are, basically, spectrum allocation constraints, and must be considered separately in each case.

In this study we present the spectral properties of various groups of spreading modulation waveforms, without judgment of their relative merits. The actual choice in a particular system design will be dictated by many factors, including hardware issues and postulated jamming scenarios; but the spectral properties of the waveform chosen will play a central role in this choice.

II. WAVEFORM CLASSES AND METHOD OF COMPUTATION OF SPECTRA

An initial decomposition of spreading modulations is based upon two features: the constancy (or lack of it) of the phase within each chip, and the continuity (or lack of it) of phase at the chip boundaries. Our first class consists of the "constant phase" waveforms, in which the carrier phase remains constant during each chip, with discontinuous change at chip boundaries permitted. The value of the phase in a given chip is determined by a particular subset of the code bit sequence which corresponds to the pulse in question. In the simplest case, we assign the bits to the chips in a one-for-one manner, and the only other case discussed here utilizes two bits per chip in some way. The bit, or bits, assigned to a given chip can determine the phase absolutely, or control an increment to be applied to the phase of the preceding chip. When two bits are used per chip, they can be two "new" bits for every chip, or a two-bit window can slide along the bit sequence, controlling phase in some way. These possibilities are discussed in detail in Section III.

The other major class of modulations combines varying phase (throughout the chip) with phase continuity at chip boundaries. The waveforms are most naturally described in terms of the possible frequency modulation patterns employed. One can have a repertoire of 2^n possible patterns for any chip, selected according to the values of a set of n consecutive bits in the code sequence. One could then take n new bits for each chip, or slide an n -bit window along the sequence, yielding a correlation between successive frequency modulation patterns. An example of this latter group called "tamed FM" has been discussed in the literature⁽²⁾ as an information modulation, but the remainder of this study is devoted to the so-called "binary FM" waveforms, of which there are several well-known examples.

The binary FM waveform uses just one bit for each chip, hence one of two frequency modulation patterns is applied. We further specialize this class by the assumption that one of these patterns is the negative of the other (with respect to a suitable carrier frequency), so that the frequency modulation in the n^{th} chip will be $\pm \phi(t-n\Delta)$, where $\phi(t)$ is the basic frequency modulation

pattern of the waveform, Δ is the chip duration, and the algebraic sign is fixed by the n^{th} bit of the spreading code. If $\phi(t)$ is a constant, the frequency-shift keying (FSK) waveform results, the simplest example of a binary FM waveform. Binary FM waveforms are discussed in detail in Sections IV, V and VI.

The two other classes allowed by our original division are excluded from this study for the following reasons. The first class would consist of constant-phase waveforms with phase continuity at chip boundaries, i.e., unmodulated pulses, and these are of no interest as spreading modulations. The remaining class allows phase discontinuities at chip boundaries along with phase variation within the chip. The phase jumps of such waveforms impart to them the same slow decay of spectral density with frequency as is exhibited by BPSK (namely inverse square), which defeats the primary purpose of the variable phase waveforms. It will be shown in Section IV that the asymptotic spectral properties are determined by the number of continuous derivatives of phase at chip boundaries, and the frequency modulation patterns, $\phi(t)$, of different binary FM waveforms are chosen with this property in mind. To allow phase discontinuities to occur (deliberately or accidentally) would ruin the good features otherwise attainable in the waveform design, and this can be clearly demonstrated in specific cases. In the binary FM waveforms, the frequency modulation function is bounded, and the resulting phase variation is continuous over the entire waveform. If, in addition, the frequency modulation function is zero at the beginning and end of a chip, then the overall frequency modulation of the waveform is continuous, regardless of the original bit sequence, and this leads to faster spectral decay with frequency. Further details are given in Section IV.

Our basic method of computing spectra begins with an explicit expression for the waveform as a function of time and the code sequence. Next, we compute the Fourier transform of this time function, still as a function of the code bits. The square of the Fourier transform gives the energy spectrum, and the desired power spectrum of the original waveform is obtained by dividing $N\Delta$, the total duration of the signal, which is N chips long. Finally, the spreading modulation spectrum is found by taking an ensemble

average over the bits of the spreading code. These bits are treated as "purely random", i.e., independent and equally likely to assume either value.

The "purely random" assumption places some limitation on the applicability of our results, but in many applications one strives for an approximation to this quality in real code sequences. This is not a basic limitation of the method, however, which would still be applied if the statistical properties of the code sequence in use were well enough known.

The spectra of individual waveforms will vary considerably, depending on the actual bits of the code, but the ensemble averages computed here are still relevant for the behavior of the system, so long as code sequences change continually, as we have assumed from the start.

Other methods of spectral computation are equivalent, but tend to be more difficult to apply. For example, a spreading waveform can be modelled as a stationary random process by extending it indefinitely in time and treating the start time of some reference chip as a random variable, uniformly distributed over an interval of length Δ , while the chip spacing remains rigid. One can then compute a covariance function and finally, by Fourier transformation, a power spectrum. Other authors have used Markov chain models to describe the sequence of phase variations in the waveform, and these too tend to become complicated.

The essential feature of the method used here is a representation theorem, which permits the expression of any binary FM waveform in a form formally very similar to the representation of a constant-phase waveform. This form permits easy application of the approach outlined above. The representation theorem is proved in Section IV, and the basic spectrum calculation is given in Section III.

III. CONSTANT-PHASE WAVEFORMS

A constant-phase waveform, N chips long, is uniquely specified by the sequence of carrier phases $\theta_0, \theta_1, \dots, \theta_{N-1}$. This sequence, in turn, is determined from an input bit sequence according to an algorithm characteristic of the modulation scheme. The modulation waveform itself can be written as a summation of adjacent rectangular pulses, each one chip in duration, and having the appropriate values of phase. The rectangular pulse function is defined as

$$P_0(t) \equiv \begin{cases} 1 & ; 0 < t < \Delta \\ 0 & ; \text{otherwise,} \end{cases}$$

and the complex modulation function which describes this waveform is then

$$Z(t) = \sum_{n=0}^{N-1} e^{i\theta_n} P_0(t - n\Delta) .$$

This function vanishes outside the interval $0 < t < N\Delta$, and the underlying carrier is arbitrary (although practical generation techniques often make use of an integral relationship between chip duration and carrier period).

The familiar Fourier transform of the rectangular pulse is denoted $k_0(\omega)$, as follows:

$$\begin{aligned} k_0(\omega) &\equiv \frac{1}{\Delta} \int_0^{\Delta} P_0(t) e^{-i\omega t} dt \\ &= e^{-i\omega\Delta/2} \frac{\sin(\omega\Delta/2)}{(\omega\Delta/2)} . \end{aligned}$$

In terms of $k_0(\omega)$, the Fourier transform of the modulation itself is

$$\begin{aligned} K(\omega) &= \int_0^{N\Delta} Z(t) e^{-i\omega t} dt \\ &= \sum_{n=0}^{N-1} e^{i\theta_n} \int_{n\Delta}^{n\Delta+\Delta} P_0(t - n\Delta) e^{-i\omega t} dt \\ &= \Delta k_0(\omega) \sum_{n=0}^{N-1} e^{i(\theta_n - n\omega\Delta)} . \end{aligned}$$

The quantity $|K(\omega)|^2$ is the energy spectrum of the waveform, and (according to Parseval's theorem)

$$\frac{1}{2\pi} \int_{-\infty}^{\infty} |K(\omega)|^2 d\omega = \int_0^{N\Delta} |Z(t)|^2 dt = N\Delta,$$

since $|Z(t)|$ is identically unity. Thus $|K(\omega)|^2/N\Delta$ is the desired power spectrum, whose ensemble average is given by

$$\begin{aligned} G(f) &= \frac{1}{N\Delta} \overline{|K(\omega)|^2} \\ &= \Delta |k_0(\omega)|^2 \frac{1}{N} \overline{\left| \sum_{n=0}^{N-1} e^{i(\theta_n - n\omega\Delta)} \right|^2}. \end{aligned}$$

We write spectral densities as functions of ordinary frequency, with the understanding that $\omega = 2\pi f$. The overbar denotes ensemble average, which can be evaluated after the specific dependence of the phase sequence on the code bit sequence is given.

The separation of $G(f)$ into a "pulse factor", in this case, $|k_0(\omega)|^2$, and a code factor (the ensemble average) is typical of all the spreading modulations considered in this study. The code factor is periodic in frequency, with period equal to the chipping rate, $f_{\text{chip}} = 1/\Delta$, hence the spectral behavior for all constant-phase waveforms, at large frequency (i.e., far from band center), is given by the pulse factor, which in this case decays as f^{-2} . Because of our normalization of the modulation waveform, the power spectral density integrates to unity:

$$\int_{-\infty}^{\infty} G(f) \frac{d\omega}{2\pi} = 1.$$

The code factor is expanded as follows:

$$\begin{aligned} &\frac{1}{N} \overline{\left| \sum_{n=0}^{N-1} e^{i(\theta_n - n\omega\Delta)} \right|^2} \\ &= \frac{1}{N} \overline{\sum_{n,m=0}^{N-1} e^{i(\theta_m - \theta_n) - i(m-n)\omega\Delta}} \end{aligned}$$

$$\equiv \sum_{\ell=-(N-1)}^{N-1} C_{\ell} e^{-j\ell\omega\Delta},$$

where, for $\ell > 0$,

$$C_{\ell} \equiv \frac{1}{N} \sum_{n=0}^{N-1-\ell} e^{j(\theta_{n+\ell} - \theta_n)}.$$

When $\ell < 0$,

$$C_{\ell} = \frac{1}{N} \sum_{n=|\ell|}^{N-1} e^{j(\theta_{n+\ell} - \theta_n)},$$

and it follows that

$$C_{-\ell} = C_{\ell}^*,$$

and that

$$C_0 = 1.$$

The numbers, C_{ℓ} , form the truncated autocorrelation sequence of the finite, random sequence, $e^{j\theta_n}$.

If the phases are statistically independent, and if

$$\overline{e^{j\theta_n}} = 0,$$

then all the C_{ℓ} will vanish, except for C_0 , and the spectral density will be given by the pulse factor alone:

$$\begin{aligned} G(f) &= \Delta |k_0(\omega)|^2 \\ &= \Delta \frac{\sin^2(\omega\Delta/2)}{(\omega\Delta/2)^2}. \end{aligned}$$

This is the case for BPSK, since each phase angle is equally likely to assume either of two values, 180 degrees apart. If the code bit sequence is written b_0, b_1, \dots, b_{N-1} , and if each b_n is a binary variable taking only the values ± 1 , then the BPSK phase sequence can be defined by the statement

$$e^{j\theta_n} = b_n,$$

for $0 < n < N-1$. The same power spectral density describes the QPSK waveform (quadrature phase shift keying), at the same chipping rate, since QPSK can be described in terms of a sequence of $2N$ bits as follows:

$$e^{i\theta_n} = \frac{1}{\sqrt{2}} (b_{2n} + ib_{2n+1}).$$

Four phase values are possible, but the average value of $\overline{e^{i\theta_n}}$ is still zero.

If the phases are independent, but if $\overline{e^{i\theta_n}}$ is not zero, for example if

$$\overline{e^{i\theta_n}} = \rho,$$

then lines appear in the spectrum. It is not hard to show that, for large N , the fraction $1 - |\rho|^2$ of the power is found in a spectral density just like that of BPSK, while the remaining fraction, $|\rho|^2$, is in a line at $\omega = 0$ (band center). This kind of spectral density is undesirable in a spreading modulation, hence this case is not discussed in further detail.

A number of constant-phase waveforms exhibit correlation, at least over adjacent chips. An example is SQPSK (staggered, or offset QPSK), in which the correspondence of code bits and waveform phases is best shown by a diagram:

Q	b _{n-1}		b _{n+1}		
	b _n		b _{n+2}		
I	θ _{n-2}	θ _{n-1}	θ _n	θ _{n+1}	θ _{n+2}

Here, I and Q refer to in-phase and quadrature signals, which are separately modulated by alternate bits, as shown, and then combined to form the resultant phase sequence. From this diagram, we can write

$$e^{i\theta_{n-1}} = \frac{1}{\sqrt{2}} (b_n + ib_{n-1}),$$

$$e^{i\theta_n} = \frac{1}{\sqrt{2}} (b_{n+1} + ib_n),$$

$$e^{i\theta_{n+1}} = \frac{1}{\sqrt{2}} (b_{n+2} + ib_{n+1}),$$

etc.

Only adjacent phases are correlated, and we have

$$\overline{e^{i(\theta_n - \theta_{n-1})}} = \frac{1}{2} \overline{(b_n + ib_{n+1})(b_n - ib_{n-1})} = \frac{1}{2},$$

since $\overline{b_n b_{n+k}} = \overline{b_n} \overline{b_{n+k}} = 0$, for $k \neq 0$, and $\overline{b_n^2} = 1$. Similarly we have

$$\overline{e^{i(\theta_{n+1} - \theta_n)}} = \frac{1}{2} \overline{(b_{n+2} + ib_{n+1})(b_n - ib_{n-1})} = \frac{1}{2},$$

and this equation is thus true for both even and odd values of n . We have therefore found that

$$C_\ell = 0, \quad |\ell| > 1$$

and

$$C_1 = \frac{1}{N} \sum_{n=0}^{N-2} \overline{e^{i(\theta_{n+1} - \theta_n)}} = \frac{1}{2} \frac{N-1}{N} = C_{-1}.$$

For large N , which is always the case of interest here, we can take $C_{\pm 1} = 1/2$ and thus

$$\begin{aligned} G(f) &= \Delta |k_o(\omega)|^2 \left\{ 1 + \frac{1}{2} (e^{-i\omega\Delta} + e^{i\omega\Delta}) \right\} \\ &= \Delta \frac{\sin^2(\omega\Delta/2)}{(\omega\Delta/2)^2} (1 + \cos \omega\Delta) \\ &= 2\Delta \frac{\sin^2(\omega\Delta/2) \cos^2(\omega\Delta/2)}{(\omega\Delta/2)^2}, \end{aligned}$$

or

$$G(f) = 2\Delta \frac{\sin^2(\omega\Delta)}{(\omega\Delta)^2}.$$

In this case, the result is the same as the spectrum of BPSK or QPSK at one-half the chipping rate. In terms of our diagram, it means that the Q-channel signal could be advanced (or delayed) by one chip length, thus aligning the bits to produce conventional QPSK with chips twice as long as the original ones, all without changing the spectrum.

A second example exhibiting one-chip correlation is illustrated in the following diagram:

Q	b_{n-3}	b_{n-2}	b_{n-1}	b_n
I	b_{n-2}	b_{n-1}	b_n	b_{n+1}
	θ_{n-2}	θ_{n-1}	θ_n	θ_{n+1}

We call it PQPSK ("Poor-man's QPSK"), and, like SQPSK, the bit rates and chip rates are equal. From the diagram,

$$e^{i\theta_n} = \frac{1}{\sqrt{2}} (b_n + ib_{n-1})$$

and

$$e^{i(\theta_{n+1} - \theta_n)} = \frac{1}{2} \frac{(b_{n+1} + ib_n)(b_n - ib_{n-1})}{(b_n + ib_{n-1})(b_n - ib_{n-1})} = 1/2 .$$

For large N,

$$C_1 = 1/2 , \quad C_{-1} = -1/2,$$

and the spectral density is

$$\begin{aligned} G(f) &= \Delta |k_o(\omega)|^2 \left\{ 1 + \frac{1}{2} (e^{-i\omega\Delta} - e^{i\omega\Delta}) \right\} \\ &= \Delta \frac{\sin^2(\omega\Delta/2)}{(\omega\Delta/2)^2} (1 + \sin \omega\Delta) . \end{aligned}$$

If I and Q channels are interchanged in this example, the second factor in the spectral density is changed to $(1 - \sin \omega\Delta)$.

A final example, which has been called⁽³⁾ UPSK (unidirectional PSK), shows correlation of phase over two chips. The defining diagram is

Q	b_{n-1}	b_n	b_{n+1}
I	b_{n-1}	b_n	b_{n+1}
	θ_{n-2}	θ_{n-1}	θ_n
	θ_{n-1}	θ_n	θ_{n+1}
	θ_n	θ_{n+1}	θ_{n+2}

and we have

$$e^{i\theta_{n-2}} = \frac{1}{\sqrt{2}} (b_{n-1} + ib_{n-1})$$

$$e^{i\theta_{n-1}} = \frac{1}{\sqrt{2}} (b_n + ib_{n-1})$$

$$e^{i\theta_n} = \frac{1}{\sqrt{2}} (b_n + ib_n)$$

$$e^{i\theta_{n+1}} = \frac{1}{\sqrt{2}} (b_{n+1} + ib_n),$$

etc. We evaluate

$$\frac{e^{i(\theta_{n-1} - \theta_{n-2})}}{e} = \frac{1}{2} (1 + i)$$

$$\frac{e^{i(\theta_n - \theta_{n-1})}}{e} = \frac{1}{2} (1 + i)$$

$$\frac{e^{i(\theta_{n+1} - \theta_n)}}{e} = \frac{1}{2} (1 + i),$$

and so on, and also

$$\frac{e^{i(\theta_n - \theta_{n-2})}}{e} = 0$$

$$\frac{e^{i(\theta_{n+1} - \theta_{n-1})}}{e} = 1/2 .$$

This last sequence continues to alternate between the values 0 and 1/2, and we find (for large N);

$$C_1 = \frac{1}{2} (1 + i), C_2 = 1/4 ,$$

and hence, after some simplification,

$$G(f) = 2\Delta \frac{\sin^2(\omega\Delta)}{(\omega\Delta)^2} (1 + \sin \omega\Delta) .$$

Again, interchange of I and Q channels in the definition replaces $(1+\sin \omega\Delta)$ by the factor $(1-\sin \omega\Delta)$.

It is convenient to replace frequency by an angle variable, θ , defined as follows:

$$\theta = \omega\Delta = 2\pi f\Delta = 2\pi f/f_{\text{chip}},$$

and to use a corresponding, dimensionless spectral density:

$$g(\theta) \equiv G(f)/\Delta.$$

Then $g(\theta)$ is normalized according to

$$\frac{1}{2\pi} \int_{-\infty}^{\infty} g(\theta) d\theta = 1 .$$

The spectral densities of the constant-phase waveforms discussed so far can be summarized as follows:

$$\text{BPSK, QPSK:} \quad g(\theta) = \frac{\sin^2(\theta/2)}{(\theta/2)^2}$$

$$\text{SQPSK:} \quad g(\theta) = 2 \frac{\sin^2 \theta}{\theta^2}$$

$$\text{PQPSK:} \quad g(\theta) = \frac{\sin^2(\theta/2)}{(\theta/2)^2} (1 \pm \sin\theta)$$

$$\text{UPSK:} \quad g(\theta) = 2 \frac{\sin^2 \theta}{\theta^2} (1 \pm \sin\theta) .$$

These spectra are shown in Fig. III-1, where spectral density is plotted on a linear scale. The plots are made from the $g(\theta)$ -formulas, but with the abscissa labelled by the ratio $(f/f_{\text{chip}}) = \theta/2\pi$. The spectral differences here are not significant, from a spreading point of view, and the disadvantage shared by all is the inverse-square decay of spectral density with frequency.

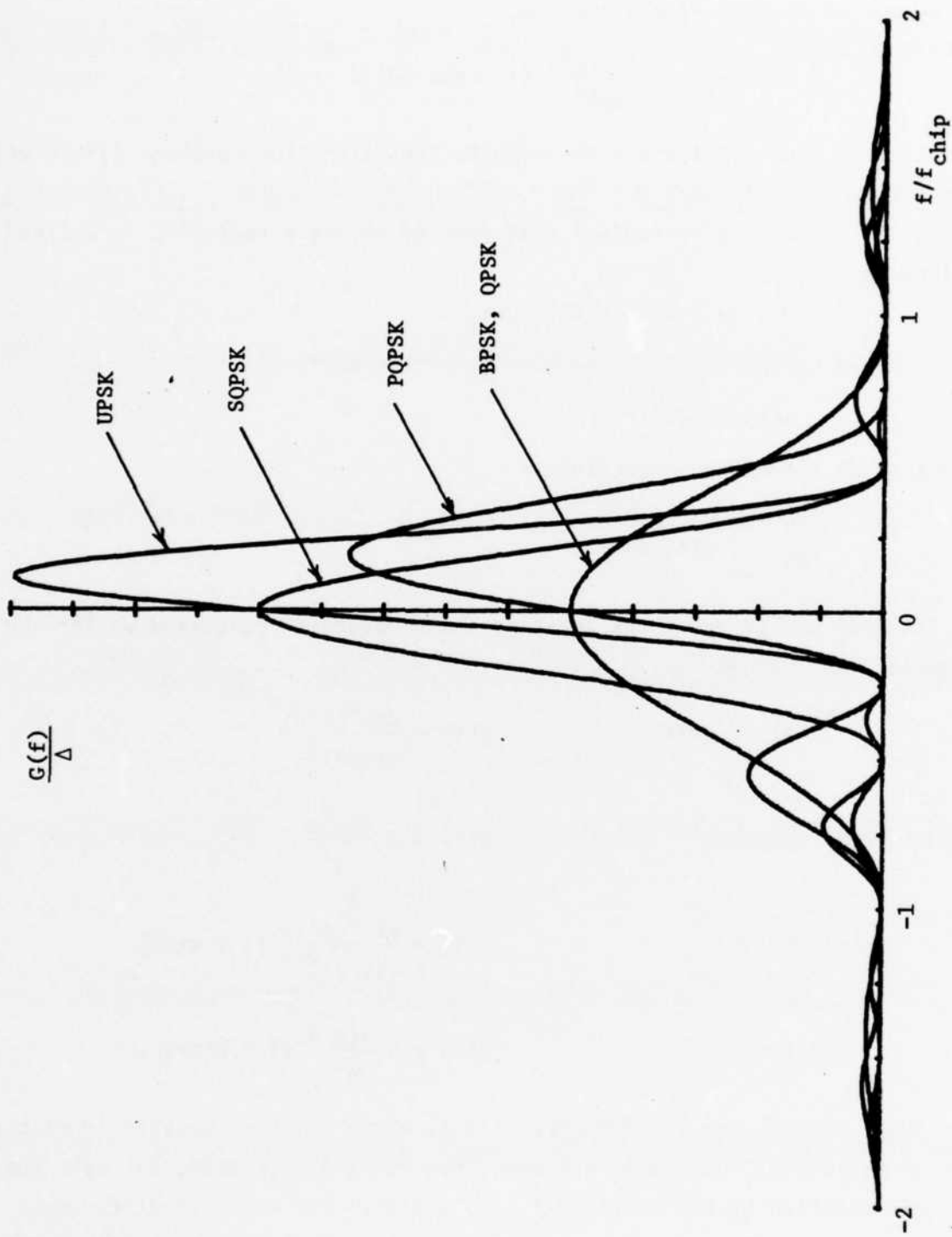


Fig. III-1. Spectra of constant-phase waveforms

TR-596(III-1)

Another variation of the constant phase theme assigns statistically independent increments, ψ_n , to the initial phase of each chip of the waveform. Then

$$\theta_n = \theta_0 + \sum_{m=1}^n \psi_m ,$$

and

$$e^{i(\theta_{n+l} - \theta_n)} = \exp\left(i \sum_{m=n+1}^{n+l} \psi_m\right) .$$

If the increments, ψ_m , form a stationary, independent sequence, determined by the input bit sequence, then

$$\overline{e^{i(\theta_{n+l} - \theta_n)}} = \rho^l ,$$

where

$$\rho \equiv \overline{e^{i\psi_m}} .$$

The code factor of the spectral density is then given by

$$1 + 2\text{Re} \sum_{\ell=1}^{N-l} \frac{N-l}{N} \rho^\ell e^{-i\ell\omega\Delta} ,$$

which becomes, in the limit of large N ,

$$\frac{1 - |\rho|^2}{1 + |\rho|^2 - 2\text{Re}(\rho e^{-i\omega\Delta})} .$$

In general, the correlation introduced by specifying increments (instead of phases directly) leads to ripples in the spectral density, as given by this code factor. If, however, $\rho=0$, then the BPSK spectrum reappears, no matter how many bits are used to specify each phase increment.

An interesting case occurs if each phase increment is either $\pm\psi$, according to the corresponding code bit. We can write

$$\psi_n = b_n \psi$$

and evaluate

$$\rho = \overline{e^{i\psi_n}} = \cos\psi .$$

The spectrum of any waveform featuring independent phase increments can be matched by one of these special waveforms, with appropriate choice of ψ . The code factor, expressed in terms of ψ , is

$$\frac{\sin^2 \psi}{1 + \cos^2 \psi - 2\cos \psi \cos(\omega\Delta)}$$

in this case, and we shall meet this factor again, in a similar context, in connection with binary FM waveforms.

In terms of $\theta = \omega\Delta$, the complete spectral density for this waveform, which we call IPSK (incremental phase shift keying) is

$$g(\theta) = \frac{\sin(\theta/2)^2}{\theta/2} \frac{\sin^2 \psi}{1 + \cos^2 \psi - 2\cos \psi \cos \theta} .$$

Linear plots of $g(\theta)$ for a range of ψ -values are given in Fig. III-2. As $\psi \rightarrow 0$, the spectral density approaches a line at zero frequency (band center), and when $\psi \rightarrow \pi$, lines appear at frequencies $\pm f_{\text{chip}}/2$ on either side of band center. The relative density, $G(f)/G(0)$ is shown, for a range of ψ -values, in Fig. III-3, expressed in dB. The null positions are independent of ψ , and the slow decay with frequency is evident. It should also be noted that sidelobe levels increase with increasing values of ψ in this range.

TR-596(III-2)

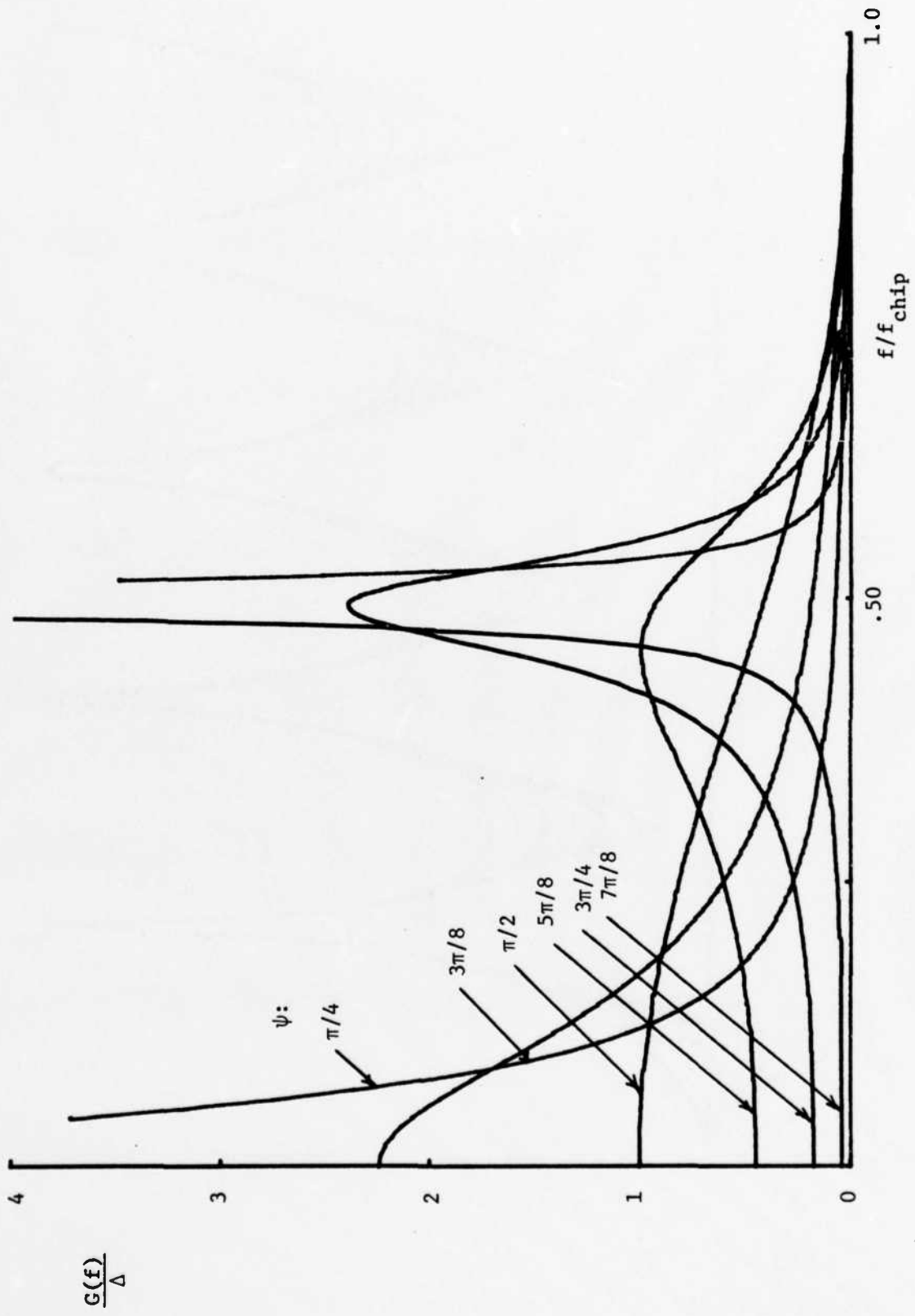


Fig. III-2. IPSK spectra

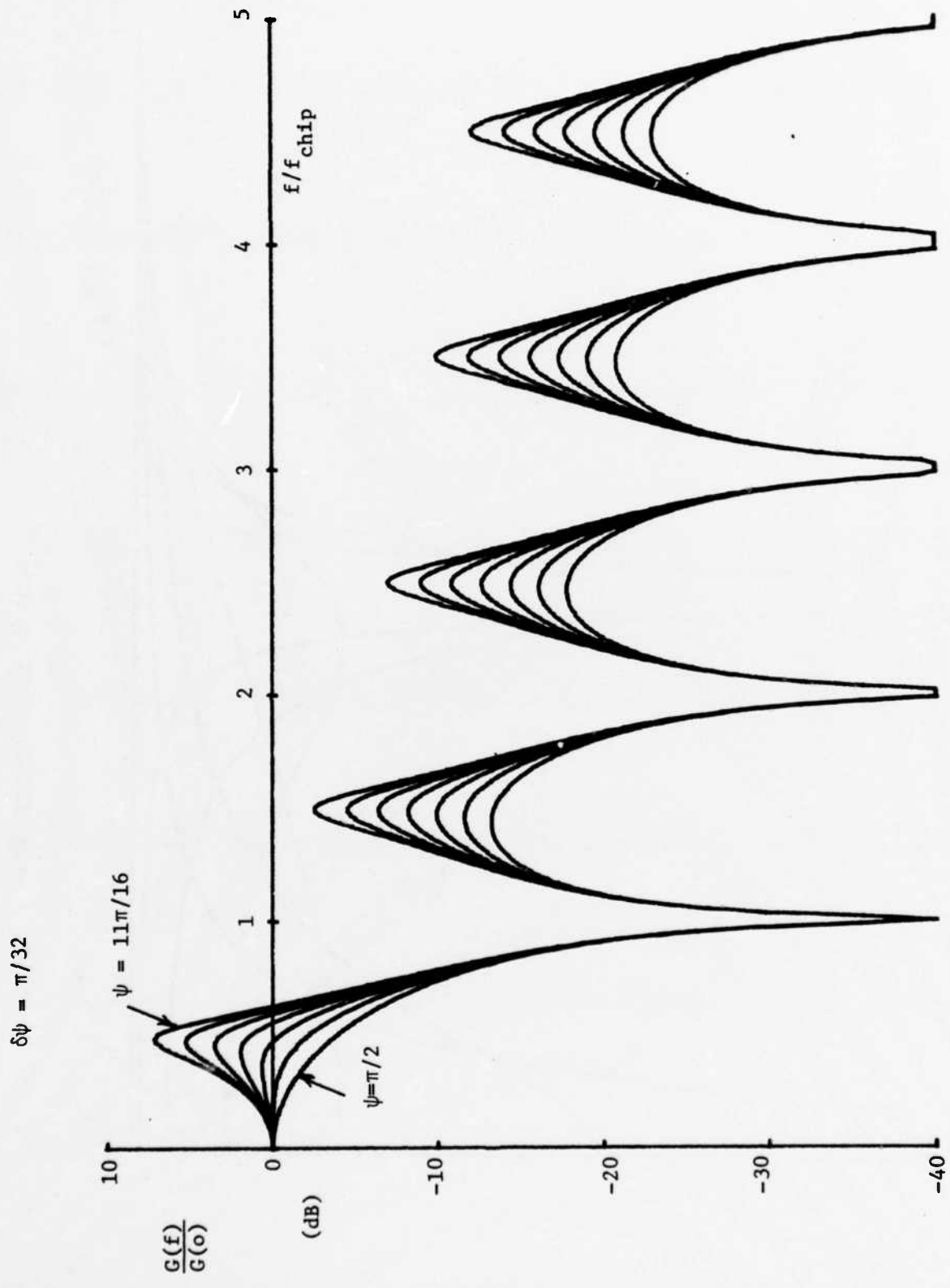


Fig. III-3. Relative spectra of IPSK.

IV. BINARY FM WAVEFORMS

A binary FM spreading modulation is completely specified by its characteristic frequency modulation function, $\dot{\phi}(t)$, which is defined only over the interval $0 < t < \Delta$, one chip in duration. During the n^{th} chip of the waveform, which starts at $t = n\Delta$, the instantaneous frequency is defined to be

$$\dot{\phi}(t) = b_n \dot{\phi}(t - n\Delta),$$

where b_n is the n^{th} bit of the spreading code. The initial phase (at $t=0$) is taken to be zero, so that the modulation waveform is

$$Z(t) = e^{i\phi(t)},$$

where

$$\phi(t) = \int_0^t \dot{\phi}(s) ds.$$

The last chip ends at $t = N\Delta$, and $Z(t)$ is taken to be zero outside the interval $0 < t < N\Delta$.

The characteristic phase variation is

$$\phi(t) = \int_0^t \dot{\phi}(s) ds,$$

and we define

$$\psi \equiv \phi(\Delta).$$

This parameter, ψ , is of basic importance in the study of these waveforms; it represents the magnitude of the phase change which takes place across every chip. The actual phase increments accumulate, with appropriate signs, so that the waveform phase at time $t = n\Delta$, which we call θ_n , is given by

$$\theta_n = \phi(n\Delta) = (b_0 + b_1 + \dots + b_{n-1})\psi.$$

Of course, $\theta_0 = 0$, and within the n^{th} chip, we have

$$\phi(t) = \theta_n + b_n \phi(t - n\Delta),$$

where

$$n\Delta < t < (n+1)\Delta.$$

We assume now that $\sin\psi$ does not vanish, deferring discussion of this special case (where ψ is an integral multiple of π) until later. With this restriction we introduce the "pulse function", $P(t)$, which is non-zero only over an interval two chips long, by the equations

$$P(t) = \begin{cases} \csc\psi \sin[\psi - \phi(t)]; & 0 < t < \Delta \\ \csc\psi \sin[\phi(t + \Delta)]; & -\Delta < t < 0 \\ 0 & ; \text{ otherwise .} \end{cases}$$

Note that $P(t)$ is continuous, being zero at $t = \pm\Delta$ and unity at $t=1$, but not necessarily symmetric. Finally, consider the waveform

$$Z_1(t) \equiv \sum_{m=0}^N e^{i\theta_m} P(t - m\Delta),$$

where $\theta_m = (b_0 + \dots + b_{m-1})\psi$ as before.

For a time, t , within the n^{th} chip (i.e., if $n\Delta < t < (n+1)\Delta$), only the terms $m=n$ and $m=n+1$ of the sum defining $Z_1(t)$ contribute, and then

$$\begin{aligned} Z_1(t) &= e^{i\theta_n} P(t-n\Delta) + e^{i\theta_{n+1}} P(t-n\Delta-\Delta) \\ &= \csc\psi \{ e^{i\theta_n} \sin[\psi - \phi(t-n\Delta)] \\ &\quad + e^{i\theta_{n+1}} \sin[\phi(t-n\Delta)] \}. \end{aligned}$$

But

$$e^{i\theta_{n+1}} = e^{i\theta_n + i b_n \psi},$$

and

$$\begin{aligned} e^{i b_n \psi} &= \cos(b_n \psi) + i \sin(b_n \psi) \\ &= \cos\psi + i b_n \sin\psi, \end{aligned}$$

since b_n is a binary variable. We therefore obtain

$$Z_1(t) = \text{csc } \psi e^{i\theta_n} \{ \sin[\psi - \phi(t - n\Delta)] + (\cos \psi + i b_n \sin \psi) \sin[\phi(t - n\Delta)] \},$$

or

$$\begin{aligned} Z_1(t) &= e^{i\theta_n} \{ \cos[\phi(t - n\Delta)] + i b_n \sin[\phi(t - n\Delta)] \} \\ &= e^{i\theta_n + i b_n \phi(t - n\Delta)} \\ &= Z(t) \end{aligned}$$

This equality of $Z(t)$ and $Z_1(t)$ holds within every chip, since the inclusion of the term $m=N$ in the sum defining $Z_1(t)$ validates our derivation for any value of n , from zero through $N-1$ (note that θ_N is just the phase of $Z(t)$ at time $t=N\Delta$). At chip boundaries, $Z(t)$ and $Z_1(t)$ are still equal, since

$$Z_1(n\Delta) = e^{i\theta_n} P(o) = e^{i\theta_n}.$$

The modulation function, $Z_1(t)$, is zero when $t < -\Delta$ and when $t > (N+1)\Delta$, and thus $Z(t)$ and $Z_1(t)$ differ only during the two intervals, each one chip long, which precede and follow the original time interval over which $Z(t)$ is non-zero. The new function is not constant-envelope in these "extra chips," but for large N their presence cannot have a large effect on the spectral properties of $Z_1(t)$, and henceforth we use the definition of $Z_1(t)$ as a representation of $Z(t)$, dropping the subscript. From another point of view, the use of the sum for $Z(t)$ is not a serious approximation because $Z(t)$, as originally defined, is only an idealization of the waveform likely to be produced in practice.

For many purposes, including the computation of spectra, the sum representation of $Z(t)$ is very much more convenient than the original definition. In fact, the general derivation of Section II needs only one change to apply to binary FM waveforms. That change is to replace $P_o(t)$ by $P(t)$, and the transform, $k_o(\omega)$, by the new transform

$$k(\omega) \equiv \frac{1}{\Delta} \int_{-\Delta}^{\Delta} P(t) e^{-i\omega t} dt.$$

Then

$$G(f) = \Delta |k(\omega)|^2 \cdot \frac{1}{N} \left| \sum_{n=0}^N e^{i(\theta_n - n\omega\Delta)} \right|^2,$$

a product of pulse factor and code factor, as before.

The code factor is simple, since

$$\begin{aligned} \frac{e^{i(\theta_{n+l} - \theta_n)}}{e^{i(b_n + \dots + b_{n+l-1})\psi}} &= \frac{e^{ib_n\psi}}{e^{ib_{n+1}\psi}} \dots \frac{e^{ib_{n+l-1}\psi}}{e^{ib_{n+l-1}\psi}} \\ &= (\cos\psi)^l. \end{aligned}$$

This follows from the independence of the b_n and the identity

$$\frac{e^{ib\psi}}{e^{i(b + \sin\psi)\psi}} = \cos\psi,$$

for any binary variable. For large N , we get

$$C_\ell = (\cos\psi)^\ell$$

for $\ell > 0$ and

$$C_\ell = C_{-\ell} = (\cos\psi)^{|\ell|}$$

for negative ℓ . The rest of the evaluation of the code factor has already been carried out in Section III (waveforms with independent increments), and we find

$$\begin{aligned} \frac{1}{N} \left| \sum_{n=0}^N e^{i(\theta_n - n\omega\Delta)} \right|^2 &= \sum_{\ell=-N}^N C_\ell e^{-i\ell\omega\Delta} = \frac{\sin^2\psi}{1 + \cos^2\psi - 2\cos\psi \cos \omega\Delta} \end{aligned}$$

Our derivation is a bit heuristic, but the result is easily established by a careful analysis, so long as $|\cos\psi| < 1$.

This code factor is unity for any binary FM waveform in which ψ is an odd multiple of $\pi/2$, and most of the modulations suggested for spreading purposes share the value $\psi = \pi/2$. It turns out that this choice leads to the simplest receiver design, if the matched filter is realized passively, but, as we shall see, other values of ψ are desirable for shaping spectra for maximum spreading effectiveness.

The asymptotic behavior of the spectral densities is determined by the pulse factor, as it was for constant-phase waveforms, but much greater variety is now possible. The discontinuous pulse function, $P_0(t)$, led to an inverse square decay in the former case, but all binary FM waveforms have spectral densities which fall off at least as fast as f^{-4} (it is assumed that the characteristic frequency modulation function, $\dot{\phi}(t)$, is bounded). To verify this property, we write

$$e^{-i\omega t} = \frac{1}{\omega} \frac{d}{dt} e^{-i\omega t},$$

and carry out a partial integration in the defining equation for $k(\omega)$:

$$\begin{aligned} k(\omega) &= \frac{1}{\Delta} \int_{-\Delta}^{\Delta} P(t) e^{-i\omega t} dt \\ &= \frac{i}{\omega\Delta} \int_{-\Delta}^{\Delta} P(t) d(e^{-i\omega t}) \\ &= -\frac{i}{\omega\Delta} \int_{-\Delta}^{\Delta} \dot{P}(t) e^{-i\omega t} dt. \end{aligned}$$

The integrated part vanishes because $P(t)$ is continuous throughout the interval, including the point $t=0$ and the points $t=\pm\Delta$, where it is zero. However, $\dot{P}(t)$ may be discontinuous at these points, and a repetition of the procedure yields

$$\begin{aligned}
k(\omega) &= \frac{1}{\omega^2 \Delta} \int_{-\Delta}^{\Delta} \dot{P}(t) e^{-i\omega t} dt \\
&= -\frac{1}{\omega^2 \Delta} \int_{-\Delta}^{\Delta} \ddot{P}(t) e^{-i\omega t} dt \\
&\quad + \frac{1}{\omega^2 \Delta} \{ \dot{P}(\Delta-) e^{-i\omega \Delta} - \dot{P}(-\Delta+) e^{i\omega \Delta} \\
&\quad - \dot{P}(0+) + \dot{P}(0-) \} .
\end{aligned}$$

The notation $\dot{P}(t\pm)$ stands for the limit of $\dot{P}(t\pm\epsilon)$ as $\epsilon \rightarrow 0$, and we see that $k(\omega)$ varies as f^{-2} (hence $G(f)$ goes like f^{-4}) if $\dot{P}(t)$ is discontinuous at $t=0$ or $t=\pm\Delta$, and if $\ddot{P}(t)$ is bounded within $(-\Delta, \Delta)$.

If $\dot{P}(t)$ is also continuous, the argument is repeated again, and so on, so that one sees that the asymptotic properties of $G(f)$ are directly correlated with the smoothness of the pulse function, $P(t)$, at the origin and at the ends of its range.

The smoothness of $P(t)$ depends, in turn, on the corresponding properties of $\phi(t)$. For instance, in the interval $-\Delta < t < 0$,

$$P(t) = \csc \psi \cos[\phi(t+\Delta)] \dot{\phi}(t+\Delta) ,$$

and hence

$$P(-\Delta+) = \csc \psi \dot{\phi}(0+)$$

and

$$P(0-) = \cot \psi \dot{\phi}(\Delta-) .$$

Similarly,

$$P(0+) = -\cot \psi \dot{\phi}(0+)$$

and

$$P(\Delta-) = -\csc \psi \dot{\phi}(\Delta-) .$$

If $\dot{P}(t)$ is to be continuous, i.e., zero, at $t=\pm\Delta$, then $\dot{\phi}(t)$ must vanish at both ends of its range of definition. This, in turn, makes $\dot{P}(t)$ continuous at $t=0$. If $\dot{\phi}(t)$ vanishes at $t=0$ and $t=\Delta$, then

$$\ddot{P}(-\Delta+) = \csc\psi \ddot{\phi}(0+)$$

$$\ddot{P}(\Delta-) = -\csc\psi \ddot{\phi}(\Delta-)$$

and so on, hence the controlling parameter in this matter is the order of the zero of $\dot{\phi}(t)$ at $t=0$ and $t=\Delta$ (or the lower, if these are unequal).

It is easy to see why this should be so, by considering two adjacent chips. At the chip boundary the instantaneous frequency changes from $\pm\dot{\phi}(\Delta-)$ to $\pm\dot{\phi}(0+)$, depending on the relevant bits, hence the more smoothly $\dot{\phi}(t)$ approaches zero at the ends of its range the smoother will be the transitions from one chip to the next.

To summarize this relationship, we can say that if $\phi^{(n)}(t)$ is the lowest-order phase derivative which fails to vanish at $t=0$ and/or $t=\Delta$, then $k(\omega)$ will decay as f^{-n-1} , and the spectral density as f^{-2n-2} , at great distance from band center. This statement is also true for constant phase waveforms, which correspond to $n=0$, while for all binary FM waveforms, $n>1$. The parameter n , along with ψ , has a major effect on the character of the spectra of binary FM waveforms.

We conclude this section with a discussion of some special values of ψ , the phase shift per chip. First, let $\psi=\pi/2$, which is typical of many waveforms used for the transmission of information. As noted, the code factor is unity for these cases, hence the spectral density of the waveform is identical to that of the pulse factor itself. The basic representation also simplifies, since

$$e^{ib\pi/2} = ib$$

for any binary variable, and therefore, for $n>0$,

$$e^{i\theta} = i^n b_0 b_1 \dots b_{n-1}$$

We can define a new bit-sequence, a_n , as follows:

$$\begin{aligned} a_0 &= 1, \\ a_1 &= b_0 = a_0 b_0, \\ a_2 &= b_0 b_1 = a_1 b_1, \\ a_n &= b_0 \dots b_{n-1} = a_{n-1} b_{n-1}, \end{aligned}$$

and then write

$$Z(t) = \sum_{n=0}^N i^n a_n P(t-n\Delta).$$

The a -sequence is purely random if the b -sequence is, and the b 's are recovered from the a 's by means of the relation

$$b_n = a_n a_{n+1}.$$

The new expression for $Z(t)$ is particularly useful for the study of techniques for generating these waveforms and for the design of matched filters for the corresponding receivers. The case $\psi = -\pi/2$ leads to the complex conjugate of this representation for $Z(t)$.

When $\psi = K\pi$, the whole analysis must be changed, and we go back to the original definition of $Z(t)$, namely,

$$Z(t) = e^{i\theta_n + ib_n \phi(t-n\Delta)},$$

for values of t in the n^{th} chip. But now,

$$e^{ib\psi} = e^{ibK\pi} = \cos(K\pi) = (-1)^K,$$

hence

$$e^{i\theta_n} = (-1)^{nK},$$

which is independent of the bit sequence. Then

$$Z(t) = (-1)^{nK} \{\cos[\phi(t-n\Delta)] + ib_n \sin[\phi(t-n\Delta)]\}$$

within the n^{th} chip, and the I-component is deterministic. If we define

$$A(t) = \cos[\phi(t)] P_0(t),$$

$$B(t) = \sin[\phi(t)] P_0(t),$$

where $P_0(t)$ is the rectangular pulse function defined in Section III, then we can write

$$\begin{aligned} Z(t) &= \sum_{n=0}^{N-1} (-1)^{nK} A(t-n\Delta) \\ &+ i \sum_{n=0}^{N-1} (-1)^{nK} b_n B(t-n\Delta) \\ &\equiv X(t) + iY(t) . \end{aligned}$$

In terms of the pulse function Fourier transforms:

$$\begin{aligned} k_x(\omega) &\equiv \frac{1}{\Delta} \int_{-\infty}^{\infty} A(t) e^{-i\omega t} dt \\ &= \frac{1}{\Delta} \int_{-\Delta}^{\Delta} \cos[\phi(t)] e^{-i\omega t} dt \end{aligned}$$

and

$$\begin{aligned} k_y(\omega) &\equiv \frac{1}{\Delta} \int_{-\infty}^{\infty} B(t) e^{-i\omega t} dt \\ &= \frac{1}{\Delta} \int_{-\Delta}^{\Delta} \sin[\phi(t)] e^{-i\omega t} dt , \end{aligned}$$

we obtain

$$\begin{aligned}
 K(\omega) &= \int_{-\infty}^{\infty} Z(t) e^{-i\omega t} dt \\
 &= \Delta k_x(\omega) \sum_{n=0}^{N-1} (-1)^{nK} e^{-in\omega\Delta} \\
 &\quad + \Delta k_y(\omega) \sum_{n=0}^{N-1} (-1)^{nK} b_n e^{-in\omega\Delta} \\
 &\equiv K_x(\omega) + iK_y(\omega) .
 \end{aligned}$$

The spectral density is now

$$G(f) = \frac{1}{N\Delta} \overline{|K(\omega)|^2} = \frac{1}{N\Delta} \overline{|K_x(\omega)|^2} + \frac{1}{N\Delta} \overline{|K_y(\omega)|^2} .$$

In the first term, we evaluate

$$\sum_{n=0}^{N-1} (-1)^{nK} e^{-in\omega\Delta} = e^{-i \frac{N-1}{2} (\omega\Delta + K\pi)} \frac{\sin \frac{N}{2} (\omega\Delta + K\pi)}{\sin \frac{1}{2} (\omega\Delta + K\pi)} ,$$

and hence

$$\begin{aligned}
 G_x(f) &\equiv \frac{1}{N\Delta} \overline{|K_x(\omega)|^2} \\
 &= \Delta |k_x(\omega)|^2 \frac{\sin^2 \frac{N}{2} (\omega\Delta + K\pi)}{N \sin^2 \frac{1}{2} (\omega\Delta + K\pi)} .
 \end{aligned}$$

For large N , the second factor represents a sum of δ -functions at the points $\omega\Delta + K\pi = 2L\pi$, for integral L , and $G_x(f)$ becomes a line spectrum. In the usual case, all but a finite number of these lines are cancelled by zeroes of the factor, $k_x(\omega)$.

The Q-component term represents a continuous spectrum:

$$\begin{aligned}
 G_y(f) &\equiv \frac{1}{N\Delta} \overline{|K_y(\omega)|^2} \\
 &= \Delta |k_y(\omega)|^2 \frac{1}{N} \overline{\left| \sum_{n=0}^{N-1} b_n e^{-in(\omega\Delta + K\pi)} \right|^2} \\
 &= \Delta |k_y(\omega)|^2,
 \end{aligned}$$

in view of the independence of the bits in the code sequence.

Since spectral lines are very undesirable in a spreading waveform, the analysis of these cases is carried no further. It is worth noting, however, that upon squaring, the phase modulation of a waveform is doubled, so that a spreading waveform with a given value of ψ will look like a waveform of the same type, but with double the ψ -value, after passing through such a non-linearity. Thus a waveform, like MSK, with $\psi = \pi/2$, will yield lines in the spectrum if squared, and this could be undesirable from the point of view of signal detection and frequency determination by a potential jammer.

V. TYPICAL BINARY FM WAVEFORMS

The simplest binary FM waveform is FSK (frequency shift keying), defined by the statement

$$\dot{\phi}(t) = \text{constant.}$$

The constant value of $\dot{\phi}$ may be written ψ/Δ , and the carrier frequency is increased or decreased by this amount during each chip, according to the sign of the corresponding code bit. Since $\dot{\phi}(t)$ is never zero, we know that the spectral density will behave like f^{-4} ($n=1$) as $f \rightarrow \infty$.

The FSK pulse function, $P(t)$, is shown in Fig. V-1 for various values of ψ . The special case, $\psi=\pi/2$, is the familiar MSK (minimum shift keying) waveform, distinguished here by the continuous slope of $P(t)$ at the origin. All binary FM waveforms having $\psi=\pi/2$ share this latter property, due to the factor $\cot\psi$ in the expressions for $\dot{P}(0\pm)$. However, the slope discontinuity of the pulse function at $t=\pm\Delta$ is then the determining factor for asymptotic spectral behavior.

The Fourier transform is easily evaluated. After noting that

$$P(t) = \text{csc}\psi \sin\left(\psi - \frac{|t|}{\Delta}\psi\right),$$

we write

$$\begin{aligned} k(\omega) &= \frac{\text{csc}\psi}{\Delta} \cdot 2 \int_0^{\Delta} \sin\left(\psi - \frac{t}{\Delta}\psi\right) \cos \omega t \, dt \\ &= \frac{\text{csc}\psi}{\Delta} \int_0^{\Delta} \left\{ \sin\left(\psi - \frac{t}{\Delta}\psi + \omega t\right) + \sin\left(\psi - \frac{t}{\Delta}\psi - \omega t\right) \right\} dt, \end{aligned}$$

or

$$k(\omega) = \frac{2\psi}{\sin\psi} \frac{\cos\psi - \cos \omega\Delta}{(\omega\Delta)^2 - \psi^2}.$$

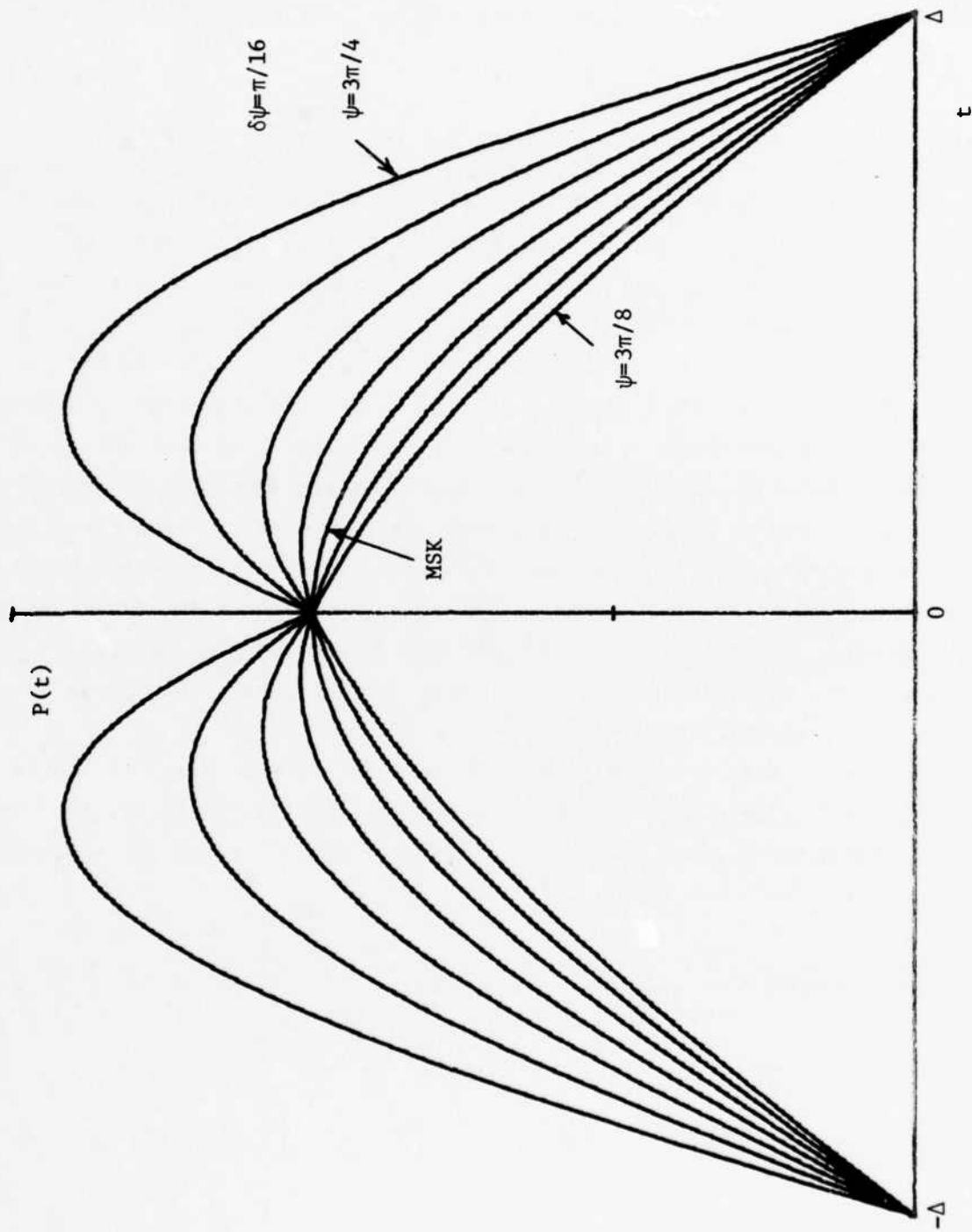


Fig. V-1. FSK pulse functions

We combine $|k(\omega)|^2$ with the code factor and express the result in terms of the angle variable, $\theta = \omega\Delta$, and the dimensionless $g(\theta) = G(f)/\Delta$, as before:

$$g(\theta) = 4\psi^2 \left\{ \frac{\cos \theta - \cos \psi}{\theta^2 - \psi^2} \right\}^2 \frac{1}{1 + \cos^2 \psi - 2\cos \psi \cos \theta} .$$

Plots of this function on a linear scale are given in Fig. V-2 for a wide range of ψ values. The effect of the denominator of the code factor is obvious, as it was in the case of IPSK, and as ψ approaches π or zero, the spectral density acquires lines.

It is apparent that $g(\theta)$ can be made fairly flat in its "mainlobe", by proper choice of ψ , and this is shown in Fig. V-3, where $g(\theta)/g(0)$ is plotted in dB, for a narrower range of ψ -values. It should be noted that the first sidelobe increases steadily with increasing ψ . In Appendix A, two quantitative measures of "spreading efficiency" are introduced, and it is shown that these quantities are optimized, in the case of FSK, for ψ -values near those which produce good "flatness" of the spectral density, in spite of the effect on the first sidelobe. Those performance measures deal with spectral occupancy constraints in a very simple way, and in some applications the sidelobe level could have more significance.

The expected behavior of $g(\theta)$ with large θ is shown in Fig. V-4, for a wide range of ψ -values. The quantity plotted is $\log R(f)$, where $R(f)$ is the fraction of the total power which lies outside a band, of width $2f$, centered on the carrier. In other words,

$$\begin{aligned} R(f) &= \left\{ \int_{-\infty}^{-f} + \int_f^{\infty} \right\} G(f) \frac{d\omega}{2\pi} \\ &= \left\{ \int_{-\infty}^{-\theta} + \int_{\theta}^{\infty} \right\} g(\theta') \frac{d\theta'}{2\pi} \end{aligned}$$

where $\theta = 2\pi\Delta$. These curves are obtained by numerical integration.

TR-596(V-2)

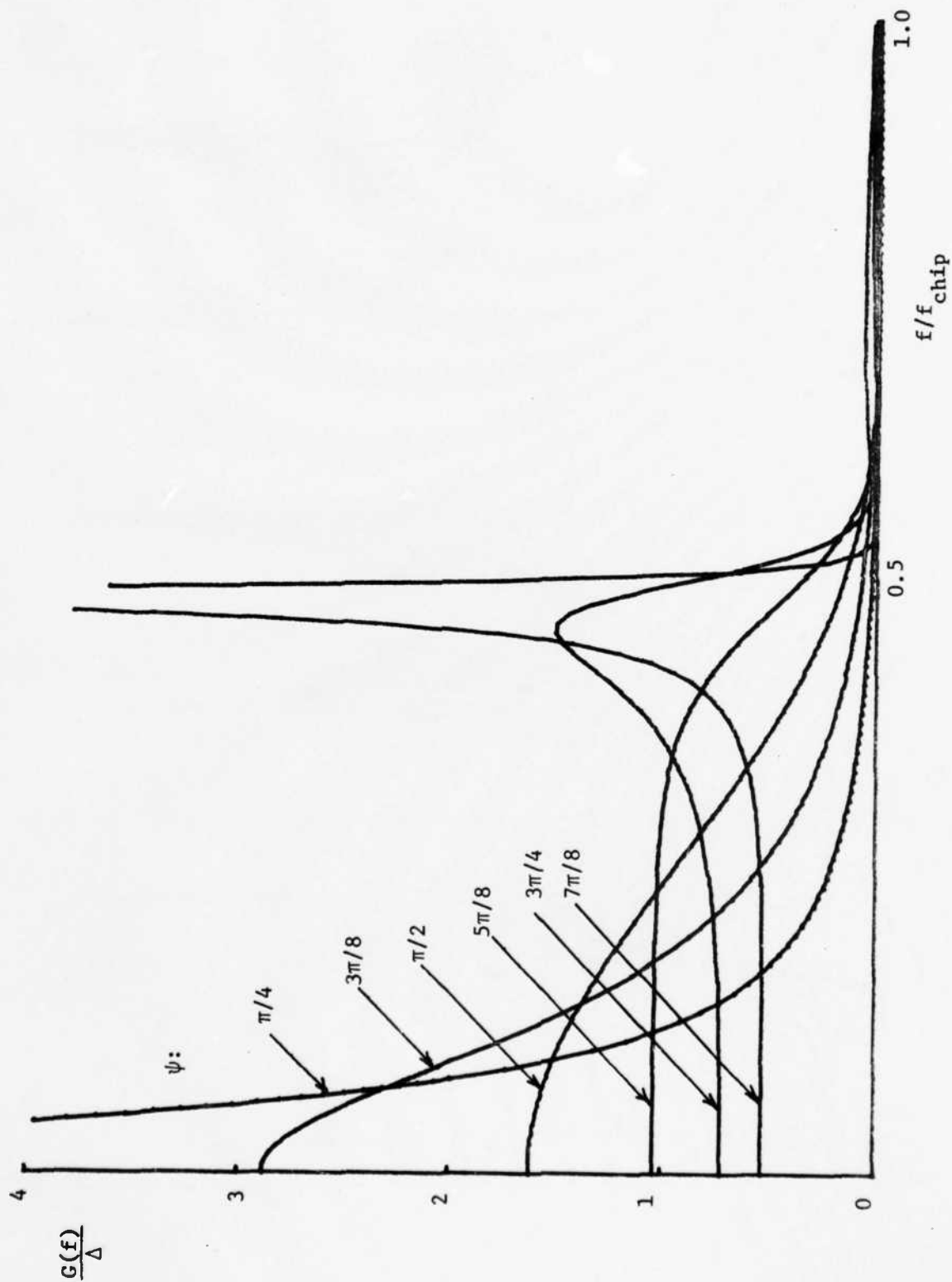


Fig. V-2. FSK spectra

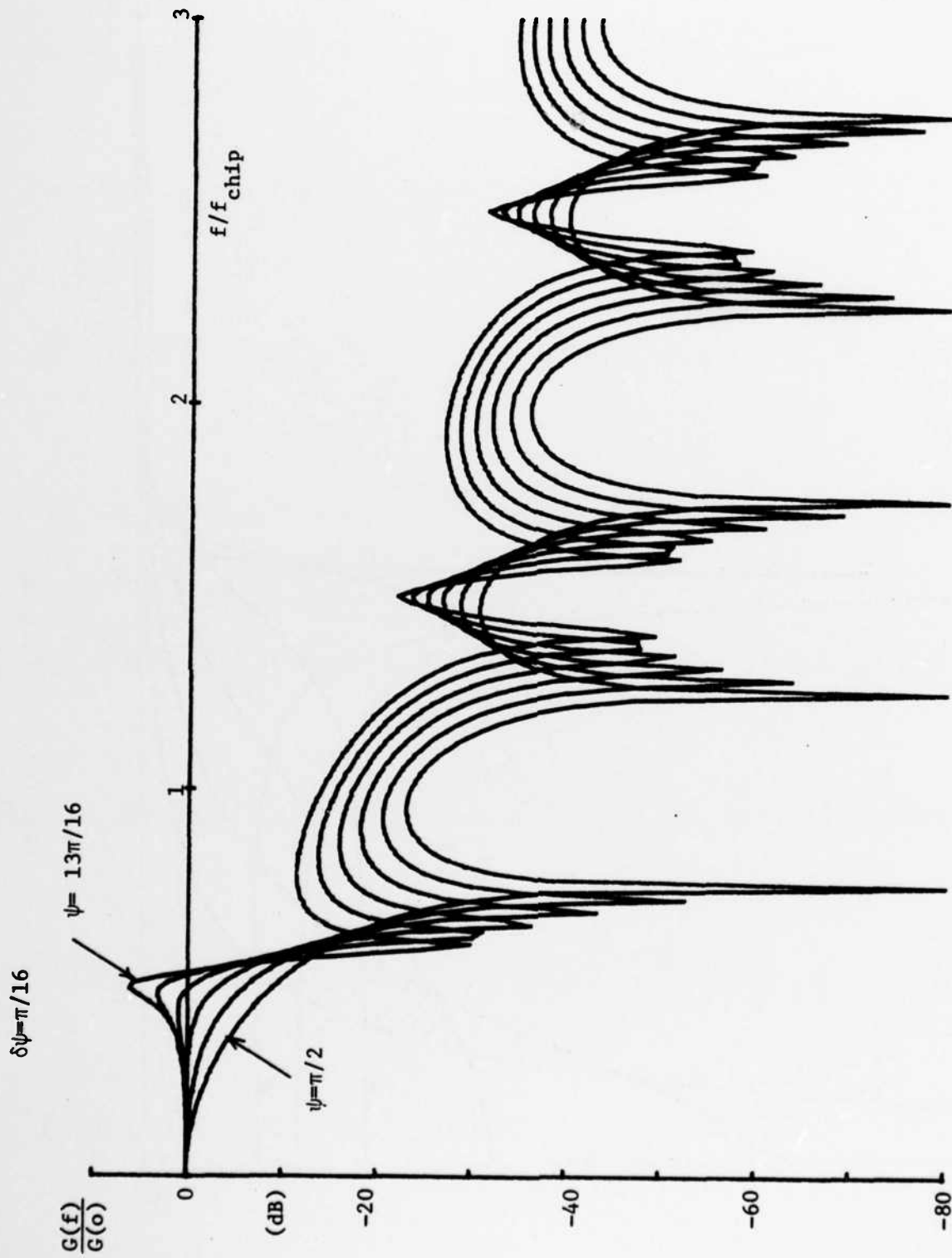


Fig. V-3. Relative spectra of FSK

TR-596(V-3)

TR-596(V-4)

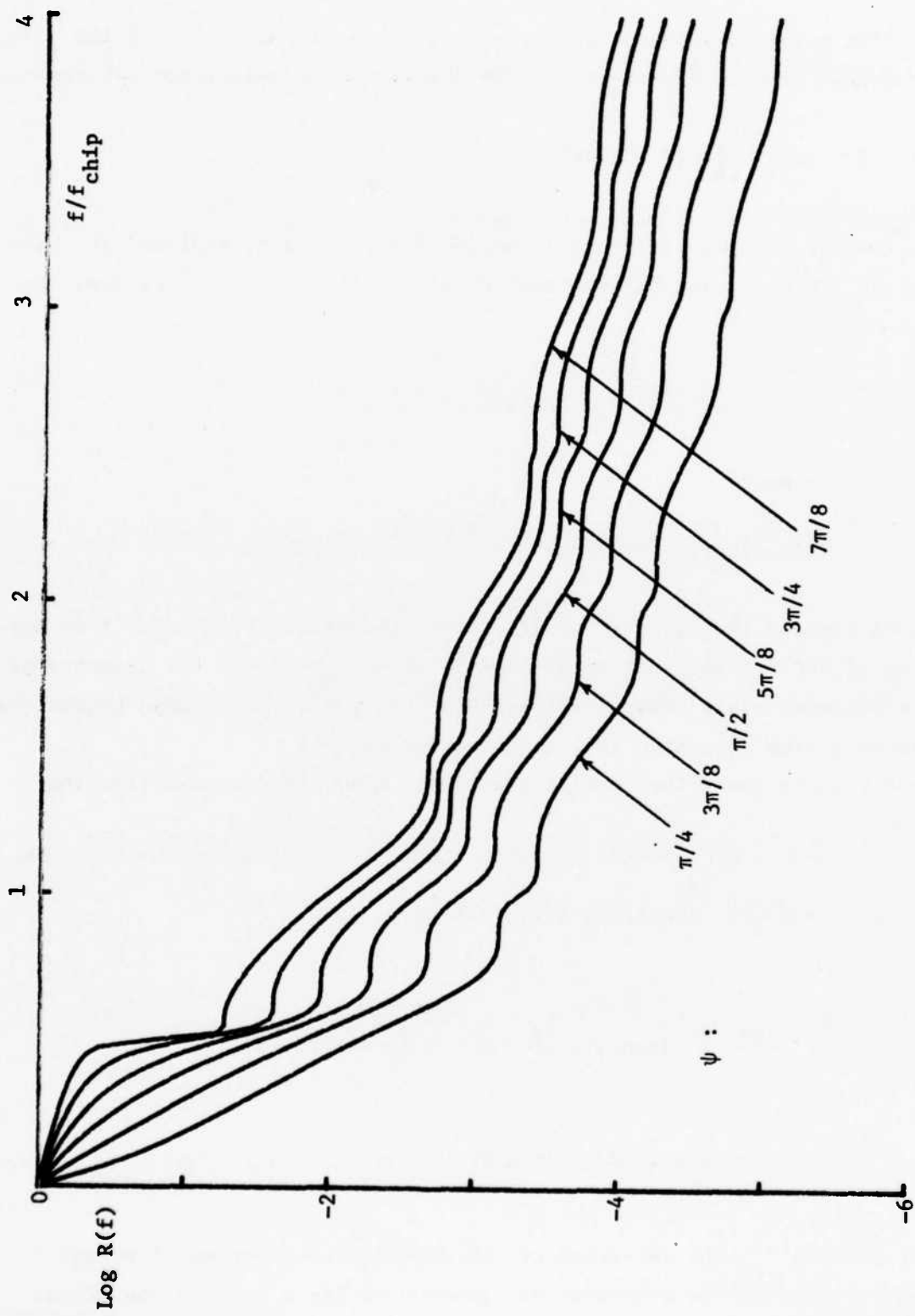


Fig. V-4. Cumulative spectra of FSK

The SFSK waveform (sinusoidal FSK), originally introduced⁽⁴⁾ in the special version with $\psi=\pi/2$, is defined by the frequency modulation pattern

$$\dot{\phi}(t) = \frac{\psi}{\Delta} [1 - \cos(2\pi t/\Delta)] .$$

Not only is $\dot{\phi}(t)$ zero at $t=0$ and $t=\Delta$ (unlike FSK), but $\ddot{\phi}(t)$ vanishes at these points also. Thus $n=3$ and the spectral density will vary as f^{-8} as $f \rightarrow \infty$. The SFSK phase variation is

$$\phi(t) = \psi \left\{ \frac{t}{\Delta} - \frac{1}{2\pi} \sin(2\pi t/\Delta) \right\} ,$$

which has the property

$$\phi(\Delta-t) = \psi - \phi(t) ,$$

as a consequence of the symmetry of $\dot{\phi}(t)$ about the midpoint, $t=\Delta/2$. From the definition of $P(t)$ we see that this symmetry of $\dot{\phi}(t)$ also implies symmetry of the pulse function about $t=0$. These symmetry properties are shared by all the binary FM waveforms discussed in the present study.

Since $P(t)$ is even, the Fourier transform, $k(\omega)$, is computed from the expression

$$\begin{aligned} k(\omega) &= \frac{2\text{csc}\psi}{\Delta} \int_0^{\Delta} \sin[\psi - \phi(t)] \cos \omega t \, dt \\ &= \frac{\text{csc}\psi}{\Delta} \int_0^{\Delta} \left\{ \sin\left[\psi - \left(\frac{\psi}{\Delta} - \omega\right)t + \frac{\psi}{2\pi} \sin(2\pi t/\Delta)\right] \right. \\ &\quad \left. + \sin\left[\psi - \left(\frac{\psi}{\Delta} + \omega\right)t + \frac{\psi}{2\pi} \sin(2\pi t/\Delta)\right] \right\} dt. \end{aligned}$$

Following Amoroso⁽⁴⁾, the integrand can be expanded in a series of Bessel functions, after which term-by-term integration yields a rapidly convergent

series. However, $k(\omega)$ can be computed equal simply by numerical integration, since the range of integration is finite and the integrand is oscillatory, so that high accuracy can be obtained with a modest number of points. Numerical integration has the advantage of applying equally well to all binary FM waveforms, and the procedure is systematized and described in Section VI.

Spectra obtained in this way are shown in Figs. V-5, V-6 and V-7, which are analogous to corresponding plots for FSK. The effectiveness of ψ in controlling flatness is again seen here, as well as the anticipated behavior at large values of f . A perhaps unexpected result is the relatively large first sidelobe, which is in all cases greater than that for FSK with the same ψ -values. This appears to be a penalty associated with increasing values of the index parameter n , as we shall see in more detail in Section VI.

Two examples of waveforms with index parameter $n=2$ ($G(f) \sim f^{-6}$) are discussed next. We call them waveforms A_2 and B_2 , and they have been briefly discussed in the literature⁽⁵⁾.

Waveform A_2 is defined by the frequency modulation pattern

$$\dot{\phi}(t) = \frac{\pi\psi}{2\Delta} \sin(\pi t/\Delta) ,$$

with the corresponding phase variation

$$\phi(t) = \frac{\psi}{2} [1 - \cos(\pi t/\Delta)] .$$

Clearly, $n=2$, since $\dot{\phi}(t)$ is itself the highest derivative of phase which vanishes at both ends of the chip interval. This waveform is similar to SFSK in the sense that its frequency modulation pattern is expressed in terms of trigonometric functions, but it is one degree less smooth at the chip boundaries. Spectral plots on linear and dB scales are given in Figs. V-8 and V-9, respectively, and Fig. V-10 shows the cumulative spectra in the form of plots of $\log R(f)$. The general behavior is similar to FSK and SFSK, and the magnitude of the first sidelobe is intermediate between these two.

Our second example having $n=2$, waveform B_2 , is defined by the frequency modulation pattern

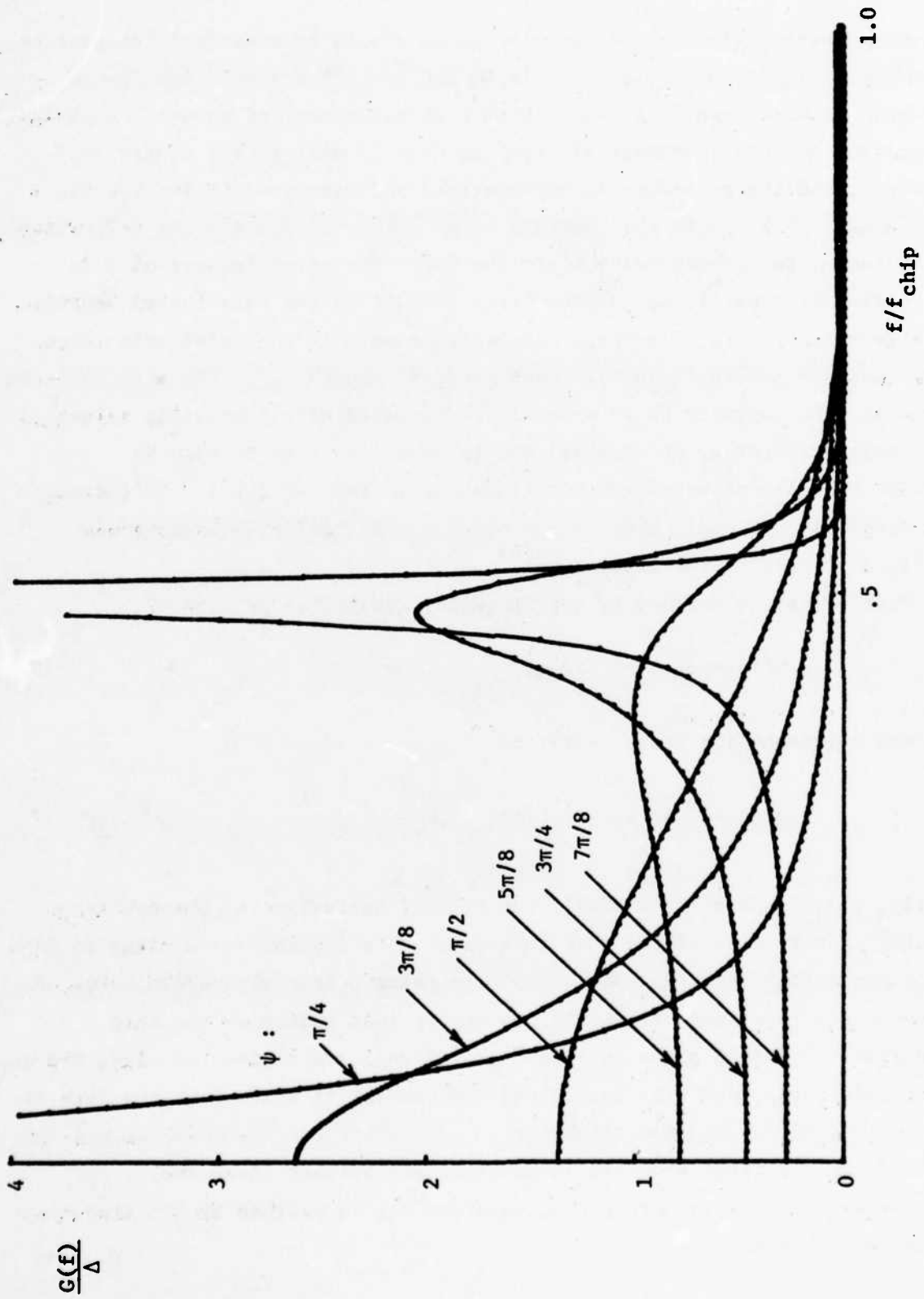


Fig. V-5. SFSK spectra

TR-596(V-5)

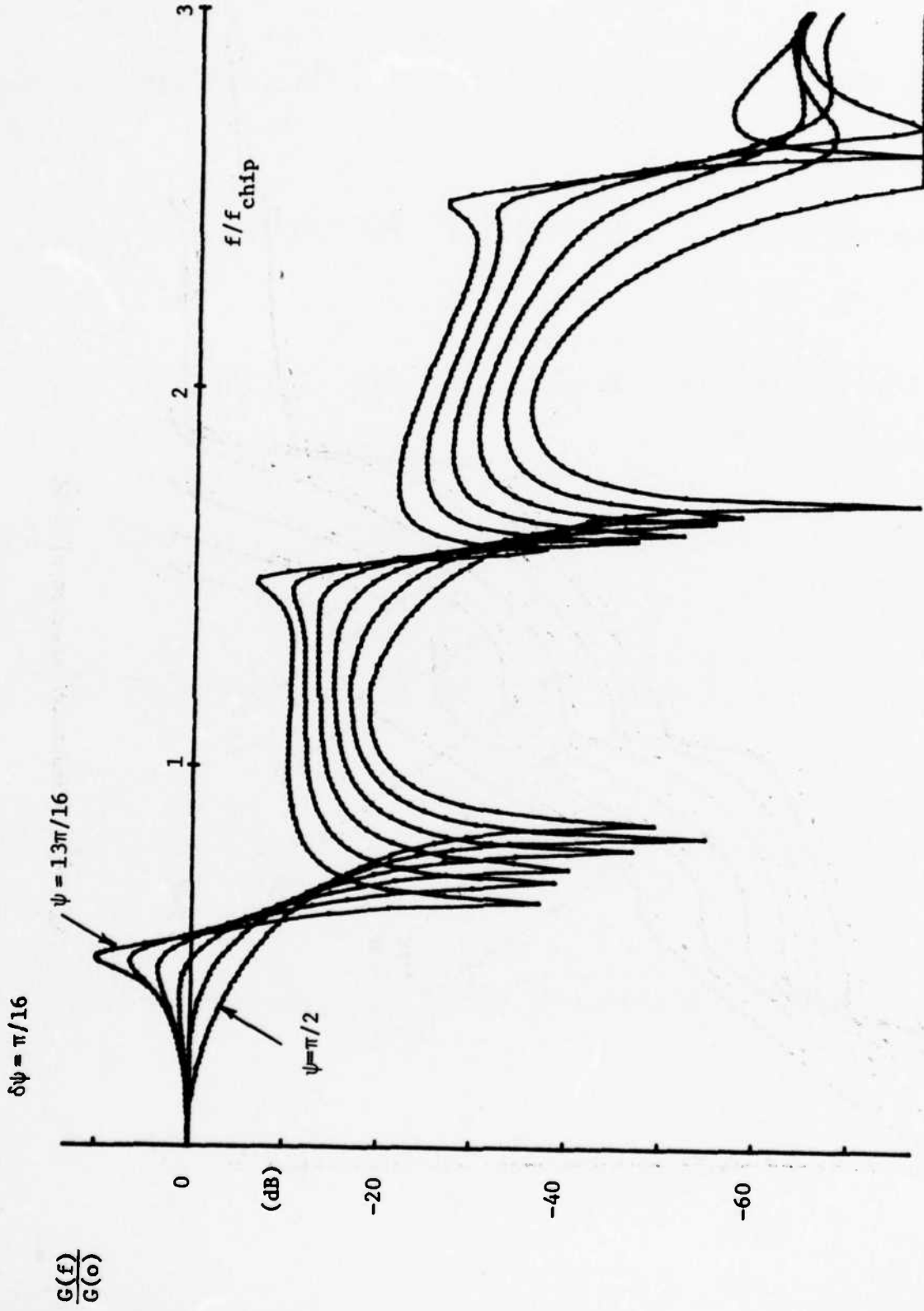


Fig. V-6. Relative spectra of SFSK

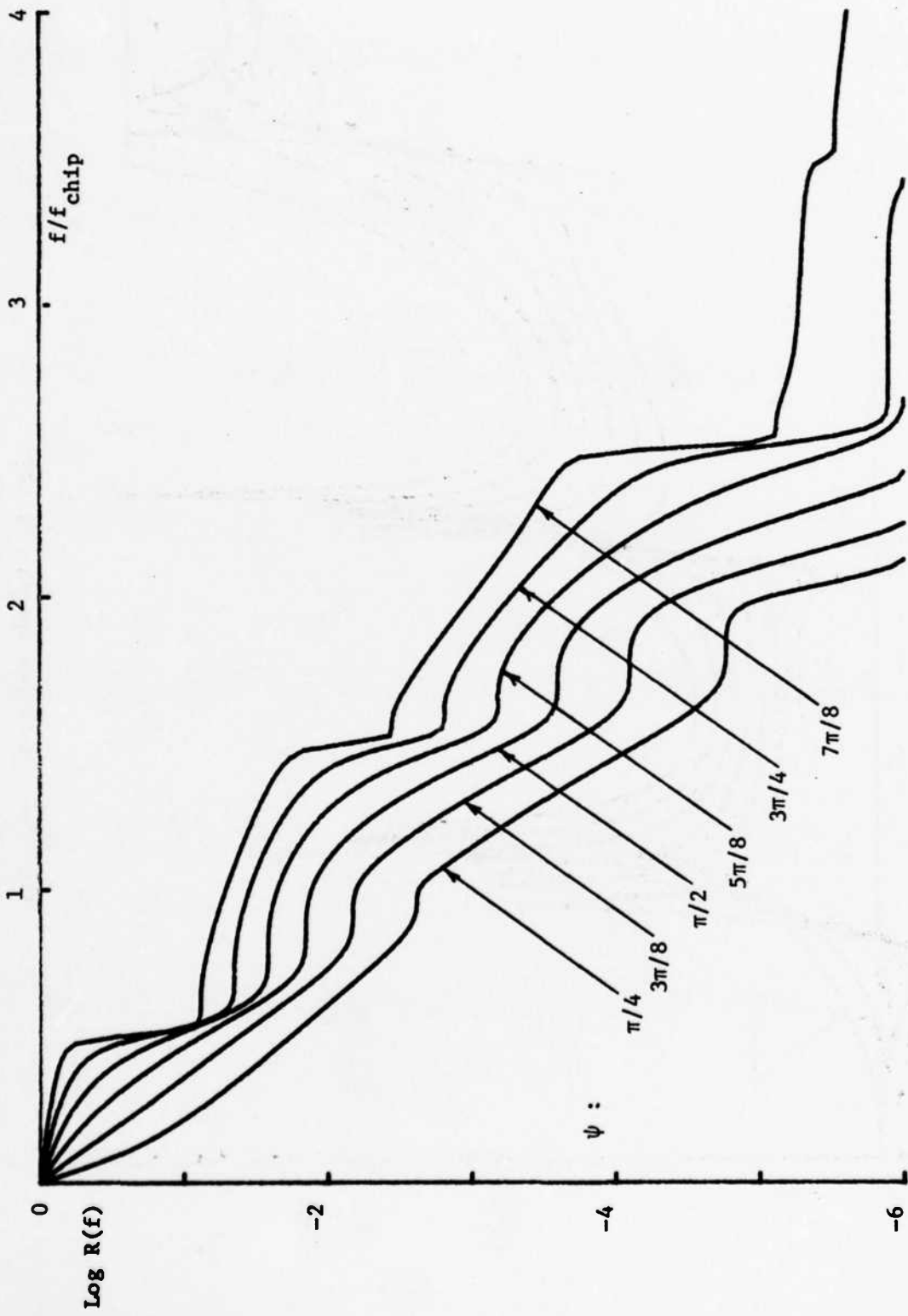


Fig. V-7. Cumulative spectra of SFSK

TR-596(V-7)

TR-596(V-8)

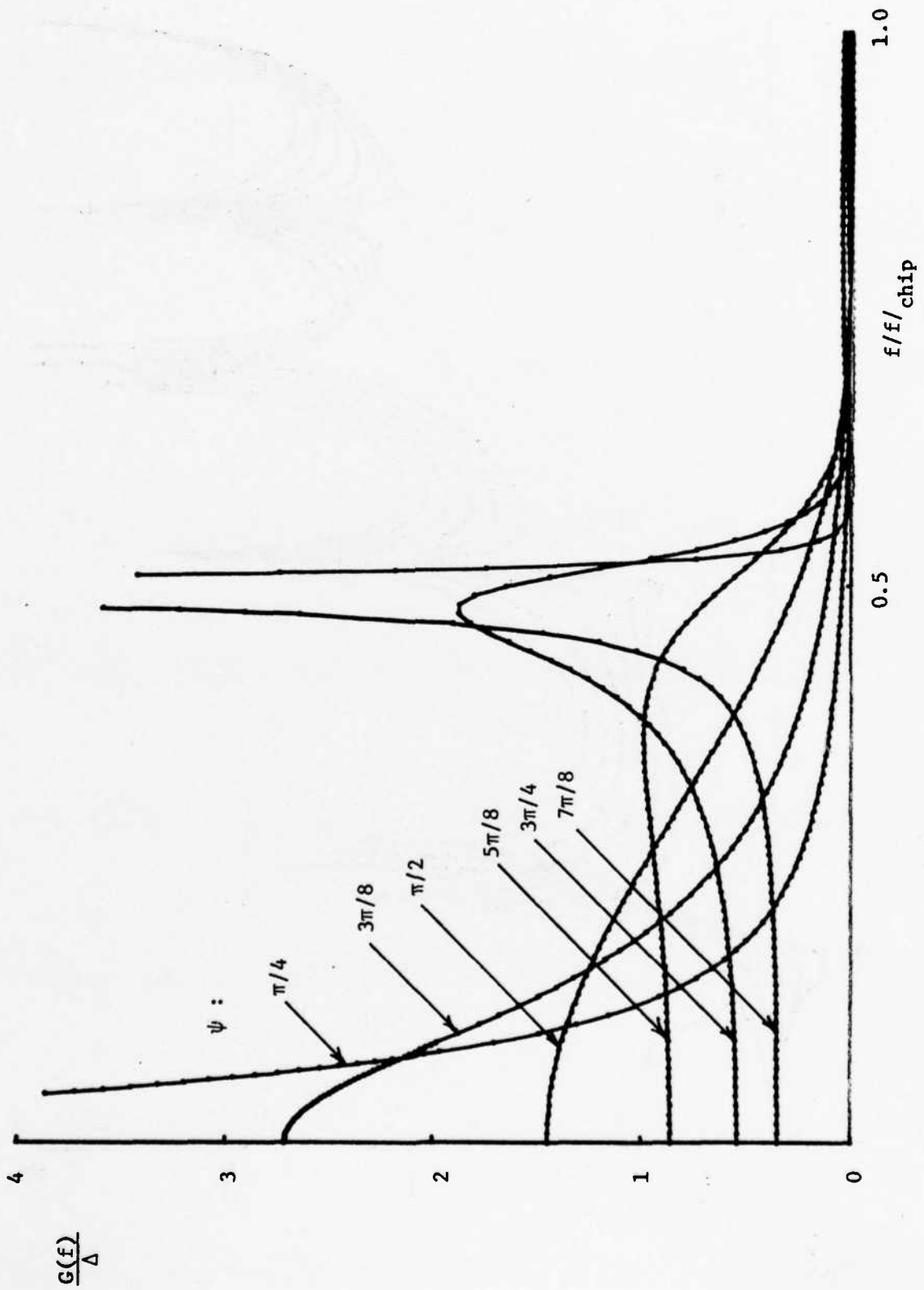


Fig. V-8. Spectra of waveform A_2

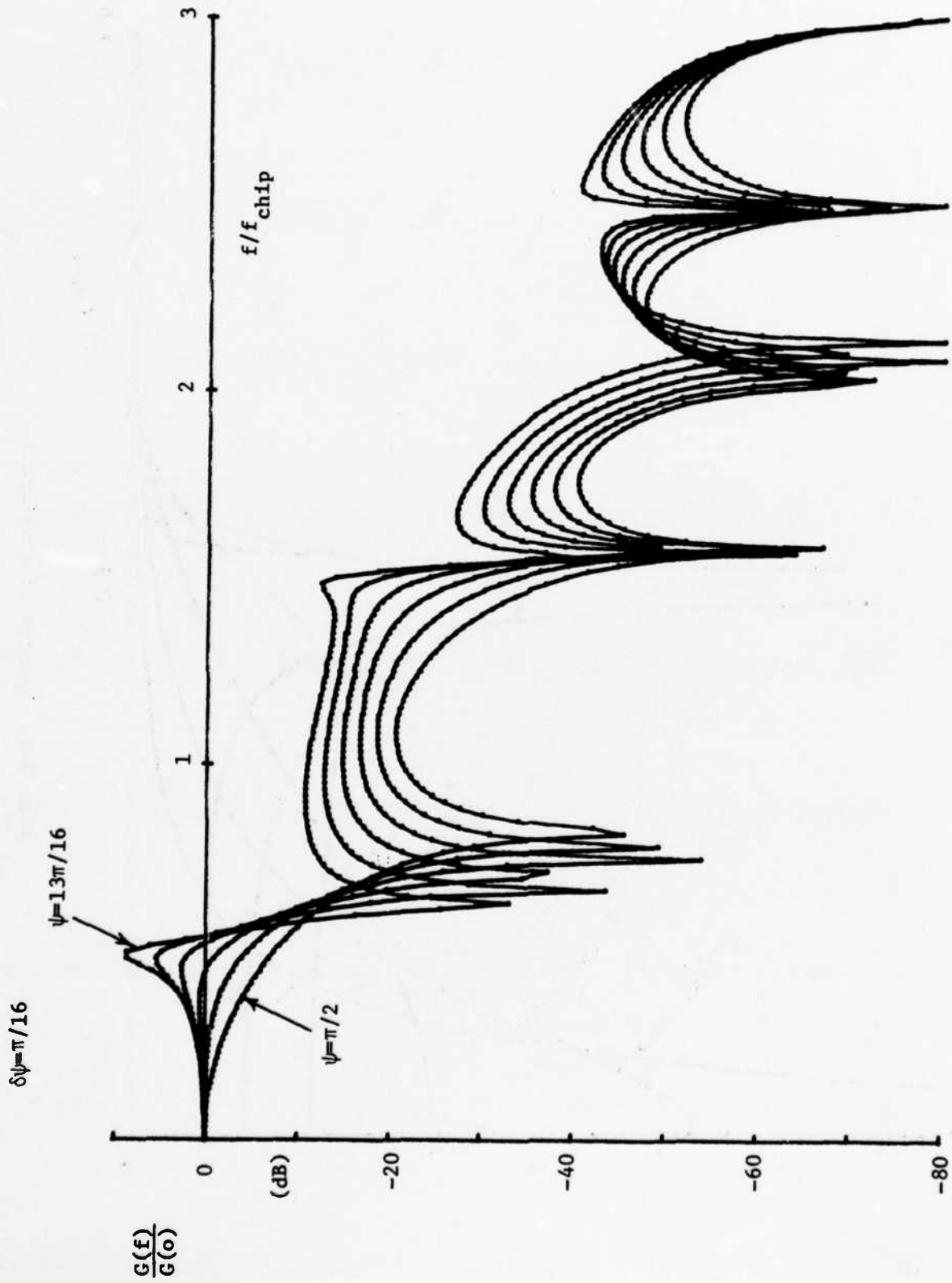


Fig. V-9. Relative spectra of waveform A₂

TR-596(V-9)

TR-596(V-10)

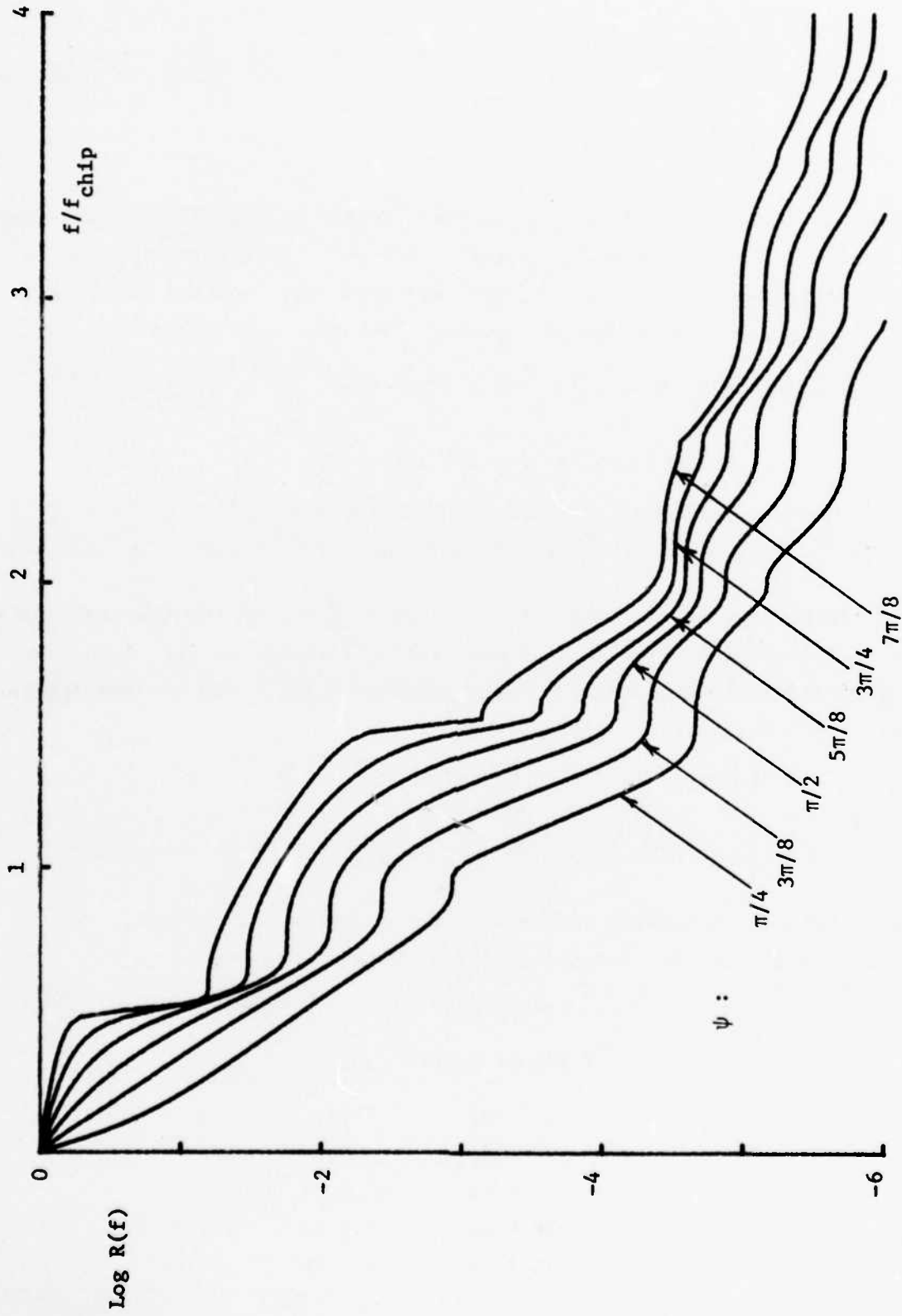


Fig. V-10. Cumulative spectra of waveform A₂

$$\dot{\phi}(t) = \begin{cases} (4\psi/\Delta)(t/\Delta) & ; \quad 0 < t < \Delta/2 \\ (4\psi/\Delta) \left(1 - \frac{t}{\Delta}\right) & ; \quad \Delta/2 < t < \Delta \end{cases} .$$

This function has a triangular shape, instead of the half sinusoid of waveform A_2 , and features a discontinuous derivative at $t=\Delta/2$. This discontinuity is of the same order as those at $t=0$ and $t=\Delta$, and therefore does not alter the expected character of the asymptotic spectra. The phase variation is

$$\phi(t) = \begin{cases} 2\psi(t/\Delta)^2 & ; \quad 0 < t < \Delta/2 \\ \psi[1-2(1-t/\Delta)^2] & ; \quad \Delta/2 < t < \Delta \end{cases} ,$$

and the spectra are presented in the same three forms as before in Figs. V-11, V-12 and V-13. These latter are closely comparable to the plots for waveform A_2 .

The normalized frequency modulation patterns, $\frac{\Delta}{\psi} \dot{\phi}$, of the four spreading modulations discussed in this section are plotted together in Fig. V-14, and the corresponding pulse functions are illustrated in Fig. V-15 for the special case $\psi=\pi/2$. In this latter case, we have

$$P(t) = \begin{cases} \cos[\phi(|t|)] & ; \quad |t| < \Delta \\ 0 & ; \quad \text{otherwise,} \end{cases}$$

which is direct generalization of the well-known expression for MSK.

The four waveforms are further compared in the Table V-1.

TABLE V-1
SIDELOBE LEVELS

Waveform	n	SL ($\pi/2$)	SL(ψ)	ψ
FSK	1	-23.0 dB	-18.2 dB	$5\pi/8$
A_2	2	-20.6 dB	-17.6 dB	$19\pi/32$
B_2	2	-20.0 dB	-17.2 dB	$19\pi/32$
SFSK	3	-18.7 dB	-16.3 dB	$37\pi/64$

TR-596(V-11)

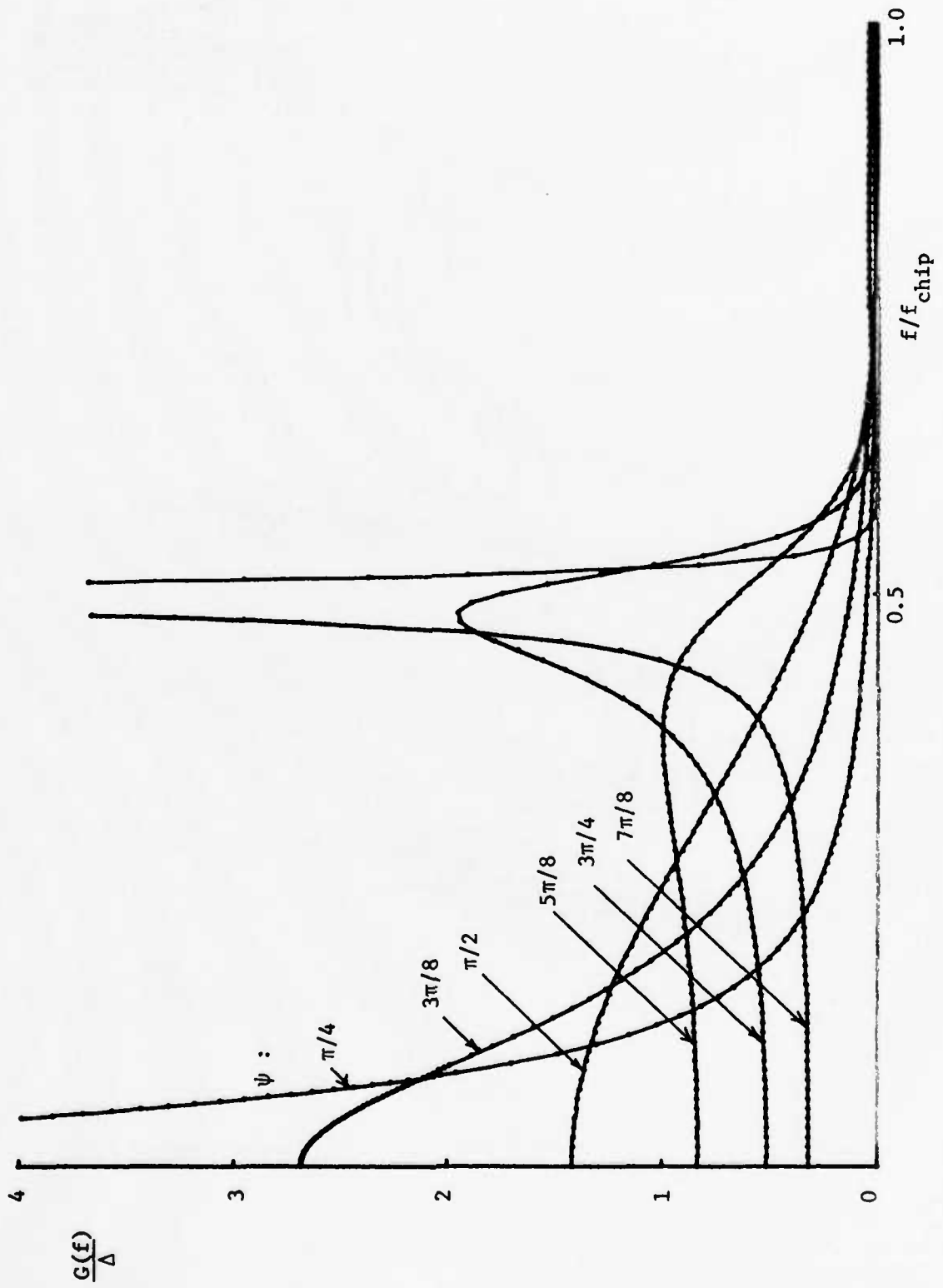


Fig. V-11. Spectra of waveform B₂

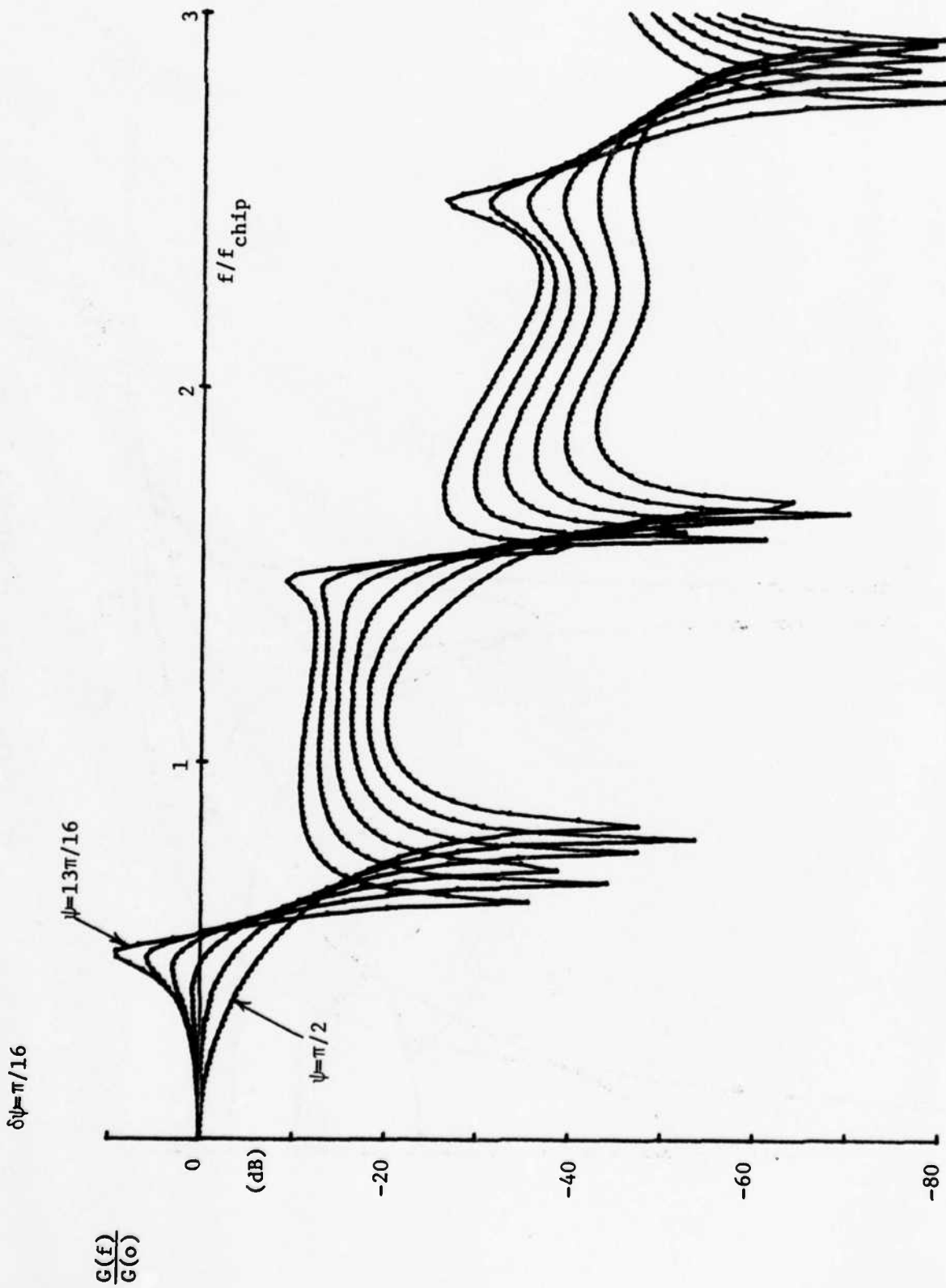


Fig. V-12. Relative spectra of waveform B₂

TR-596(V-13)

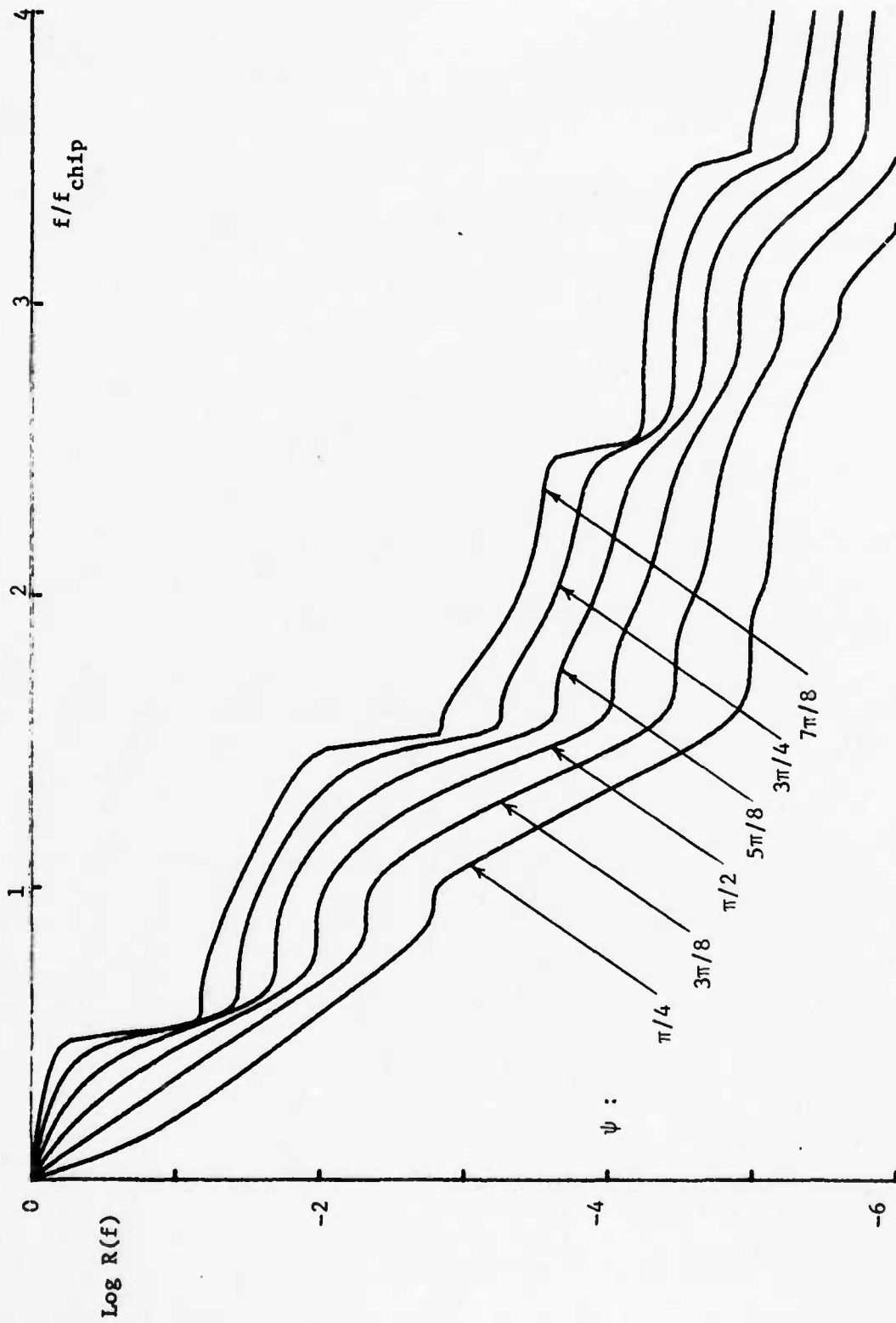


Fig. V-13. Cumulative spectra of waveform B₂

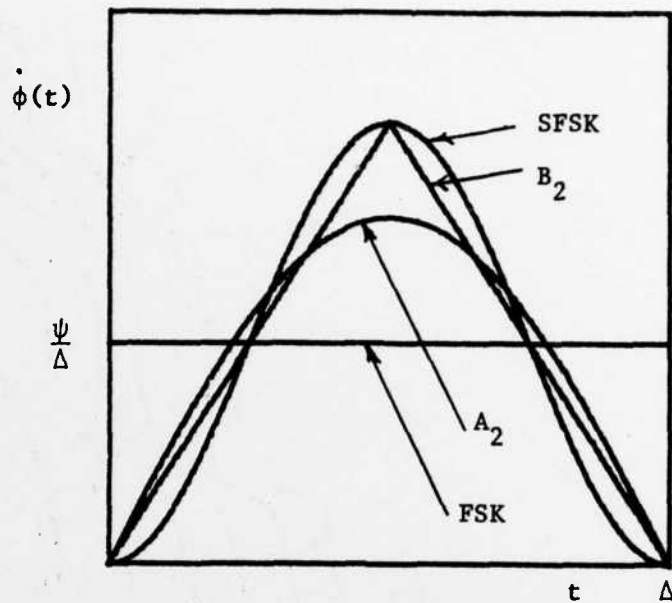


Fig. V-14. Frequency modulation patterns

TR-596(V-14)

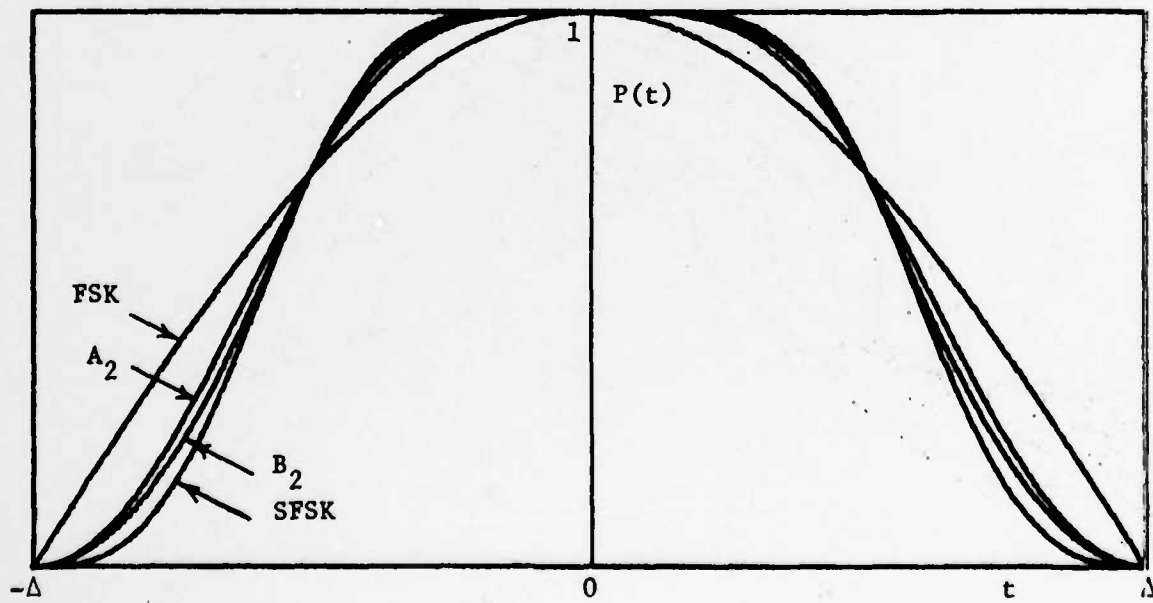


Fig. V-15. Pulse functions

TR-596(V-15)

The column $SL(\pi/2)$ gives the magnitude of the first sidelobe of each waveform for the choice $\psi=\pi/2$. The column $SL(\psi)$ gives that sidelobe level for a value of ψ which might be chosen to optimize the mainlobe spectral flatness, and the corresponding value of ψ (essentially an eyeball choice) is shown in the last column. First sidelobe levels are plotted as functions of ψ in Fig. V-16.

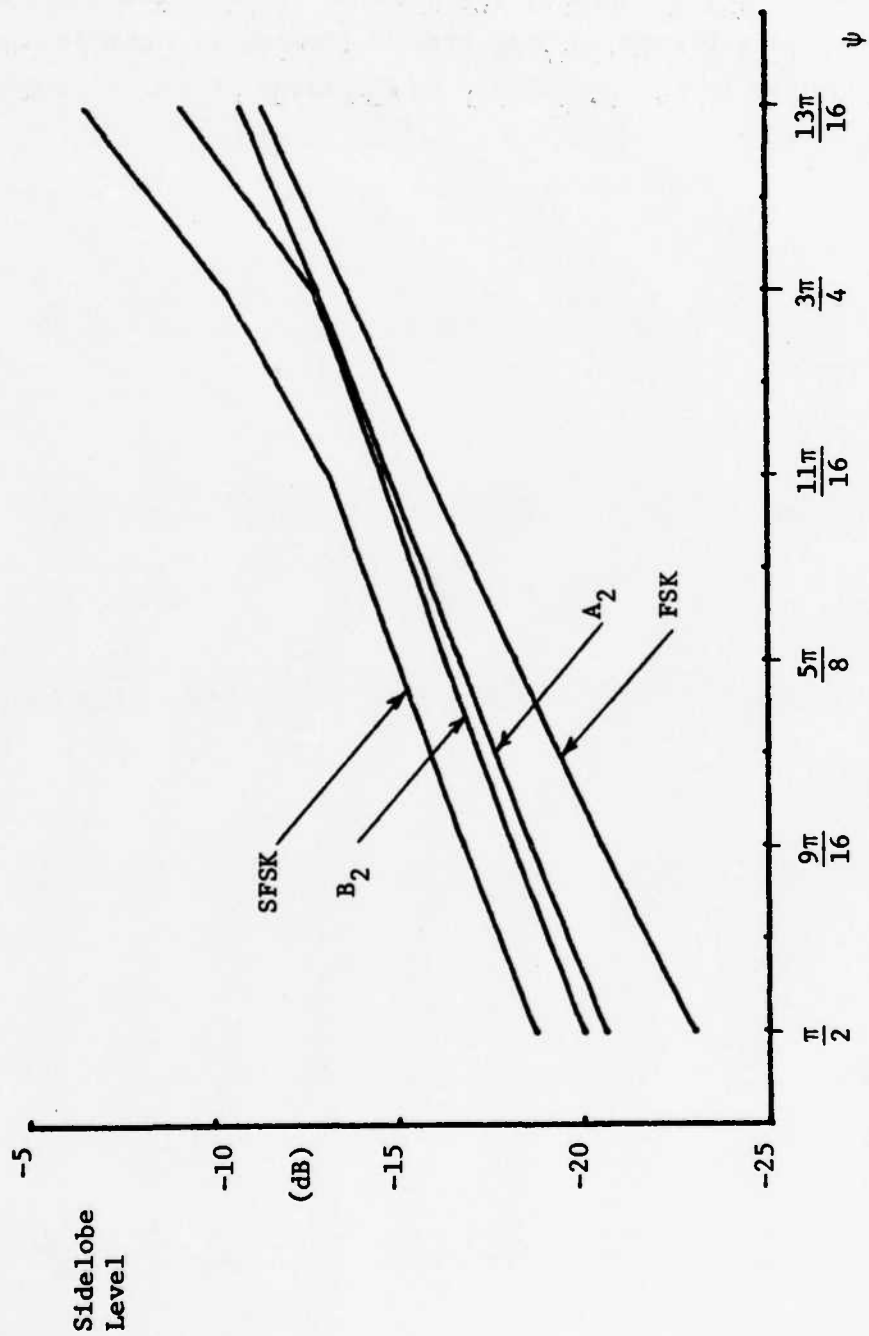


Fig. V-16. First sidelobe levels

TR-596(V-16)

VI. POLYNOMIAL FM WAVEFORMS

It is apparent from the spectra of the waveforms studied in Section V that the parameters ψ and n have a major influence on spectral properties and that waveforms such as A_2 and B_2 , with the same n -value, have very similar spectra for equal values of ψ . In order to study the effects of these parameters systematically, a special set of waveforms has been devised, with one member for each value of n . The other parameter, ψ , is simply a scale factor for the characteristic frequency modulation pattern, as usual.

To control the smoothness of $\phi(t)$ in a convenient way, we make use of simple polynomials, and postulate the general form

$$\dot{\phi}_n(t) \equiv \frac{\psi}{\Delta} K_n (t/\Delta)^{n-1} \left(1 - \frac{t}{\Delta}\right)^{n-1}.$$

The phase function itself will be proportional to t^n near $t=0$, with an analogous behavior near $t=\Delta$, hence the first phase derivative which fails to vanish at these points is the n^{th} . Thus the subscript correctly corresponds to the value of the index parameter itself. The frequency modulation patterns are symmetric about $t=\Delta/2$, and hence the pulse functions will be symmetric functions of t . These waveforms are not the same as the polynomial modulations discussed by Simon⁽⁵⁾.

The phase variations are obtained by integration:

$$\begin{aligned} \phi_n(t) &= \frac{\psi}{\Delta} K_n \int_0^t (t'/\Delta)^{n-1} \left(1 - \frac{t'}{\Delta}\right)^{n-1} dt' \\ &= \psi K_n \int_0^{t/\Delta} x^{n-1} (1-x)^{n-1} dx. \end{aligned}$$

Since $\phi_n(\Delta)$ must equal ψ , the constants K_n are determined by the requirement

$$1 = K_n \int_0^1 x^{n-1} (1-x)^{n-1} dx$$

$$= \frac{1}{2} K_n \int_{-1}^1 \left(\frac{1-u^2}{4} \right)^{n-1} du$$

$$= \frac{K_n}{4^{n-1}} \int_0^{\pi/2} (\cos\theta)^{2n-1} d\theta .$$

This is a known integral, and we find

$$K_n = \frac{(2n-1)!}{[(n-1)!]^2} = n \binom{2n-1}{n-1} .$$

It should be noted that for $n=1$, the waveform is simply FSK.

We call these waveforms "polynomial FM" waveforms, and denote them by the symbol PFM_n . The normalized frequency modulation patterns for the first five waveforms are compared in Fig. VI-1. In Fig. VI-2 we compare these patterns for PFM_2 , A_2 and B_2 , while Fig. VI-3 compares PFM_3 with SFSK. From the similarity of those frequency modulation patterns sharing a common value of n , we infer that our waveforms will provide a representative set, covering the entire class of binary FM spreading modulations.

The computation of spectra by numerical integration is facilitated by a change of variable which takes advantage of the symmetry properties of the $\dot{\phi}_n(t)$. For any frequency modulation pattern symmetric about $t=\Delta/2$, we will have the corresponding property

$$\phi(\Delta-t) = \psi - \phi(t),$$

and the pulse function will be even in t . From this last fact, we can write, as before,

$$k(\omega) = \frac{2}{\Delta} \int_0^{\Delta} P(t) \cos \omega t dt ,$$

or

$$\sin \psi k(\omega) = \frac{2}{\Delta} \int_0^{\Delta} \sin[\psi - \phi(t)] \cos \omega t dt$$

TR-596(VI-1)

TR-596(VI-2)

TR-596(VI-3)

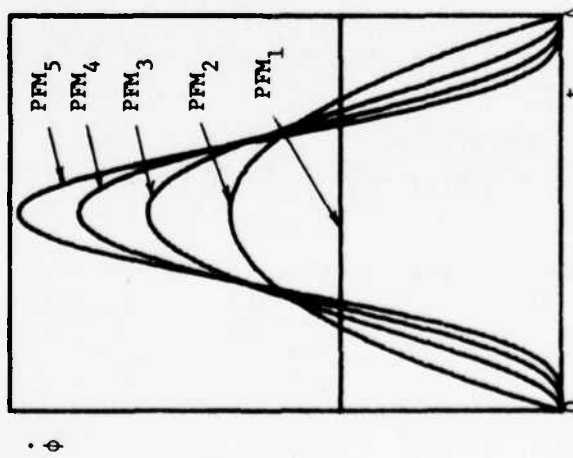


Fig. VI-1

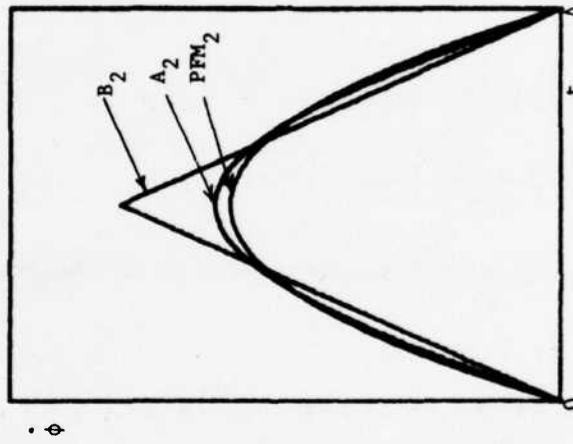


Fig. VI-2

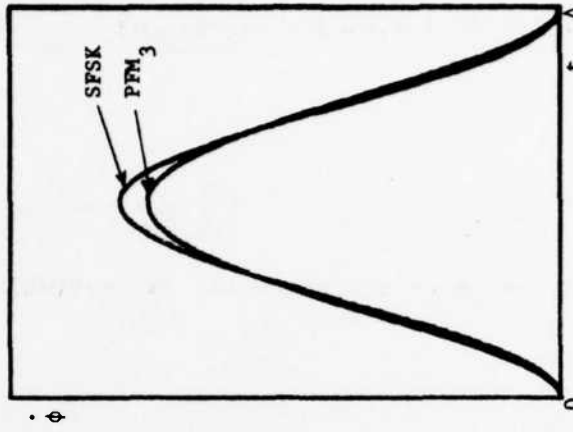


Fig. VI-3

Figs. VI-1, -2 & -3. Frequency modulation patterns

$$= \frac{1}{\Delta} \int_0^{\Delta} \{ \sin[\psi - \phi(t) + \omega t] + \sin[\psi - \phi(t) - \omega t] \} dt .$$

Now

$$\phi\left(\frac{\Delta}{2} + x\right) - \frac{\psi}{2}$$

is an odd function of x , hence we introduce the new variable, u , by means of

$$t = \frac{\Delta}{2} (1+u) ,$$

or

$$u = \frac{2t}{\Delta} - 1 .$$

This variable ranges from -1 to $+1$, and we can put

$$\phi(t) = \phi\left(\frac{\Delta}{2} + \frac{\Delta u}{2}\right) \equiv \frac{\psi}{2} [1 + h(u)] .$$

The new function, $h(u)$, is an odd function of u with the boundary values

$$h(0) = 0 , h(1) = 1 ,$$

and it describes the phase variation over half a chip in a normalized form.

In terms of the new variable, u :

$$\begin{aligned} \sin \psi k(\omega) &= \frac{1}{2} \int_{-1}^{1} \{ \sin\left[\frac{\psi}{2} - \frac{\psi}{2} h(u) + \frac{\omega \Delta}{2} + \frac{\omega \Delta u}{2}\right] \\ &+ \sin\left[\frac{\psi}{2} - \frac{\psi}{2} h(u) - \frac{\omega \Delta}{2} - \frac{\omega \Delta u}{2}\right] \} du . \end{aligned}$$

We now separate into even and odd functions of u :

$$\sin\left[\frac{\psi}{2} + \frac{\omega \Delta}{2} - \frac{\psi}{2} h(u) + \frac{\omega \Delta u}{2}\right]$$

$$\begin{aligned}
&= \sin\left(\frac{\psi+\omega\Delta}{2}\right) \cos\left[\frac{\psi h(u) - \omega\Delta u}{2}\right] \\
&\quad - \cos\left(\frac{\psi+\omega\Delta}{2}\right) \sin\left[\frac{\psi h(u) - \omega\Delta u}{2}\right] ,
\end{aligned}$$

and

$$\begin{aligned}
&\sin\left[\frac{\psi}{2} - \frac{\omega\Delta}{2} - \frac{\psi}{2} h(u) - \frac{\omega\Delta u}{2}\right] \\
&= \sin\left(\frac{\psi-\omega\Delta}{2}\right) \cos\left[\frac{\psi h(u) + \omega\Delta u}{2}\right] \\
&\quad - \cos\left(\frac{\psi-\omega\Delta}{2}\right) \sin\left[\frac{\psi h(u) + \omega\Delta u}{2}\right] .
\end{aligned}$$

The odd terms vanish upon integration, and we obtain the desired result:

$$\begin{aligned}
\sin\psi k(\omega) &= \sin\left(\frac{\psi-\omega\Delta}{2}\right) \int_0^1 \cos\left[\frac{\psi h(u) + \omega\Delta u}{2}\right] du \\
&\quad + \sin\left(\frac{\psi+\omega\Delta}{2}\right) \int_0^1 \cos\left[\frac{\psi h(u) - \omega\Delta u}{2}\right] du .
\end{aligned}$$

In terms of $\theta = \omega\Delta$ and the dimensionless spectral density, $g(\theta)$, we have

$$g(\theta) = \frac{\left[\sin\left(\frac{\psi-\theta}{2}\right) f_+(\theta) + \sin\left(\frac{\psi+\theta}{2}\right) f_-(\theta)\right]^2}{1 + \cos^2\psi - 2\cos\psi \cos\theta} ,$$

where

$$f_{\pm}(\theta) \equiv \int_0^1 \cos\left[\frac{\psi h(u) \pm \theta u}{2}\right] du .$$

These last integrals are easily computed numerically, and as few as 16 points yields adequate accuracy for most purposes.

To find $h(u)$ for a given waveform, it is simplest to begin with its derivative, $h'(u)$, which satisfies

$$\dot{\phi}(t) = \frac{\psi}{2} h'(u) \frac{du}{dt} = \frac{\psi}{\Delta} h'(u) .$$

For the PFM waveforms, we write $h'_n(u)$ for the function corresponding to $\dot{\phi}_n(t)$. Since

$$\frac{t}{\Delta} = \frac{1+u}{2} ,$$

we have

$$K_n \left(\frac{1+u}{2}\right)^{n-1} \left(\frac{1-u}{2}\right)^{n-1} = h'_n(u)$$

or

$$h'_n(u) = \frac{K_n}{4^{n-1}} (1-u^2)^{n-1} .$$

The corresponding phase function is

$$h_n(u) = \frac{K_n}{4^{n-1}} \sum_{\ell=0}^{n-1} \binom{n-1}{\ell} (-1)^\ell \int_0^u v^{2\ell} dv$$

or

$$h_n(u) = \frac{K_n}{4^{n-1}} u \sum_{\ell=0}^{n-1} \binom{n-1}{\ell} \frac{(-u^2)^\ell}{2\ell+1} .$$

It can be shown that $h_n(1)=1$, as required, and the first five polynomials are listed here for reference:

$$h_1(u) = u$$

$$h_2(u) = \frac{u}{2} (3 - u^2)$$

$$h_3(u) = \frac{u}{8} (15 - 10u^2 + 3u^4)$$

$$h_4(u) = \frac{u}{16} (35 - 35u^2 + 21u^4 - 5u^6)$$

$$h_5(u) = \frac{u}{128} (315 - 420u^2 + 378u^4 - 180u^6 + 35u^8) .$$

For comparison, the h-functions corresponding to the other waveforms studied in Section V are as follows:

$$\text{Waveform } A_2 : h(u) = \sin\left(\frac{\pi u}{2}\right)$$

$$\text{Waveform } B_2 : h(u) = u(2 - |u|)$$

$$\text{SFSK} : h(u) = u + \frac{1}{\pi} \sin(\pi u) .$$

The PFM waveforms exhibit the same kind of spectral behavior that we have seen in FSK and the other examples of Section V. For very small values of ψ , all the spectra become narrow lines at band center ($f=0$), and as ψ approaches the value π , in all cases spectral lines appear at $\omega\Delta = \pm\pi$ (i.e., $f = \pm f_{\text{chip}}/2$). The interesting region lies between these bounds and in the plotted spectra, ψ is confined to a range of values between $\pi/2$ and $11\pi/16$.

The plots in Figs. VI-4 through VI-13 show spectra for waveforms PFM₁ (FSK) through PFM₅. The FSK spectra are included again for comparison. For each waveform, linear plots out to $f=f_{\text{chip}}$ and relative spectra (in dB) out to $f=2f_{\text{chip}}$ are given. In each case, ψ ranges in increments of $\pi/32$ from the value $\pi/2$ through $11\pi/16$. The first sidelobe levels are shown, as functions of ψ , in Fig. VI-14.

The concept of spreading efficiency is discussed in Appendix A as a measure of the processing gain attainable against an optimizing noise jammer, compared to the nominal time-bandwidth product available to the system. It is shown

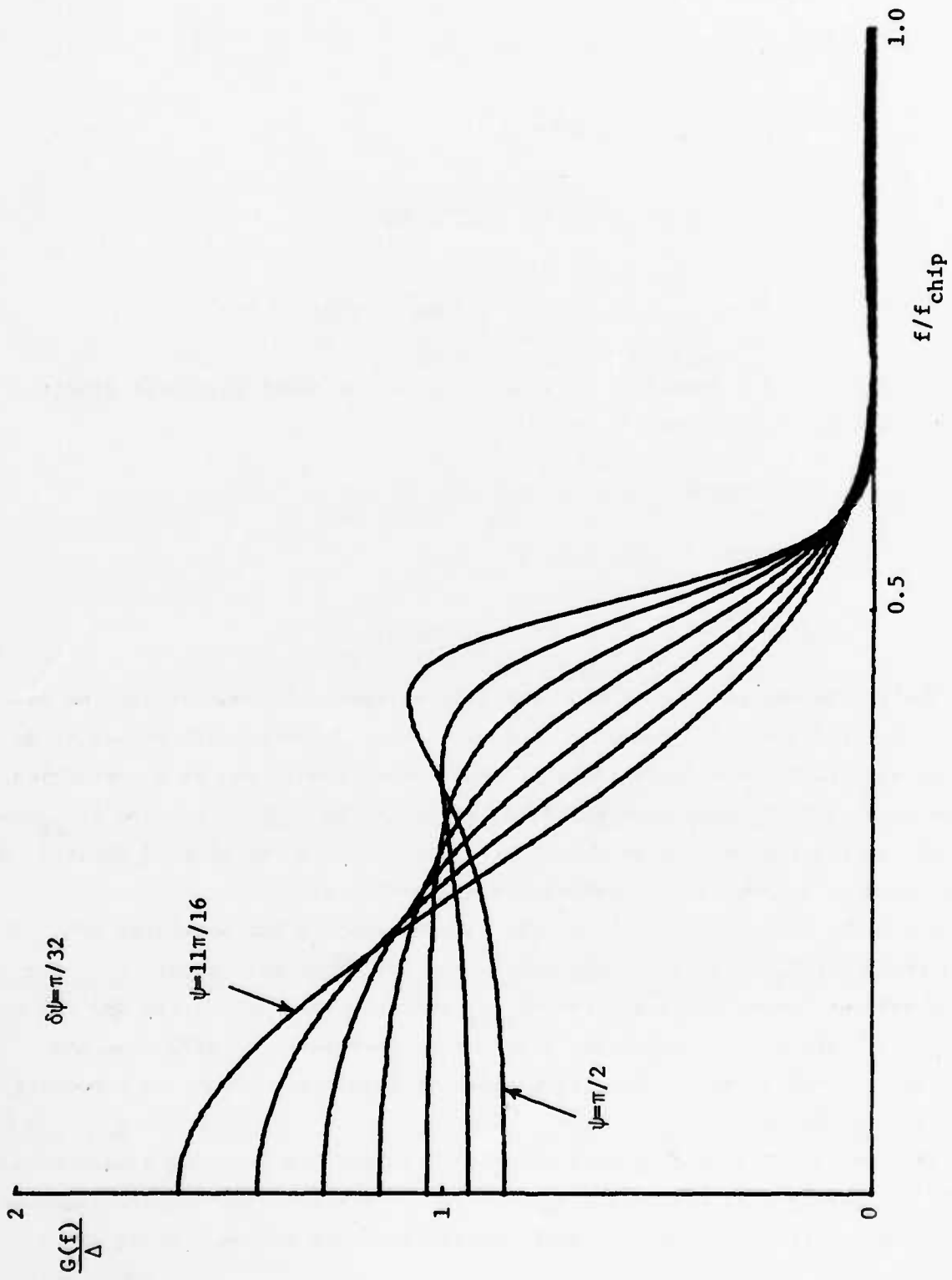


Fig. VI-4. PFM₁ (FSK) spectra

TN-596(VI-4)

TR-596(VI-5)

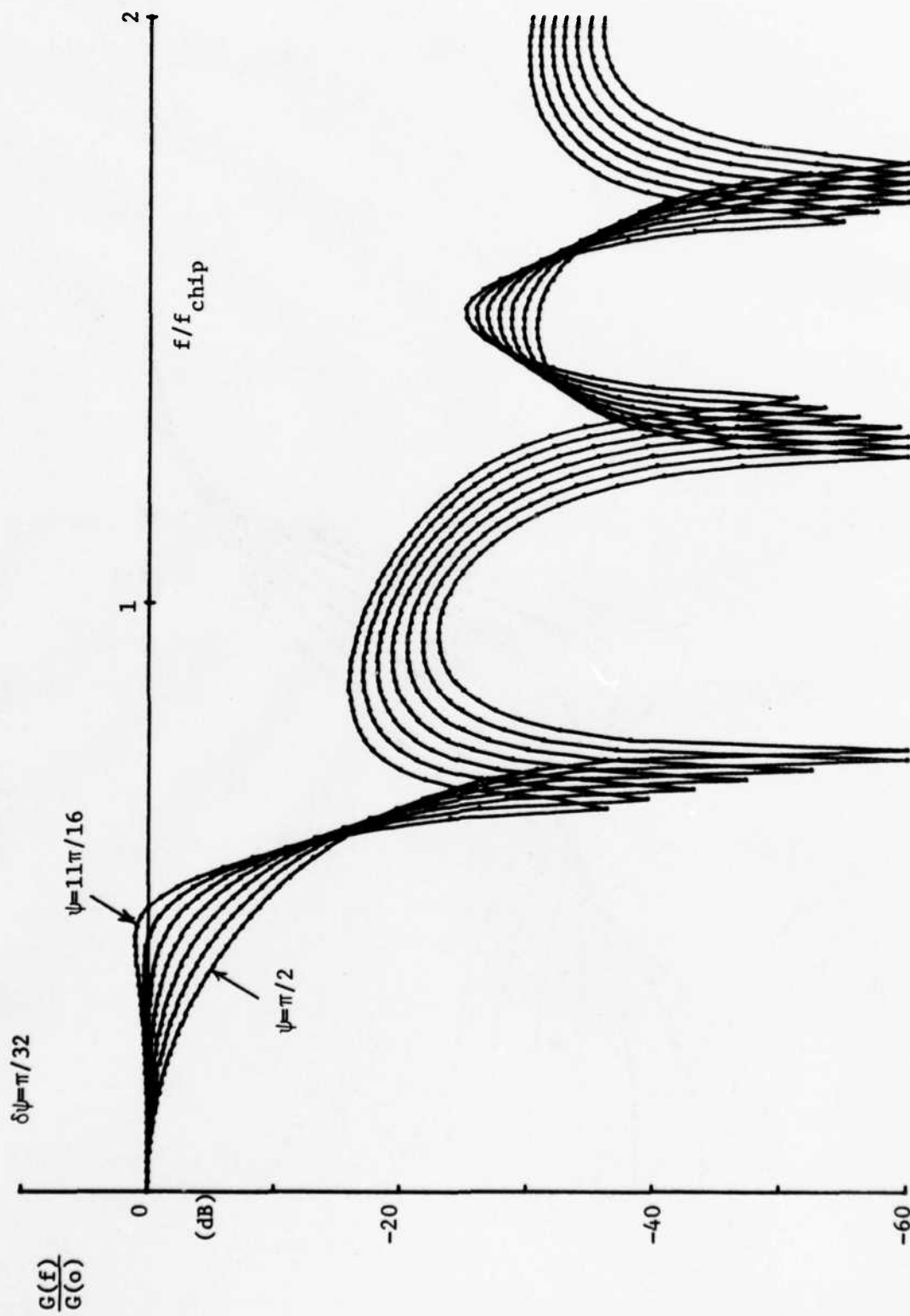


Fig. VI-5. Relative spectra of PFM₁ (FSK)

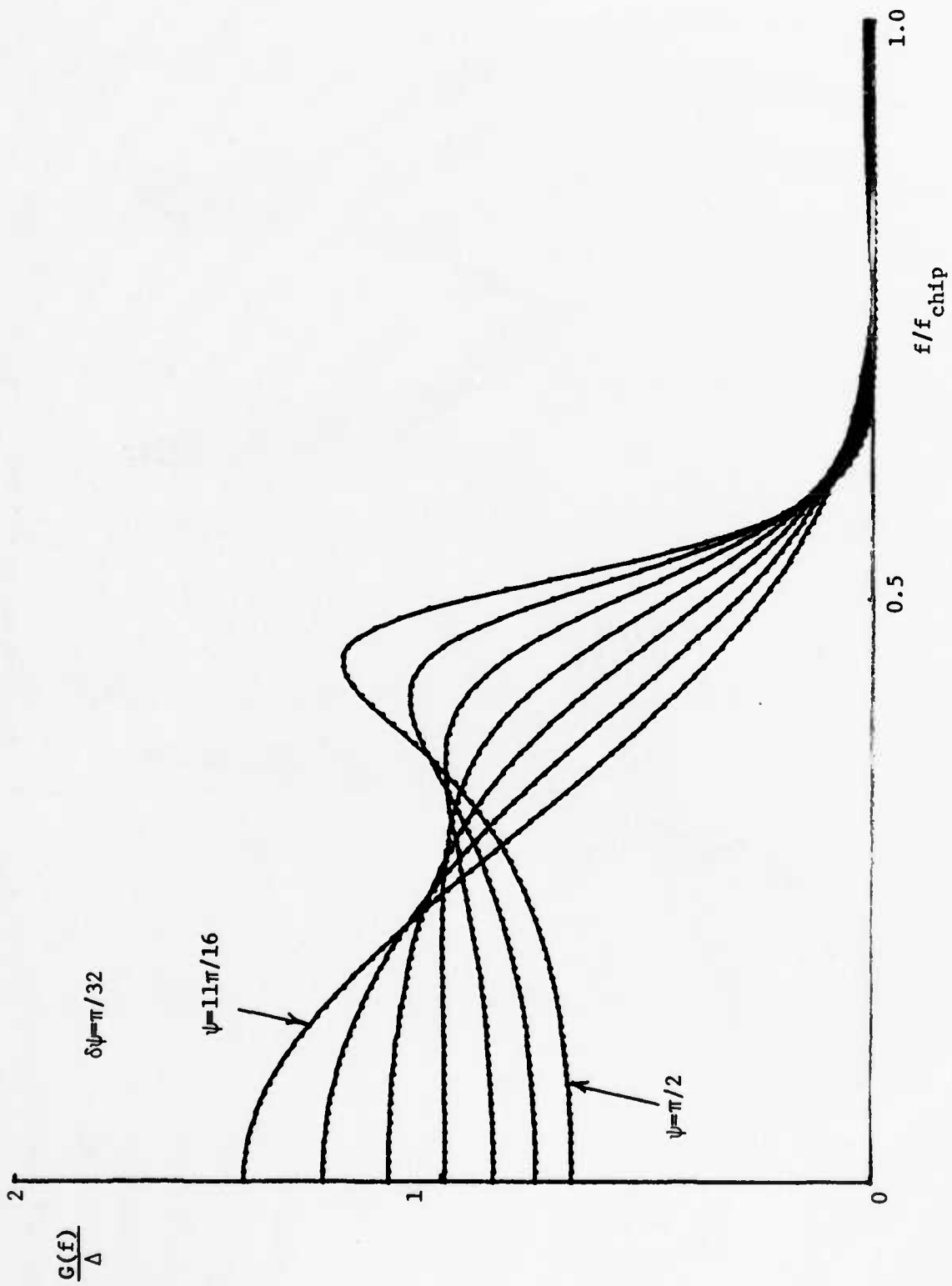


Fig. VI-6. PFM₂ spectra

TR-596(VI-6)

TR-596(VI-7)

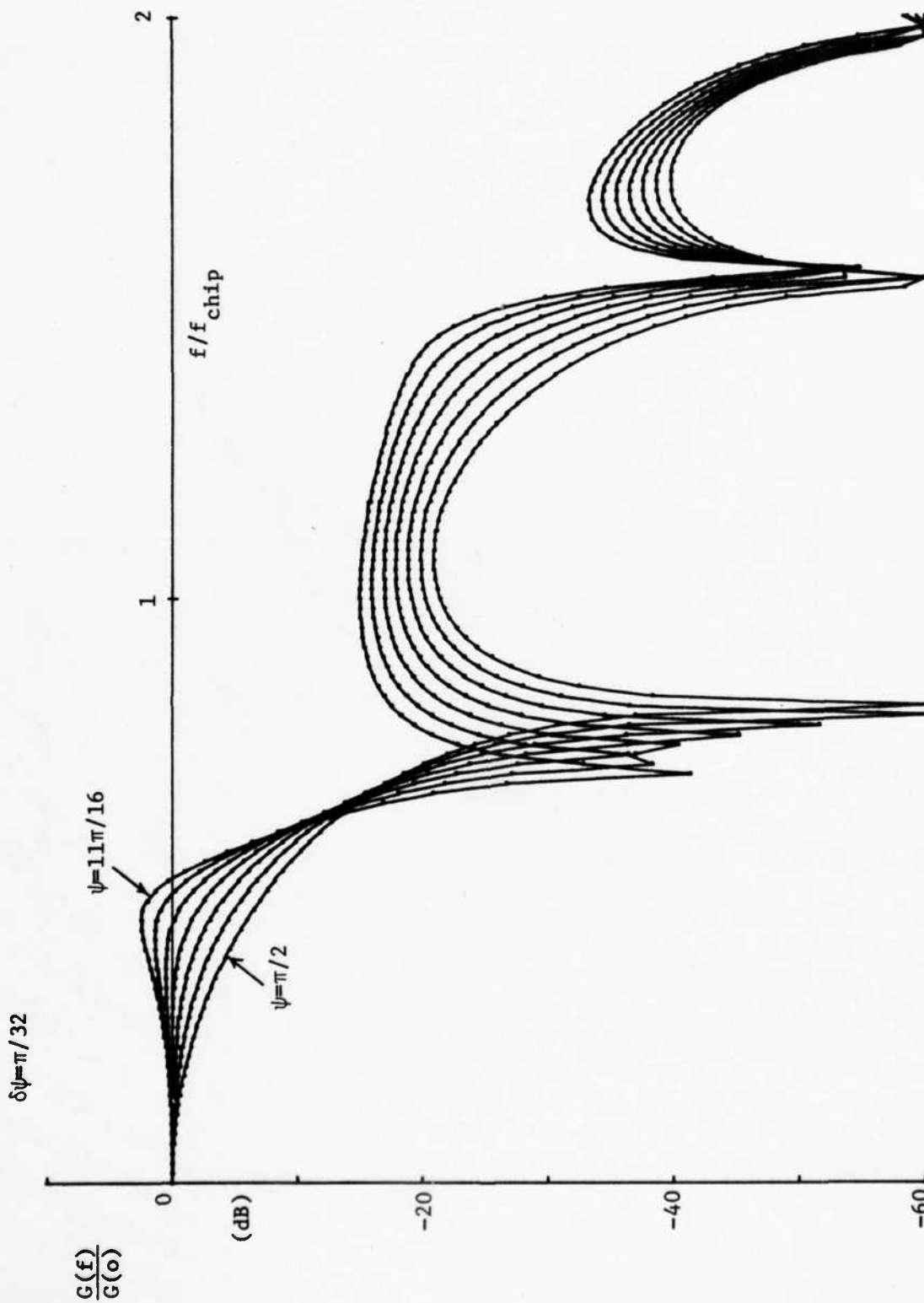


Fig. VI-7. Relative spectra of PFM₂

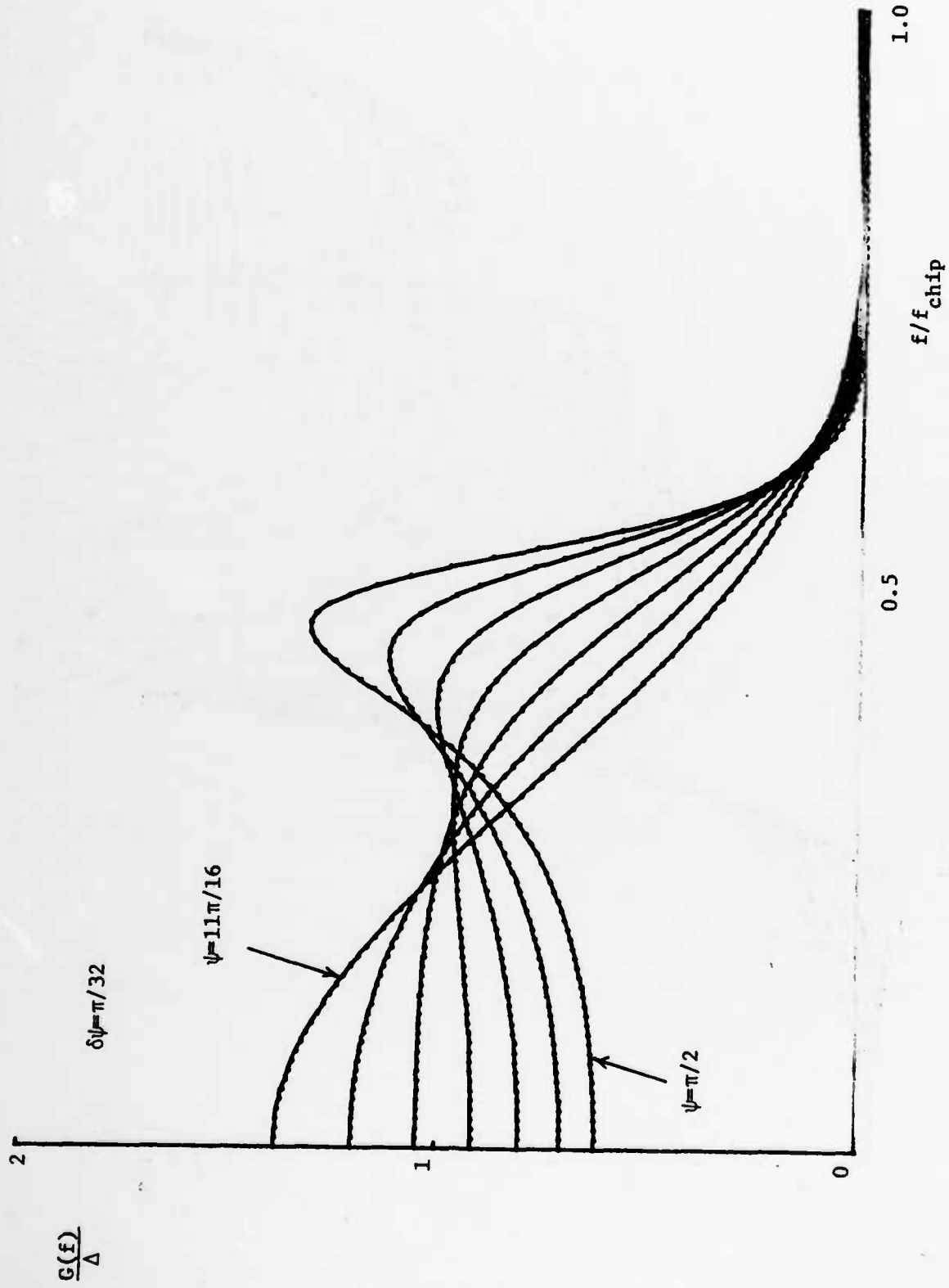


Fig. VI-8. PFM₃ spectra

TR-596(VI-8)

TR-596(VI-9)

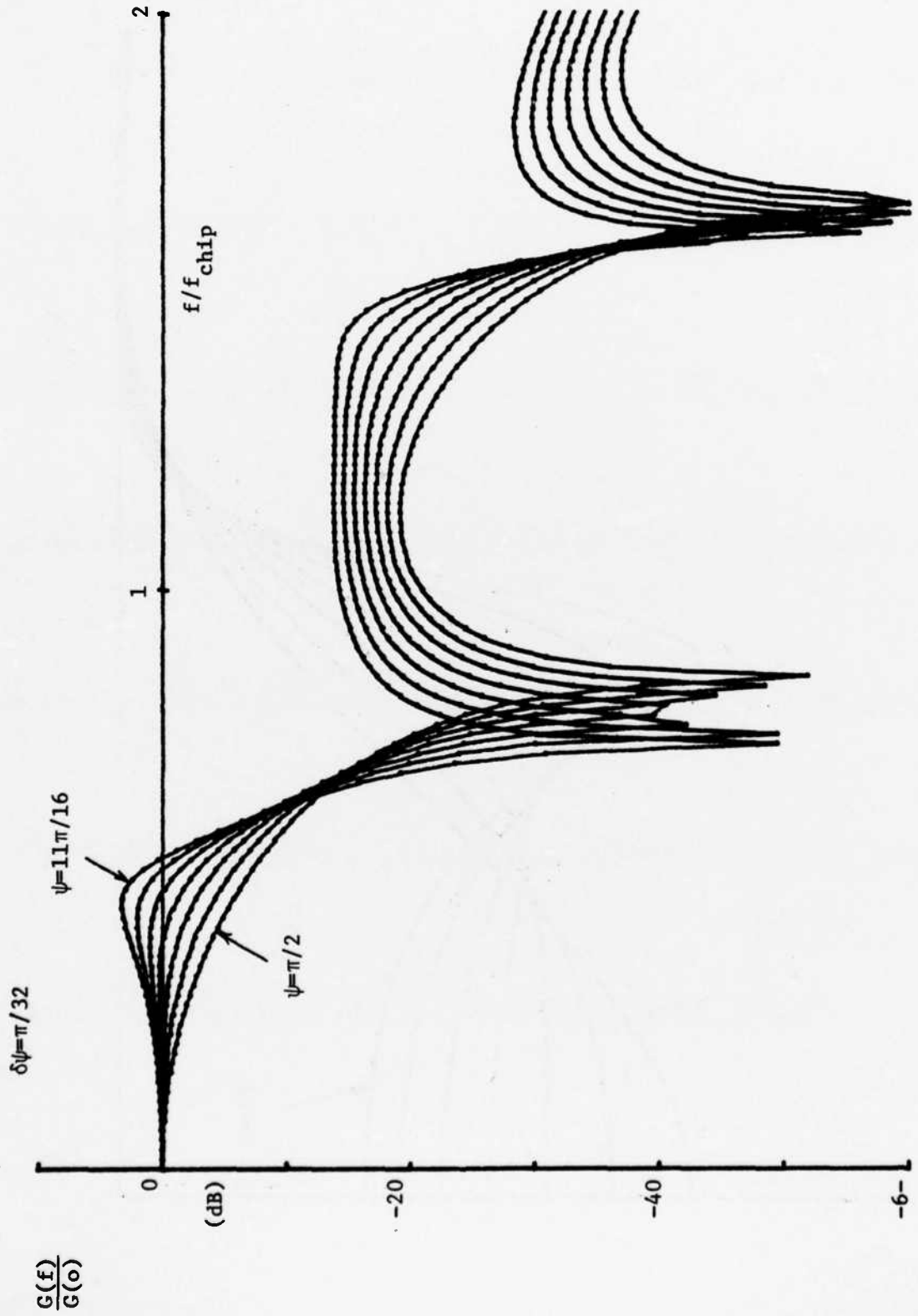


Fig. VI-9. Relative spectra of PFM₃

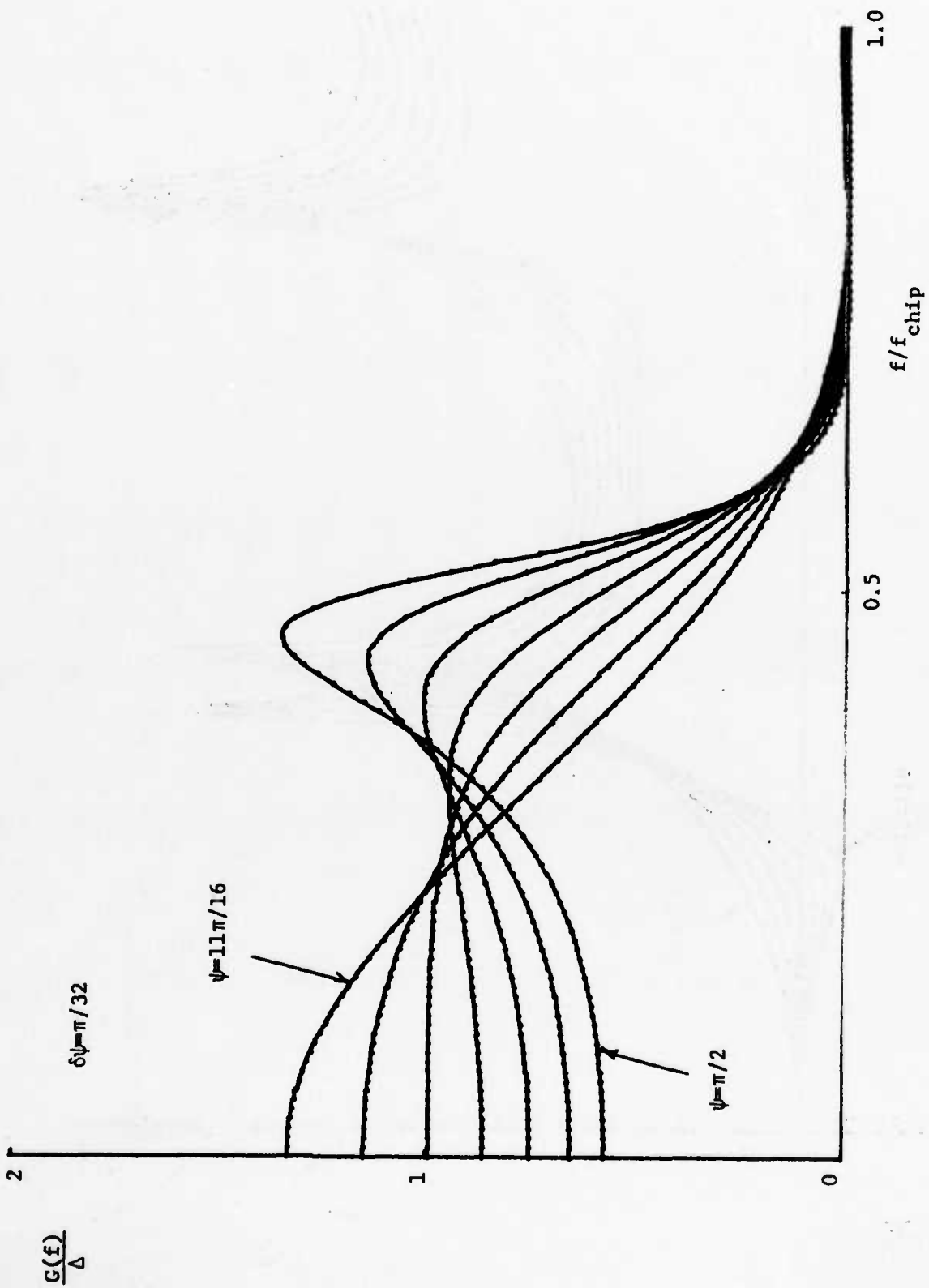


Fig. VI-10. PFM₄ spectra

TR-596(VI-11)

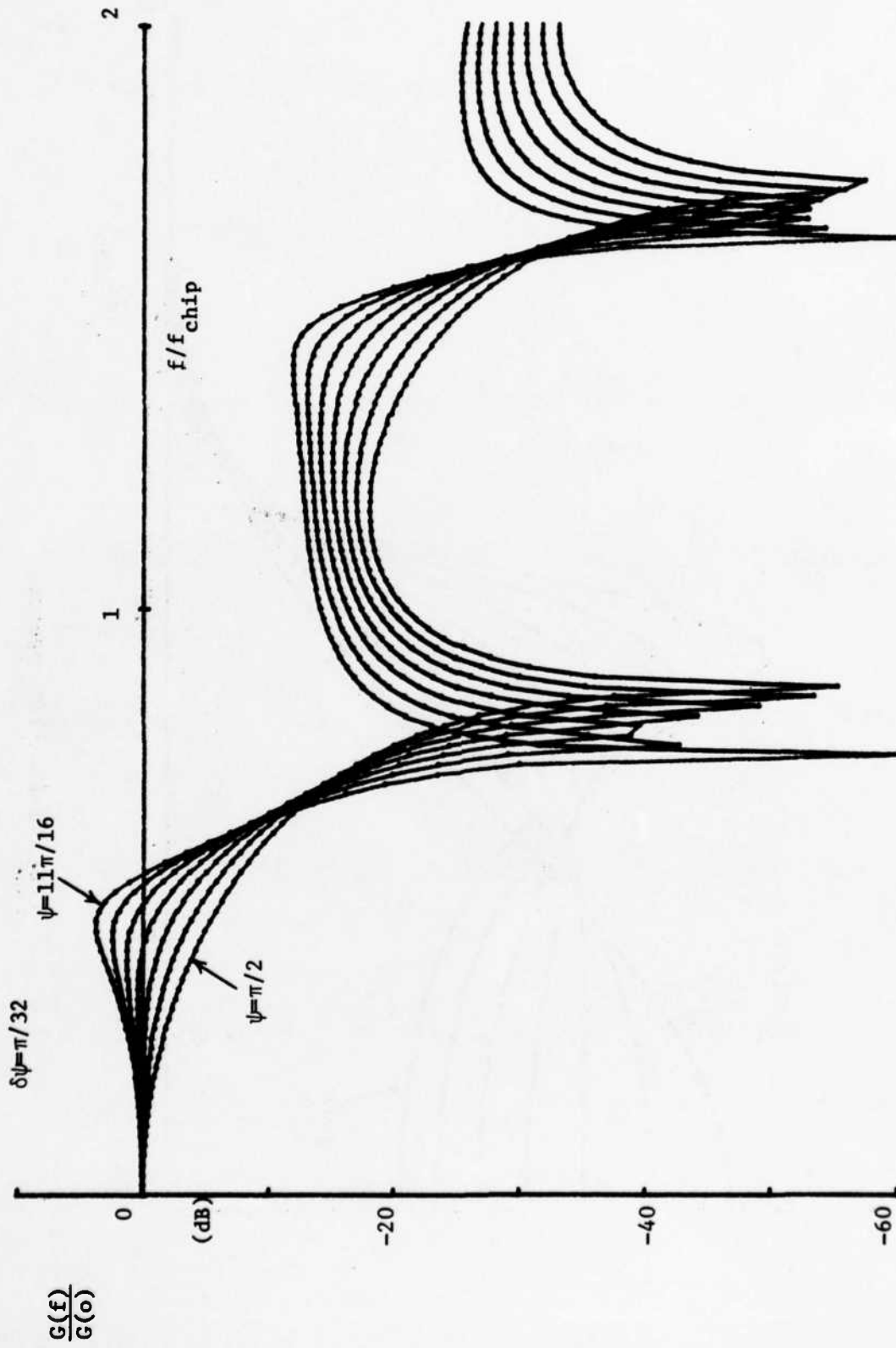


Fig. VI-11. Relative spectra of PFM₄

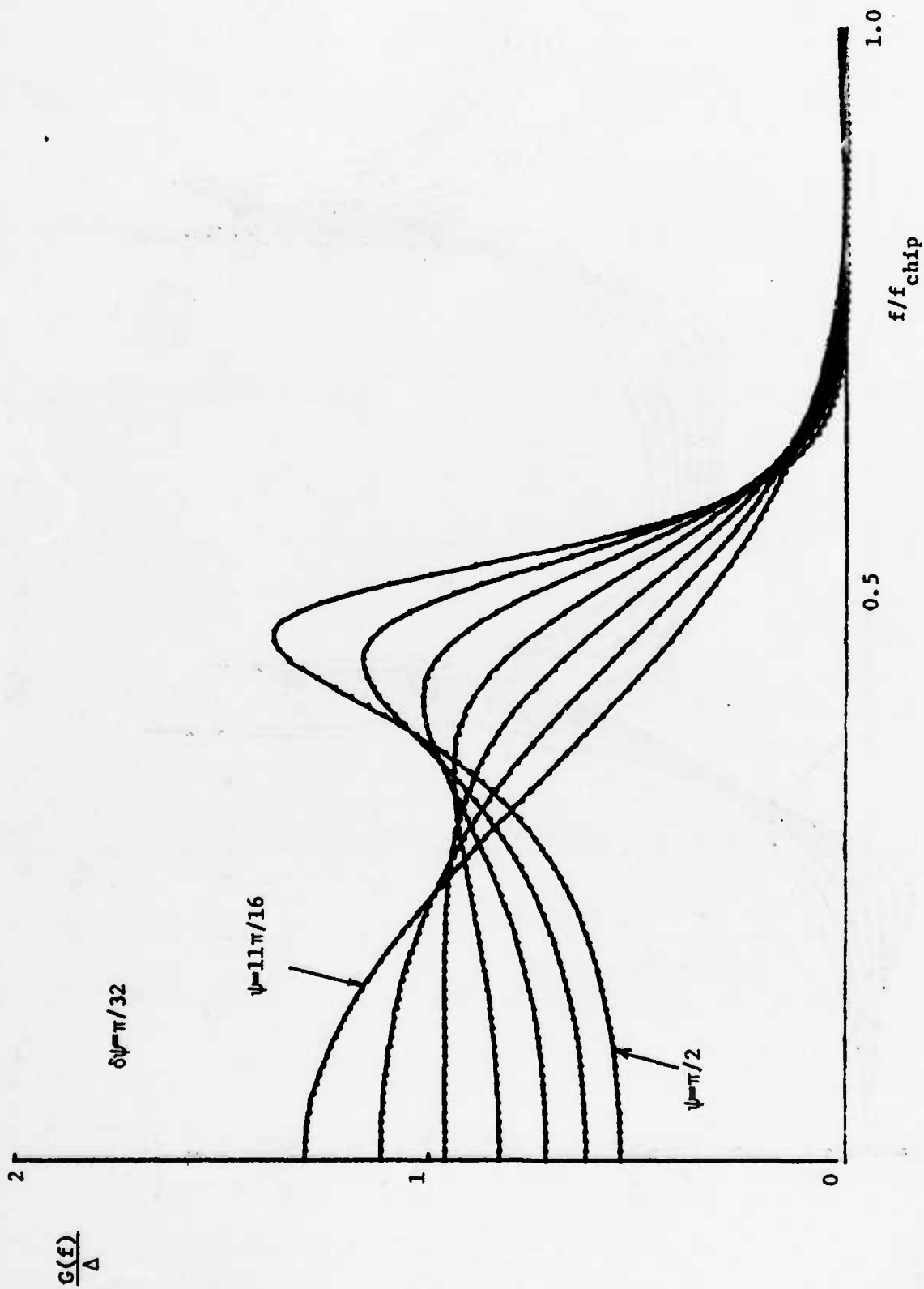


Fig. VI-12. PFM₅ spectra

TR-596(VI-12)

TR-596(VI-13)

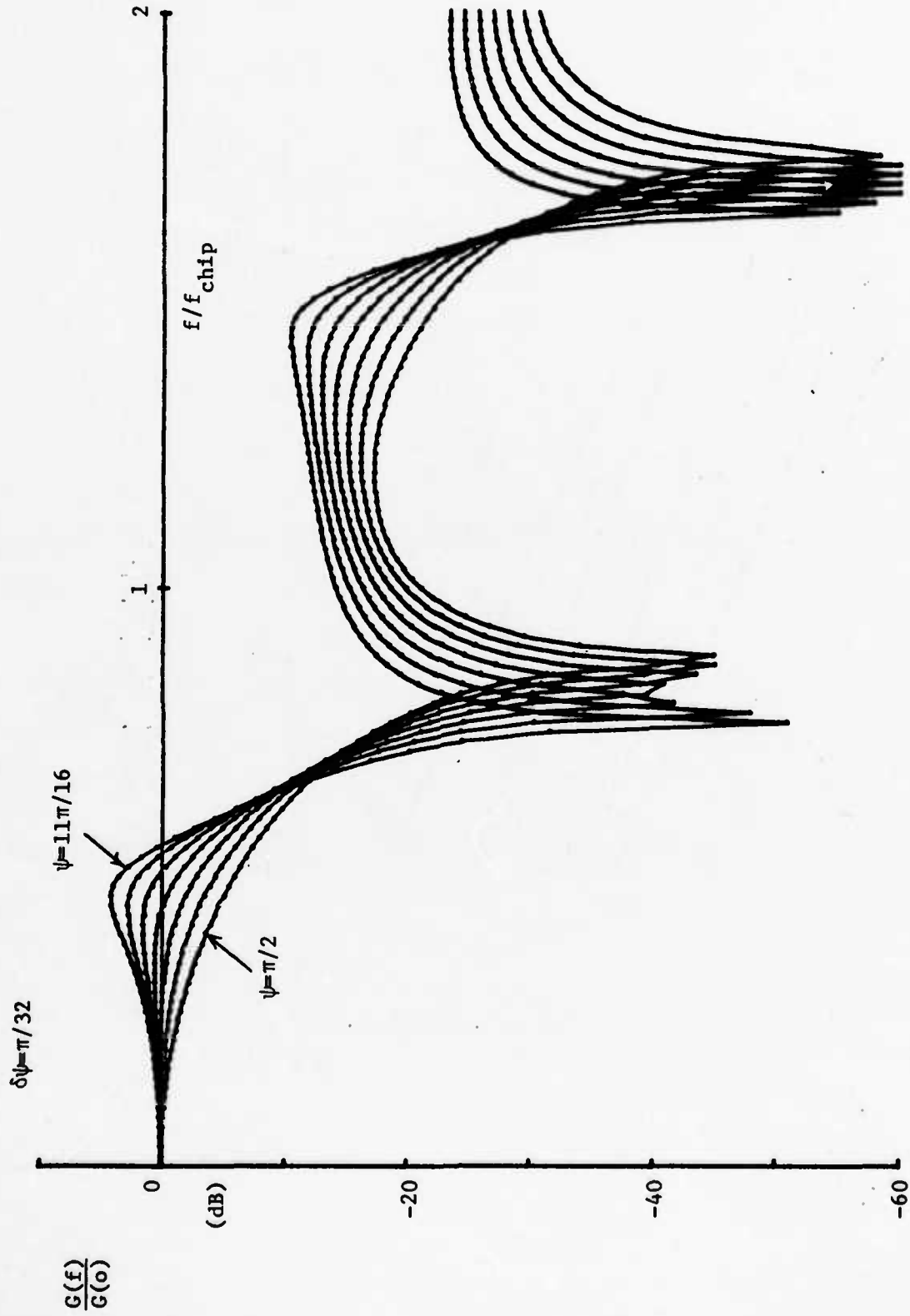


Fig. VI-13. Relative spectra of PFM₅

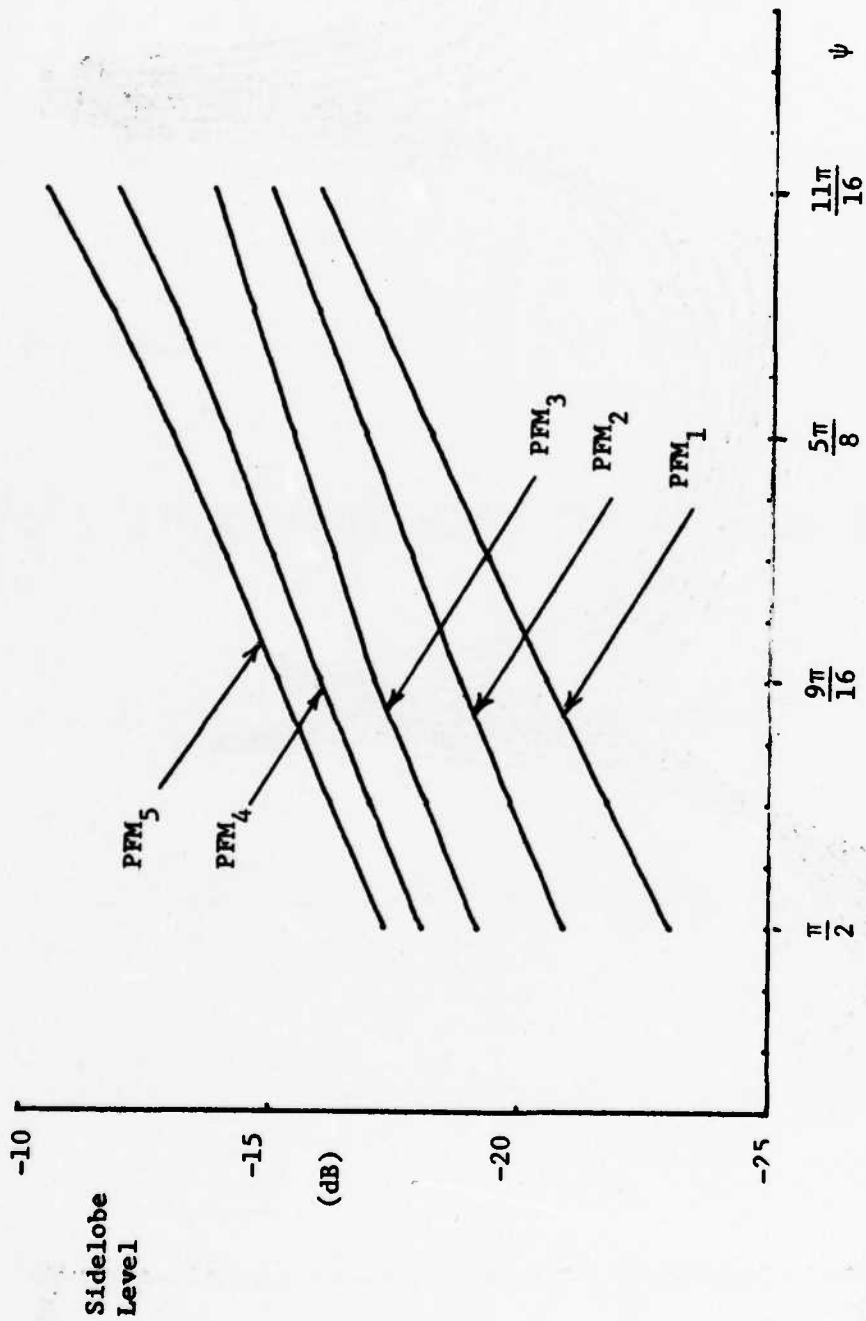


Fig. VI-14. PFM sidelobe levels versus ψ

TR-596(VI-14)

there that FSK waveforms exhibit a maximum in spreading efficiency for a particular value of ψ , and that this value corresponds closely to the "flattest" spectral density. The same behavior is shown by all the PFM waveforms, and for each of these a ψ -value has been chosen which identifies the flattest member of the set of spectra, as judged by eye.

First sidelobe levels are shown in the following table for each of the first five PFM waveforms, for two choices of ψ , namely $\pi/2$ and the value (also listed in the table) which was chosen for spectral flatness. This table may be compared directly with Table V-1.

TABLE VI-I
PFM SIDELOBE LEVELS

Waveform	SL($\pi/2$)	SL(ψ)	ψ
PFM ₁	-23.0 dB	-18.2 dB	$5\pi/8$
PFM ₂	-20.9 dB	-17.8 dB	$19\pi/32$
PFM ₃	-19.2 dB	-16.7 dB	$37\pi/64$
PFM ₄	-18.0 dB	-16.0 dB	$9\pi/16$
PFM ₅	-17.3 dB	-15.1 dB	$9\pi/16$

These sidelobe levels are plotted in Fig. VI-15.

The steady increase in sidelobe level with increasing n represents another tradeoff in spectral properties, this time between near-in and asymptotic spectral behavior.

The cumulative spectra of the PFM waveforms show the same kind of variation with ψ as do those of the four waveforms of Section V. In Fig. VI-16, the cumulative spectra of all five PFM waveforms are shown, all for the value $\psi=\pi/2$. Figure VI-17 is similar, but in each case, the ψ -value given in Table VI-1 is used, hence this plot compares spectra which are very similar (and flat) in the near-in portion. The growth of near-in sidelobes is clearly seen, together with an increase in the value of frequency at which asymptotic behavior begins to be evident.

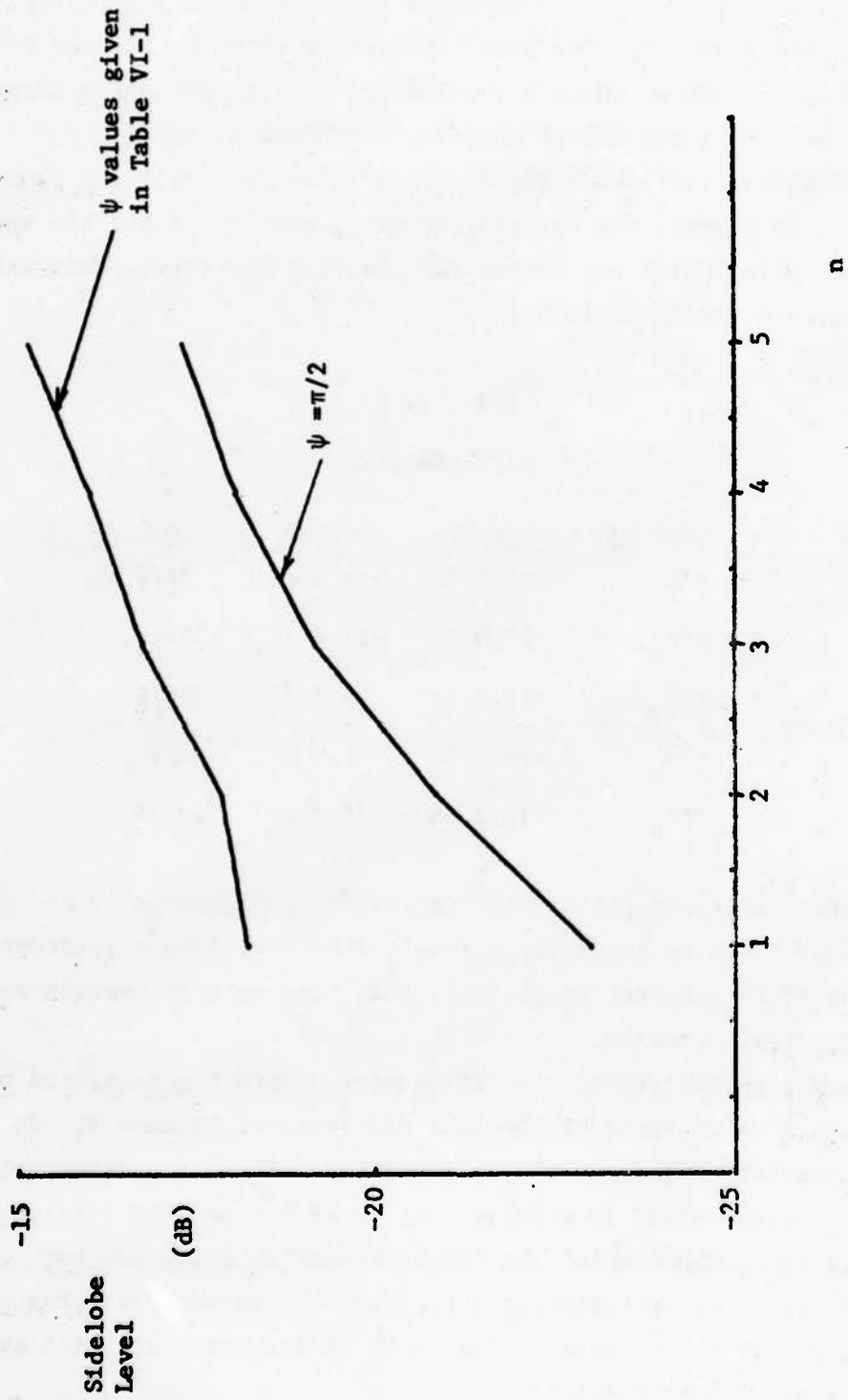


Fig. VI-15. Sidelobe levels of PFM waveforms

TR-596(VI-16)

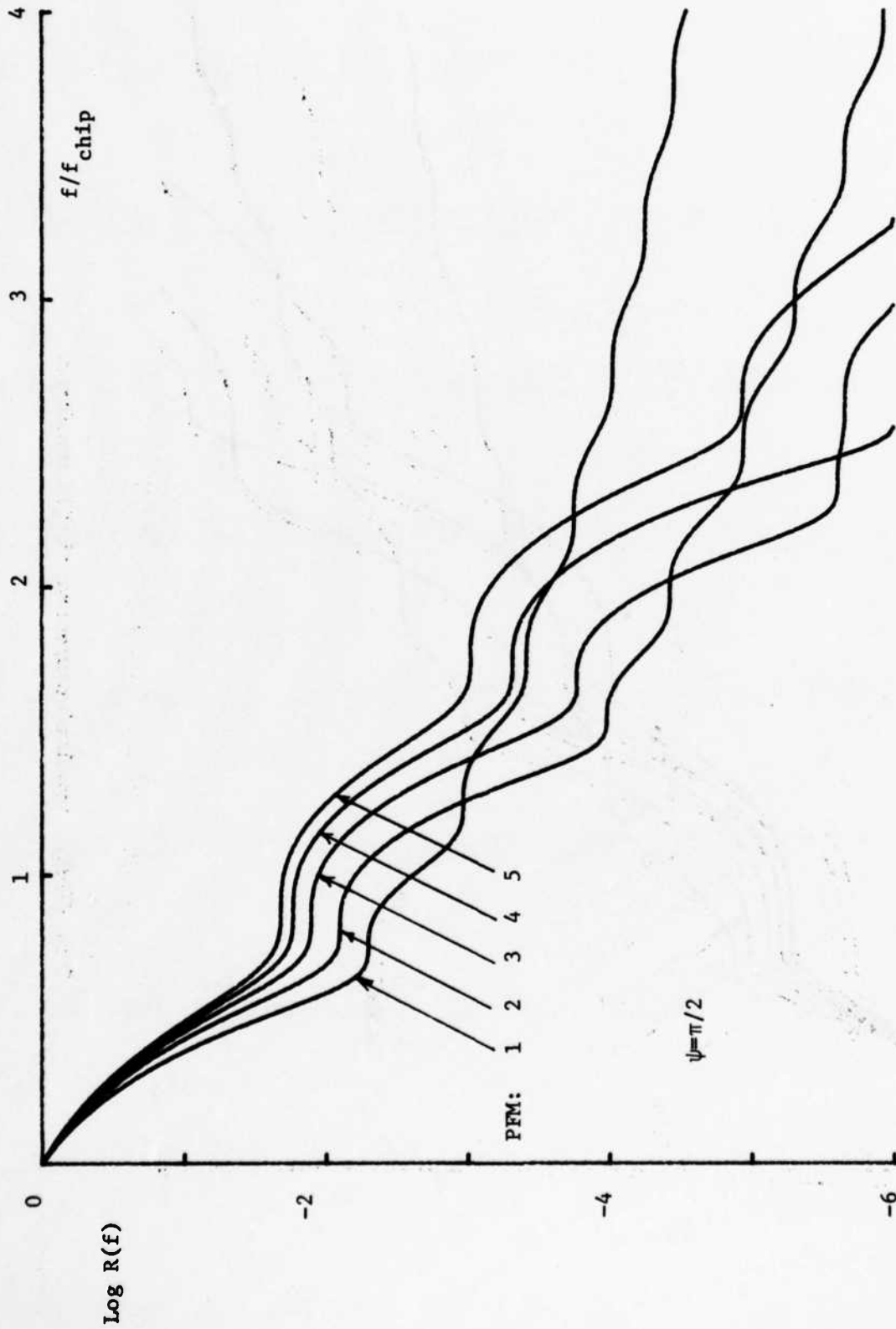


Fig. VI-16. Cumulative spectra of PFM waveforms

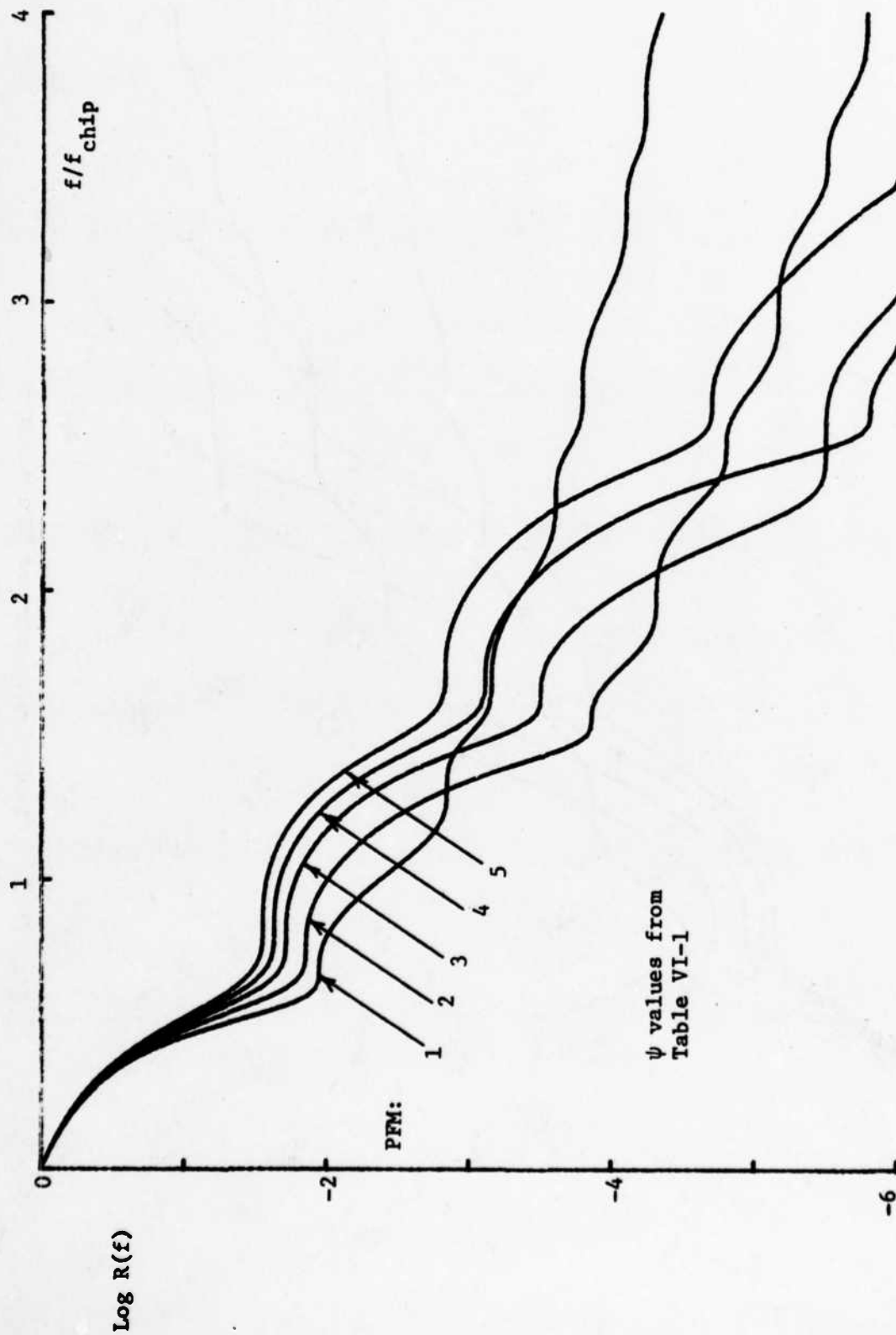


Fig. VI-17. Cumulative spectra of PFM waveforms

TR-596(VI-17)

It is interesting to consider the effect of letting n become very large. In this limit the frequency modulation pattern, $\dot{\phi}_n(t)$, approaches a delta function at mid-chip, and the phase will make an abrupt jump by $\pm\psi$. By forcing more and more smoothness on $\phi(t)$ at the chip boundaries, we have been led to a discontinuity (in the limit) at $t=\Delta/2$. This limiting waveform is just IPSK, with displaced chip boundaries, which has an asymptotic spectral density proportional to f^{-2} . The apparent paradox, that spectra behaving like f^{-2n-2} approach IPSK, is resolved by the growth of all sidelobes with increasing n , and an increase in the values of f where "asymptotic behavior" really begins. In the limit, the sidelobes continue high (in fact going like f^{-2}) for all reasonable values of f .

Our final plots in this section compare waveforms with equal values of n . In Fig. VI-18, cumulative spectra of waveforms A_2 , B_2 and PFM_2 are shown, all for $\psi=\pi/2$, and in Fig. VI-19, SFSK and PFM_3 are compared in this way, also for $\psi=\pi/2$. It is clear that the differences in spectra of waveforms having the same values of both n and ψ are small, and this is also true when these waveforms are compared with shared values of ψ other than $\pi/2$. These results appear to justify our assumption that the PFM waveforms provide a representative set with which to explore the spectral properties of binary FM waveforms in general.

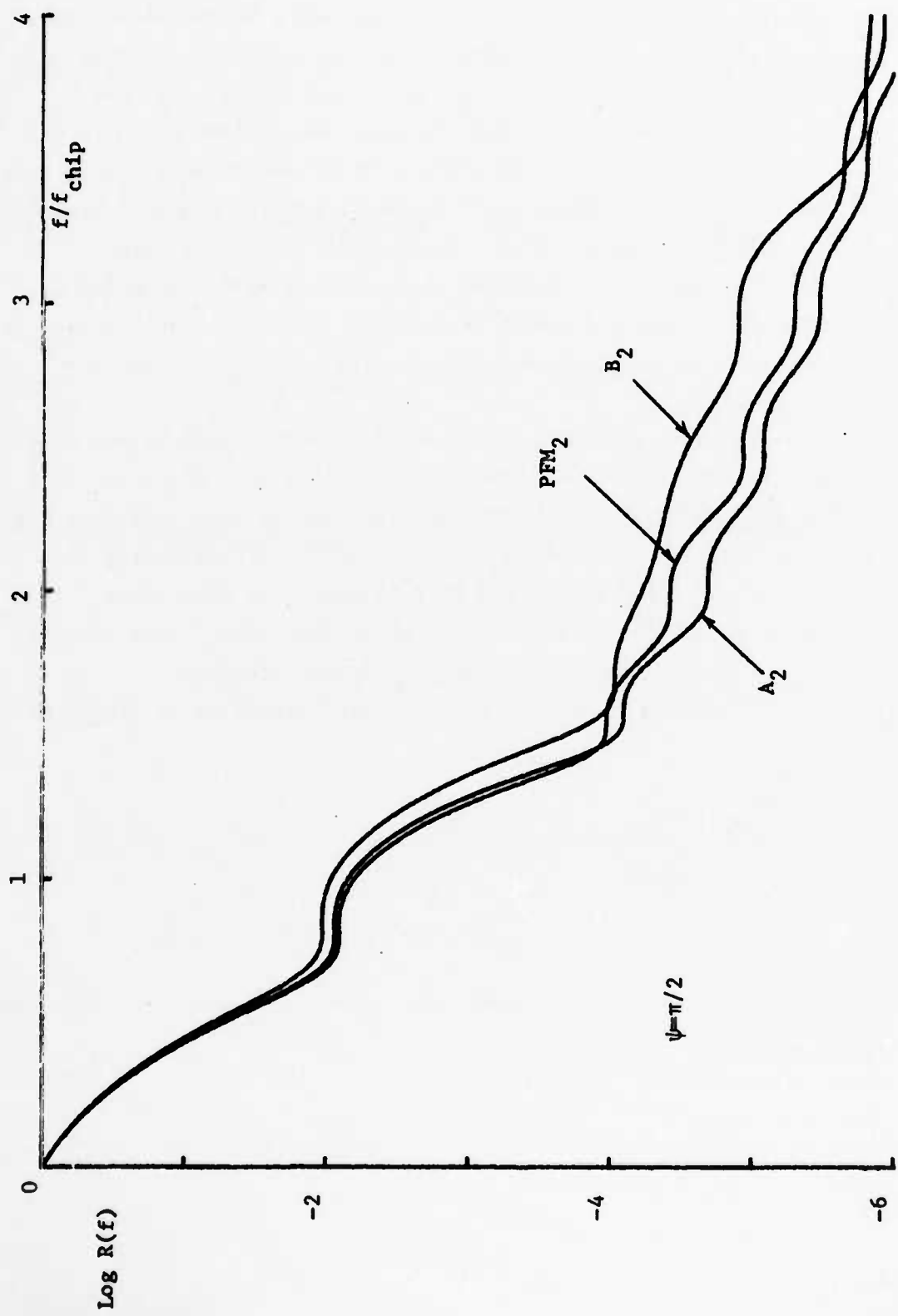


Fig. VI-18. Cumulative spectra: A_2 , B_2 and PFM_3

TR-596(VI-19)

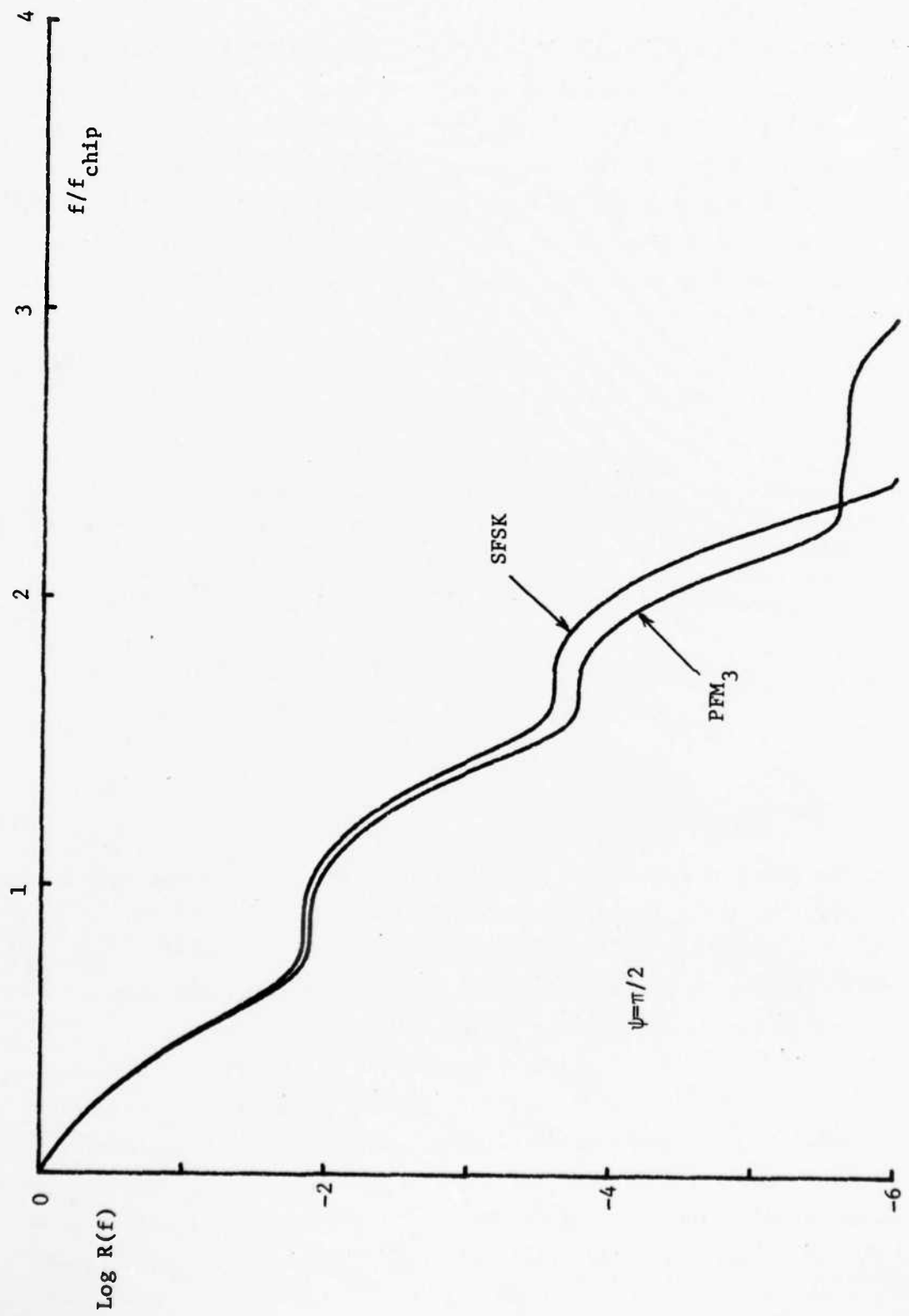


Fig. VI-19. Cumulative spectra: SFSK and PFM₃

VII. WAVEFORM COMPARISONS

If a given waveform has been selected for a particular application, the final choice which must be made concerns chipping rate. It is a mistake to choose the chipping rate equal to the nominal available bandwidth, since this may not optimize performance. Against an optimizing noise jammer, the performance of a waveform (coupled with a matched-filter receiver) is measured by its noise-equivalent-bandwidth, or NEB. If the peak of the spectral density of a particular spreading modulation occurs at frequency f_m , then by the definition already given,

$$G(f_m) \cdot \text{NEB} = \int_{-\infty}^{\infty} G(f) d\omega/2\pi .$$

By our normalization, the right side is just unity, and also

$$G(f_m) = \Delta g(\theta_m) ,$$

where θ_m is the corresponding argument of the spectral peak. Therefore we have

$$g(\theta_m) \Delta \text{NEB} = 1 ,$$

or

$$\frac{\text{NEB}}{f_{\text{chip}}} = \frac{1}{g(\theta_m)} .$$

For many of the waveforms discussed in this study, θ_m occurs at the origin, and in any case this ratio is an important attribute of the waveform. This quantity, which we call the "chipping factor", measures the amount of NEB (and hence performance) and we get per megahertz of chipping rate. In this discussion, system bandwidth is unrestricted.

For BPSK, the ratio of NEB to chipping rate is unity, and no waveform discussed in this study exceeds the value 1.3. In all the waveforms studied here, values greater than or equal to unity can be attained, by choosing a value of ψ which yields a flat spectral density in the mainlobe. For FSK, this is illustrated in Fig. VII-1, in which $\text{NEB}/f_{\text{chip}}$ is shown as a function of ψ . It should be noted that beyond a certain value of ψ (namely 1.9905 radians),

TR-596(VII-1)

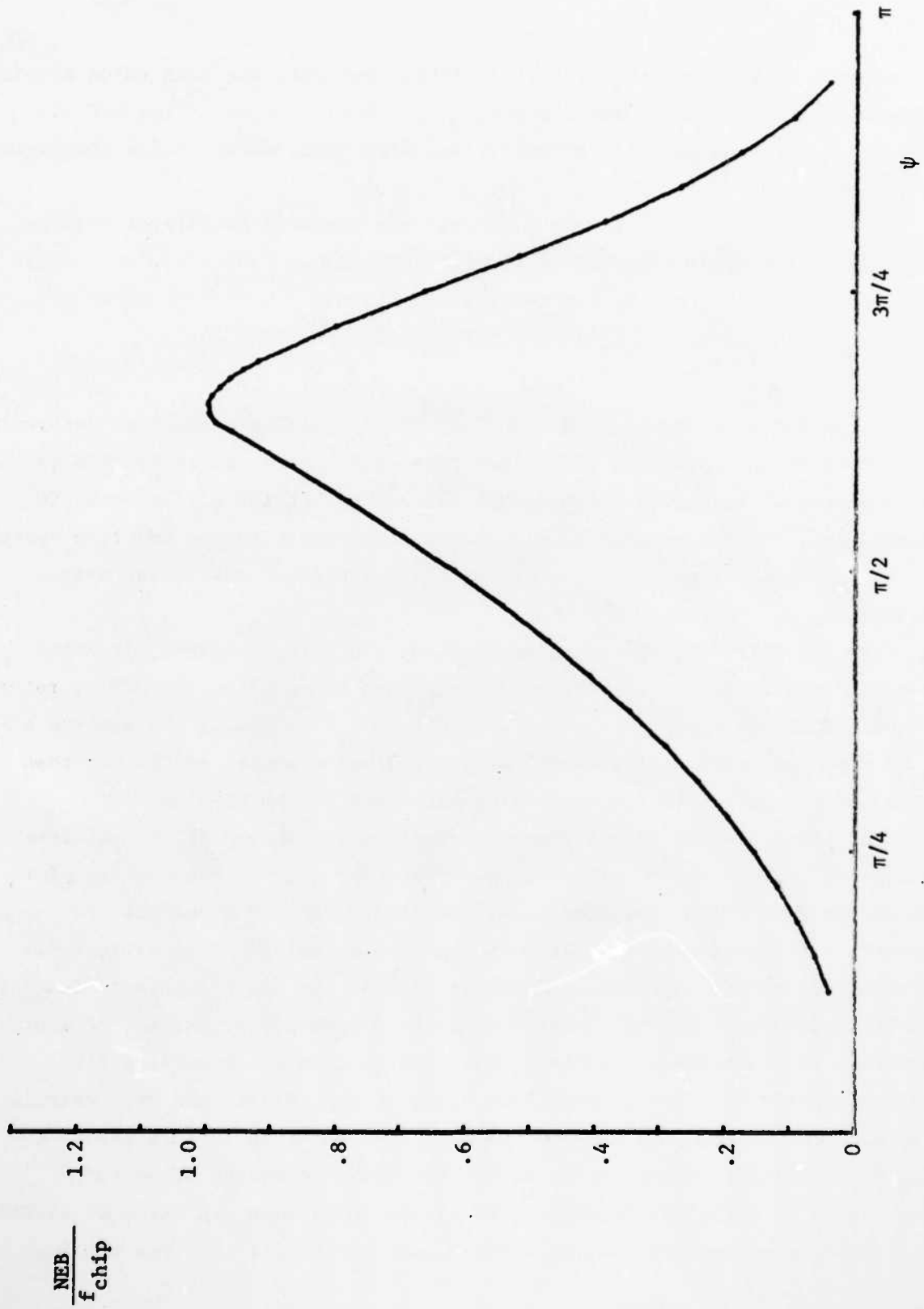


Fig. VII-1. Chipping factor for FSK

the spectral peak moves away from the origin. For FSK, the peak value attained is exactly unity. Similar results are found for all the waveforms and Fig. VII-2 shows the same data for several, including IPSK, which yields the highest ratios found.

To choose f_{chip} for a given waveform, some spectral constraint must be imposed, otherwise NEB can be made indefinitely large. The chipping rate is simply a scale factor on the frequency axis, since

$$f = f_{\text{chip}} \frac{\theta}{2\pi},$$

and the spectra depend only on θ . One way of recognizing a spectral constraint is embodied in our spreading efficiency parameter, discussed in Section VI. In that measure, it is simply assumed that all energy outside a fixed band is filtered out. More realistic models should be compared to the waveform spectra in each individual case, before a decision is made for a particular system application.

When two different spreading modulations are being compared, it makes sense to compare them with chipping rates chosen to equalize the NEB's, rather than with equal chipping rates. In this way one is comparing the spectra of two or more waveforms having essentially equal performance, and it can then be judged which better fits the spectral constraints of the problem.

Equalizing the NEB values tends to equalize the shapes of the mainlobe portions of the spectra of different waveforms for a given value of ψ . For example, in Fig. VII-3, the spectra of the first five PFM waveforms are compared, all with $\psi=\pi/2$, and all with the same chipping rates, arbitrarily taken to be 100 MHz. Spectral density is plotted, in dB, relative to its value at $f=0$. The actual spectral densities at the origin are different, of course, since each waveform has a different NEB. The spectra of these same five waveforms (still with $\psi=\pi/2$) are shown again in Fig. VII-4, but with chipping rates adjusted to equalize the NEB values. For PFM₁ (MSK in this case), the chipping rate has been kept equal to 100 MHz, and the others adjusted accordingly, as lited on the figure, to attain the common NEB value of 61.685 MHz. These waveforms now have equivalent performance (if they are not band

TR-596(VII-2)

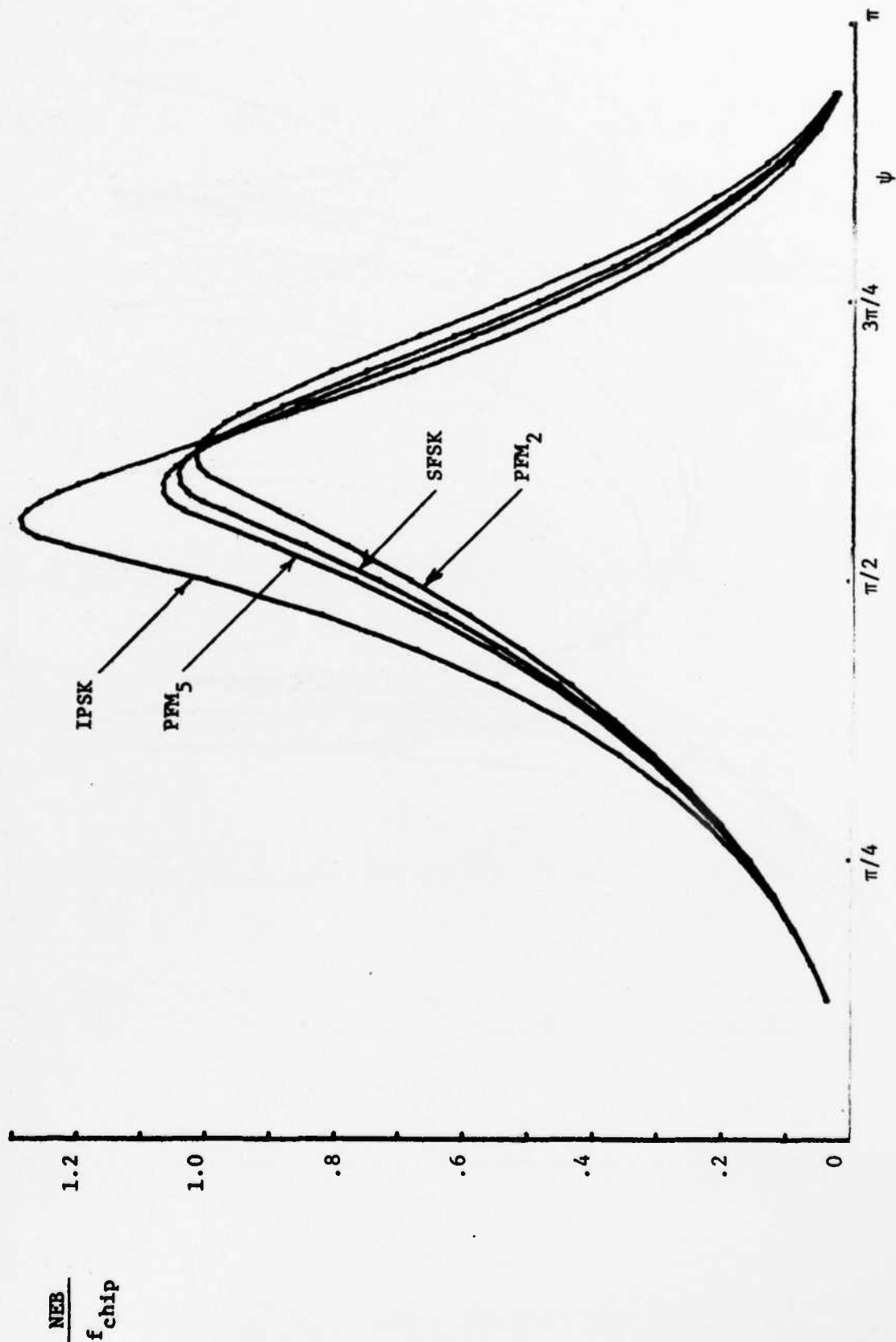


Fig. VII-2. Chipping factor curves

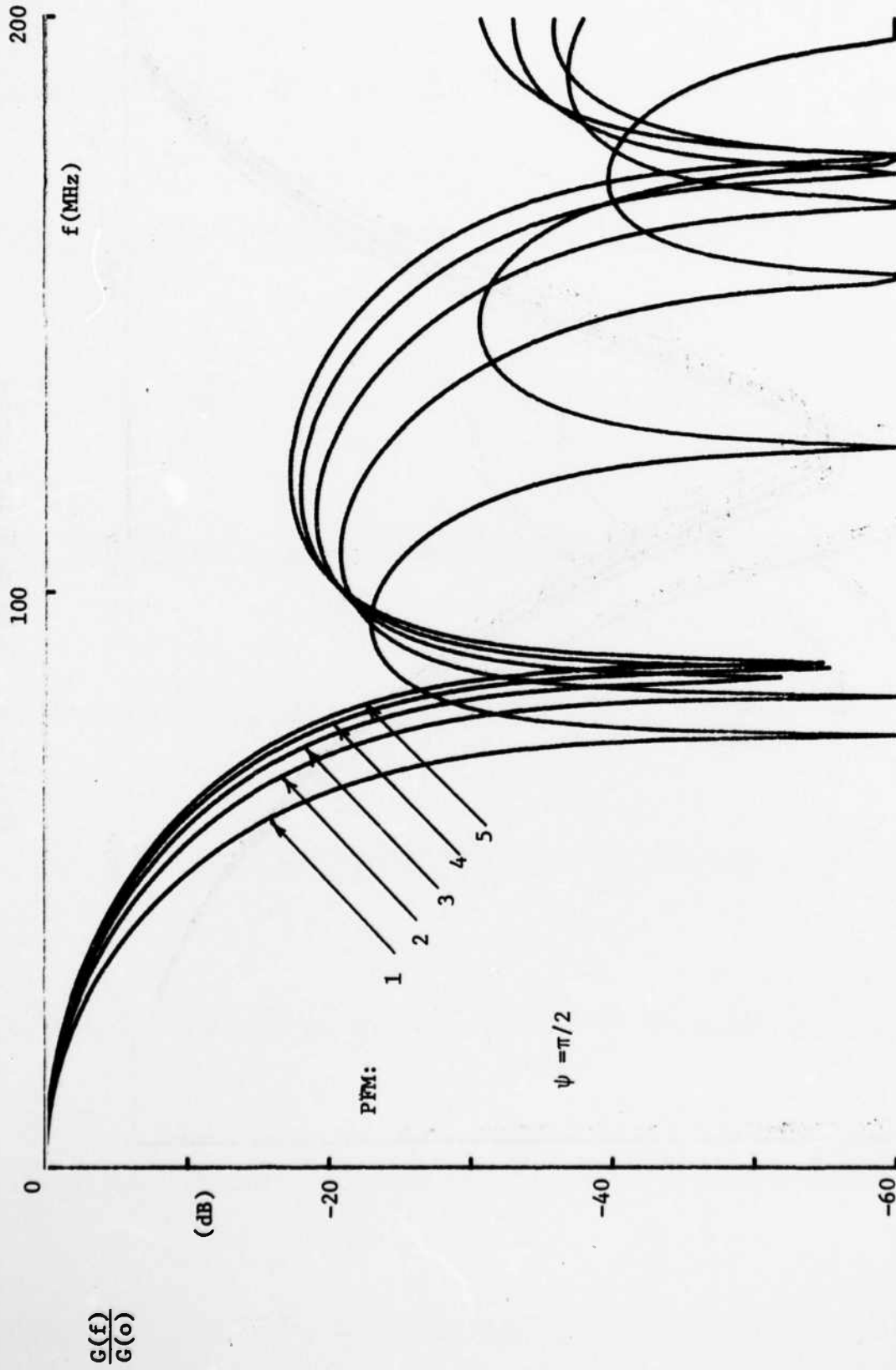


Fig. VII-3. Relative spectral densities, equal chipping rates

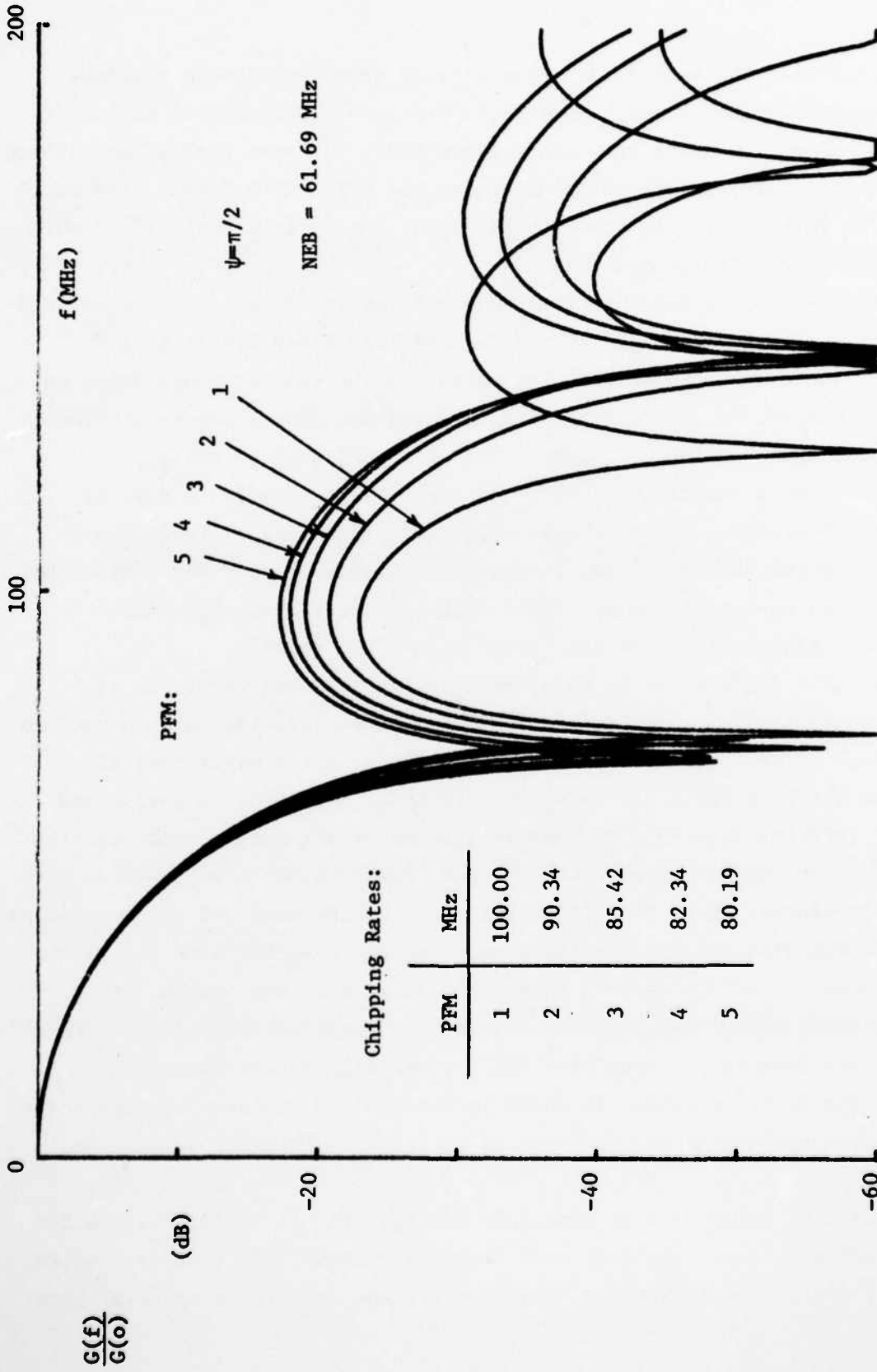


Fig. VII-4. Relative spectral densities, equal NEB

limited), but with the same differences already noted concerning sidelobe levels and asymptotic spectra. However, the figure shows another method of comparison, namely chipping rate for a given NEB. The same kind of comparison is made in Fig. VII-5 (equal chipping rates) and Fig. VII-6 (equal NEB) for the five PFM waveforms, this time with ψ -values chosen from Table VI-1, which identify "flat" spectra in each case.

Cumulative spectra for the five PFM waveforms are given, on an equal NEB basis, in Fig. VII-7 ($\psi=\pi/2$ in all cases) and Fig. VII-8 (Table VI-1 ψ -values). The corresponding chipping rates are the same as those shown on Figs. VII-4 and VII-6. The effect of equalizing the NEB values on mainlobe shape is seen again in these figures, which are analogous to the equal-chipping-rate cumulative spectra of Figs. VI-16 ($\psi=\pi/2$) and VI-17 (Table VI-1 ψ -values). All of these cumulative plots show an inversion in ordering among the PFM waveforms, in that PFM₁ has the lowest first sidelobe, and the slowest asymptotic decay, while higher-order PFM waveforms have progressively higher sidelobes and faster asymptotic decay.

Significant differences in mainlobe shape appear when waveforms with different ψ -values are compared, even when they are equalized with respect to NEB. In Fig. VII-9, relative spectra are shown for three waveforms, all adjusted to the same NEB. The waveforms are BPSK, MSK (PFM₁ at $\psi=\pi/2$) and "flat FSK" (PFM₁ at $\psi=5\pi/8$). The NEB is 100 MHz in all cases, achieved with $f_{\text{chip}}=100$ MHz for BPSK, and with the chipping rates shown in Fig. VII-10 for the other waveforms. Note that "flat FSK" attains the same NEB performance as unfiltered BPSK with essentially the same chipping rate, but with superior spectral shape out of the central band of frequencies. MSK, on the other hand, requires a higher chipping rate to match the NEB value, and exhibits a spectral decay less rapid than "flat FSK", especially before the first sidelobe. The same comparison is shown in Fig. VII-10 in terms of cumulative spectra, which emphasizes the differences in spectral behavior outside the mainlobe.

This kind of comparison is continued in Figs. VII-11 through VII-18 for the other PFM waveforms. In each case we compare BPSK, PFM_n ($\psi=\pi/2$) and PFM_n (Table VI-1 ψ -values), in both relative spectra and cumulative spectral form.

TR-596(VII-5)

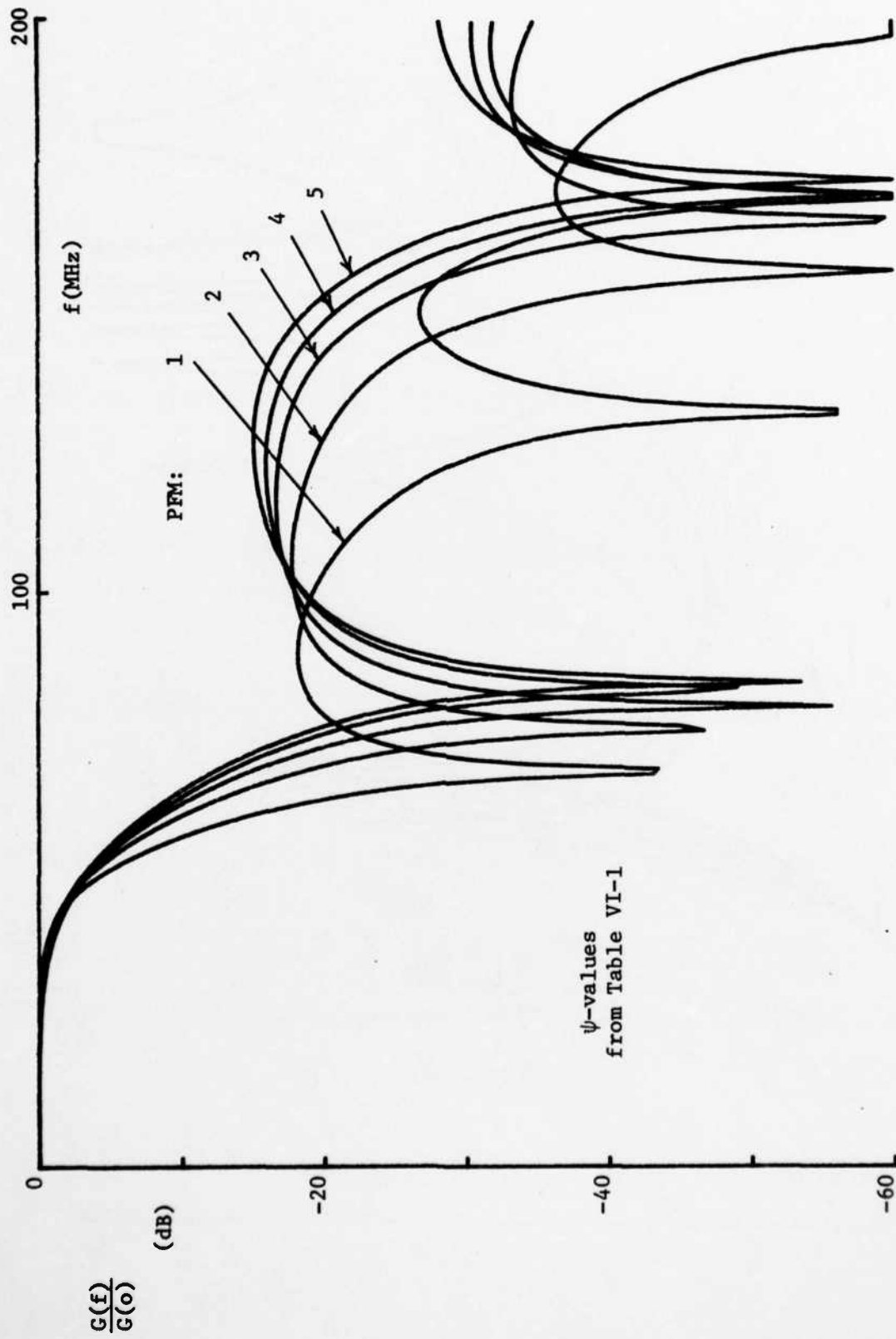


Fig. VII-5. Relative spectral densities, equal chipping rates

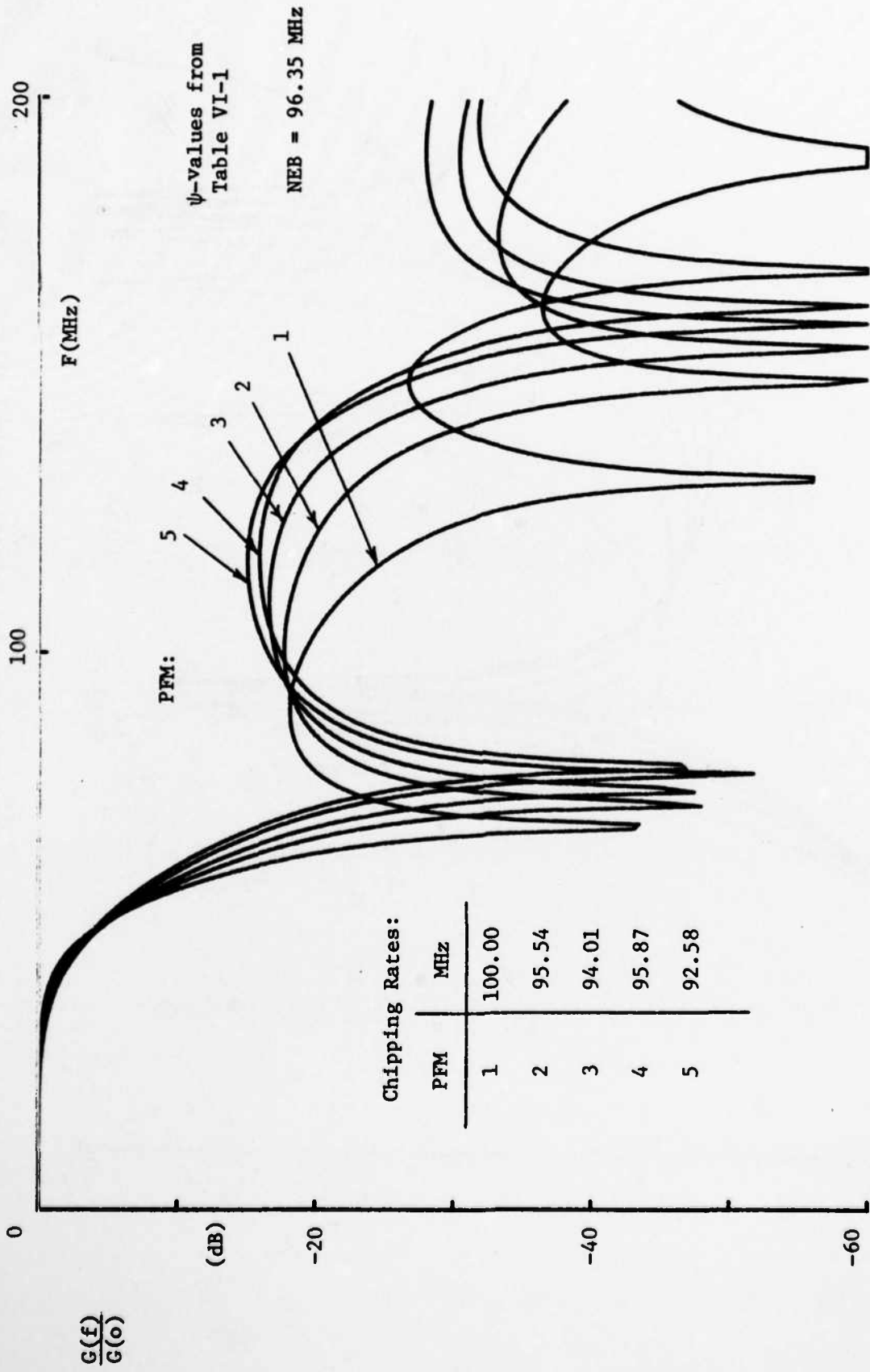


Fig. VII-6. Relative spectral densities, equal NEB

TR-596(VII-7)

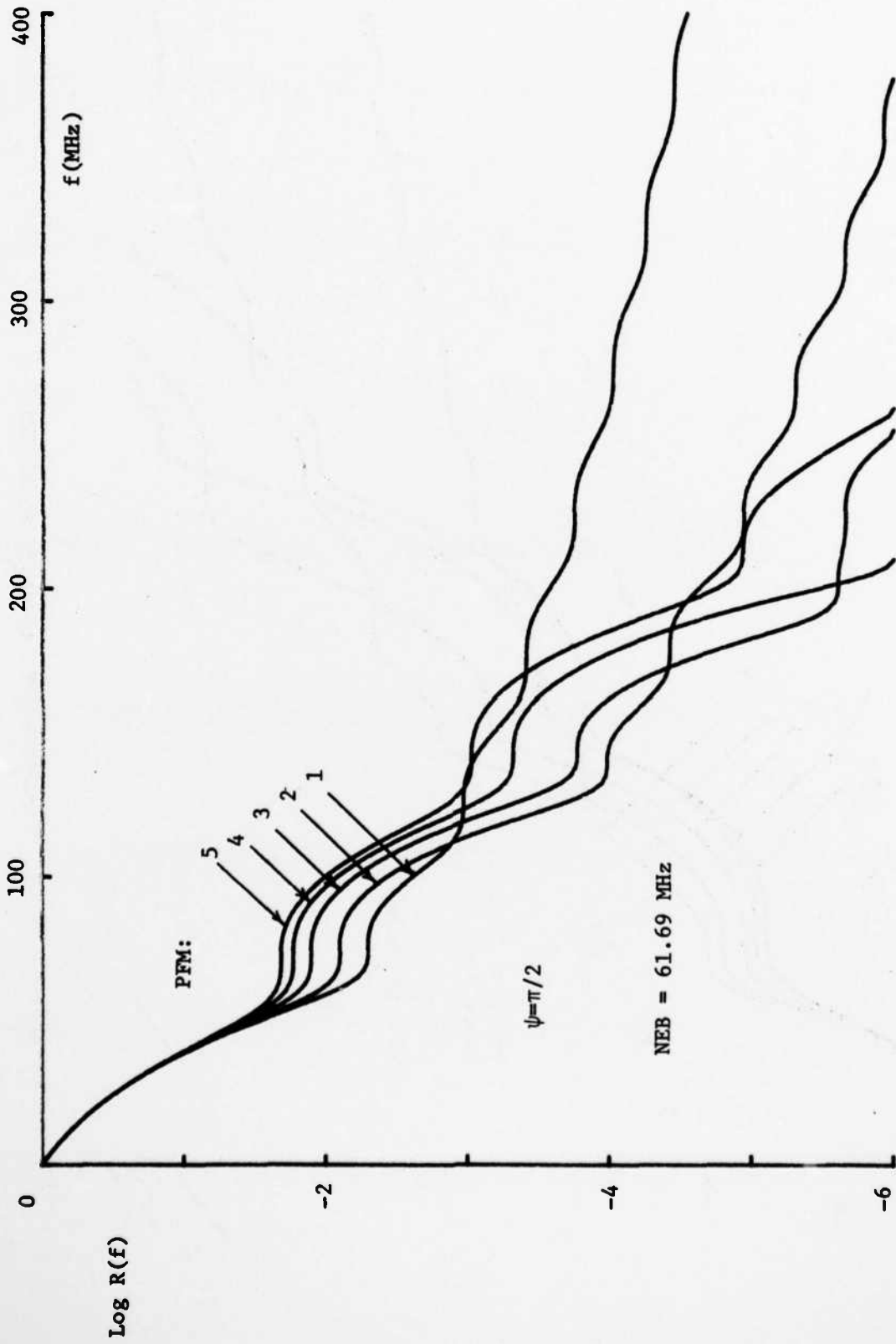


Fig. VII-7. Cumulative PFM spectra, equal NEB

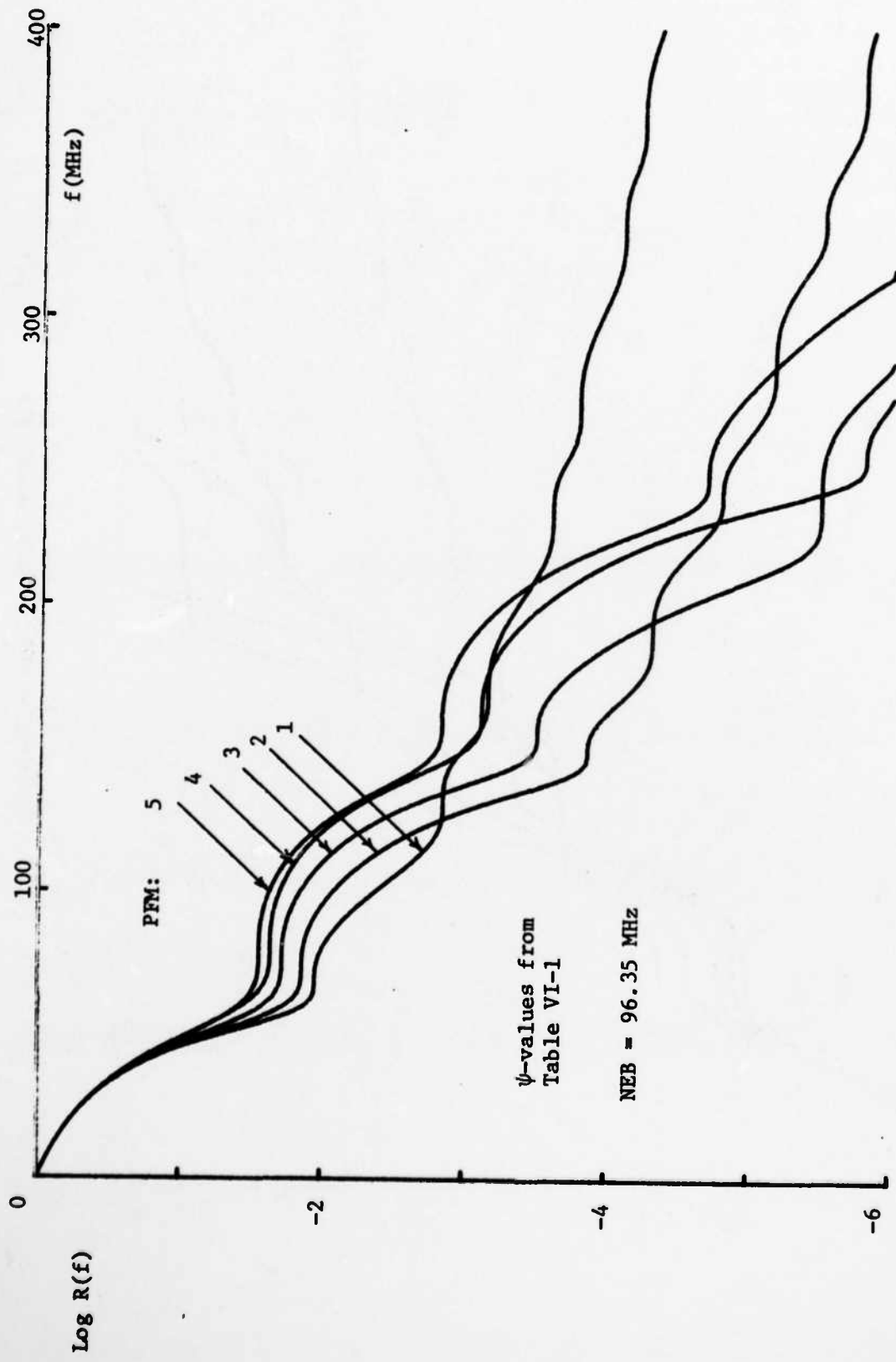


FIG. VII-8. Cumulative PFM spectra, equal NEB

TR-596(VII-8)

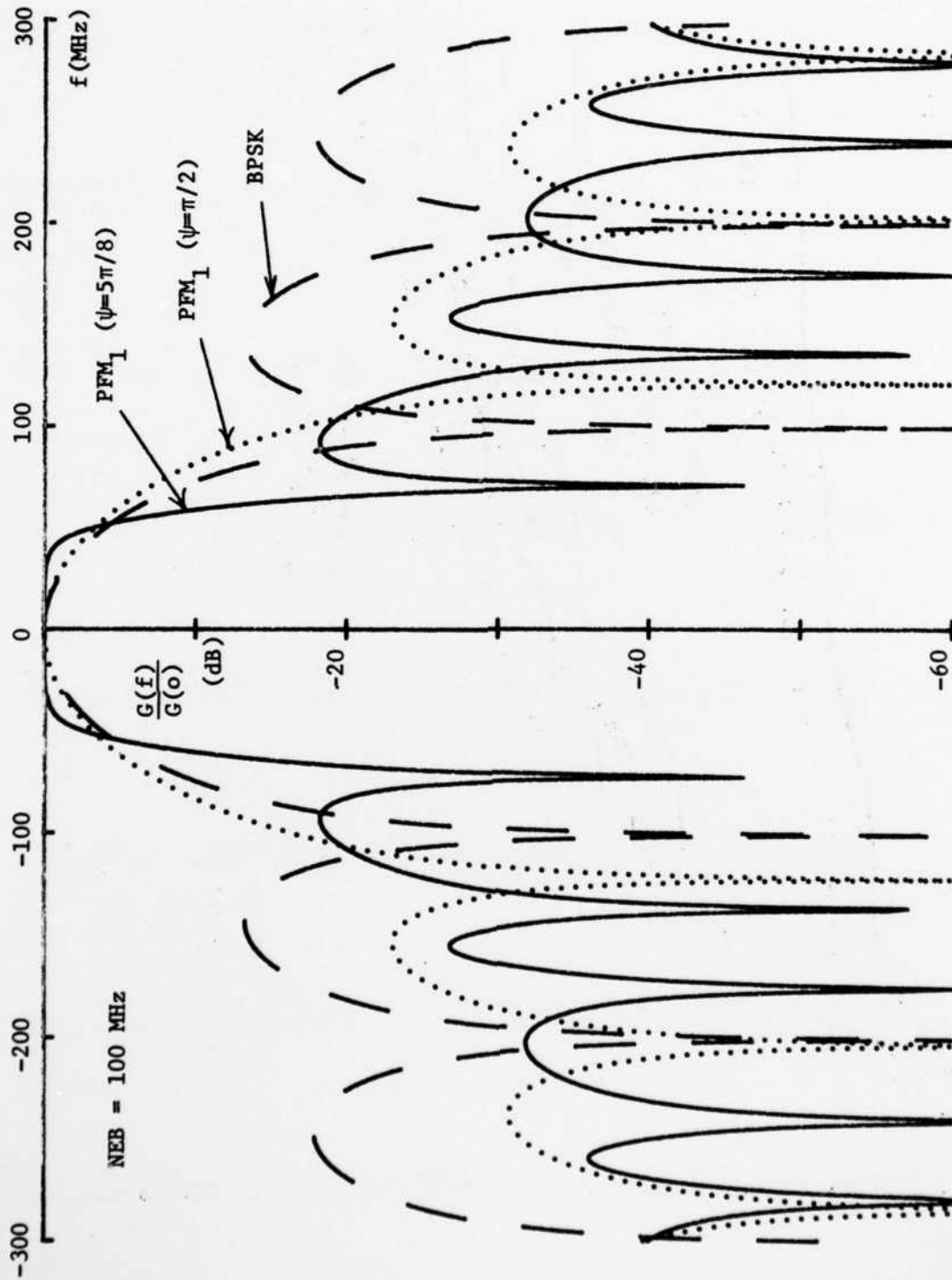


Fig. VII-9. BPSK and PFM₁ relative spectra, equal NEB

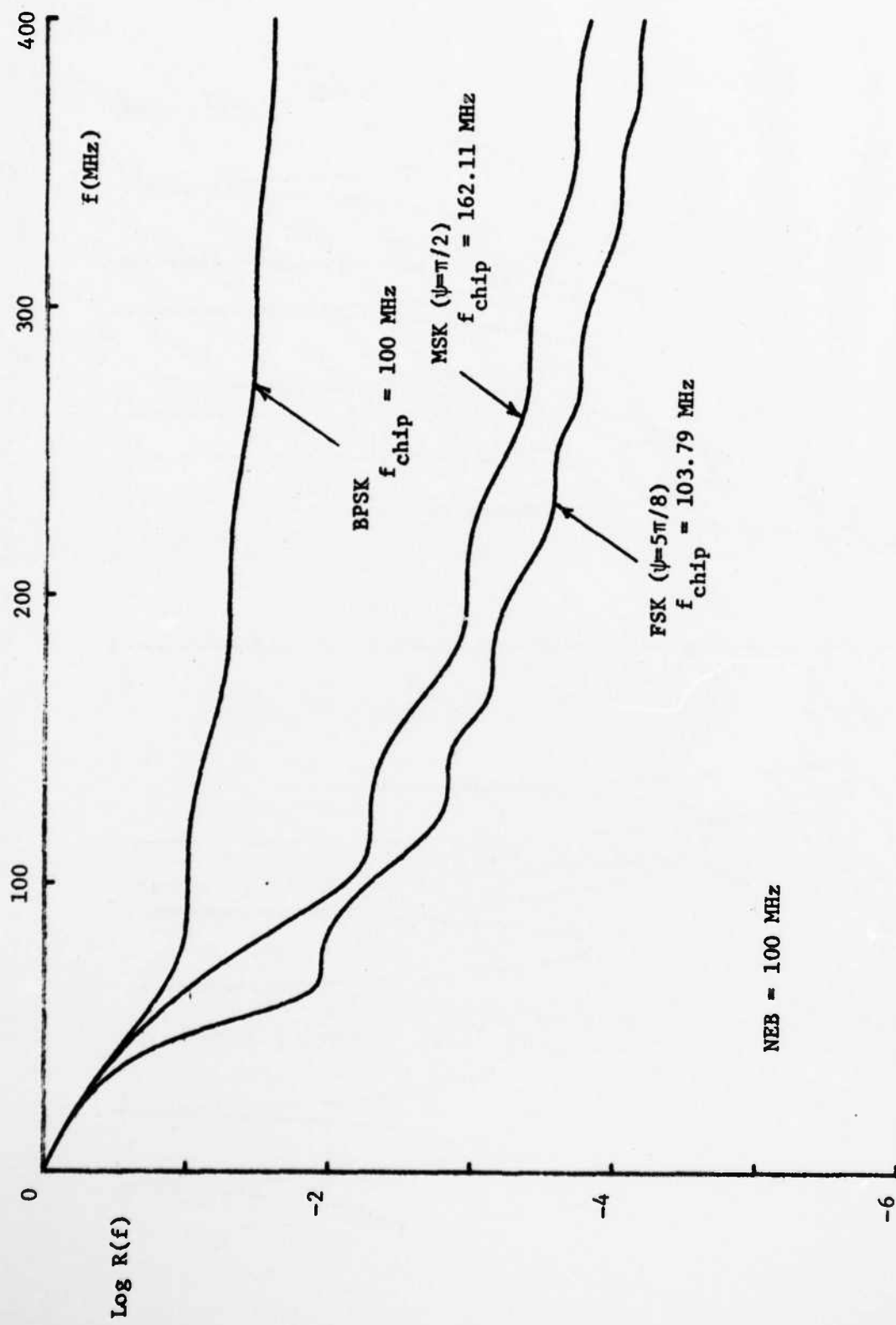


FIG. VII-10. BPSK and FSK cumulative spectra, equal NEB

TR-596(VII-11)

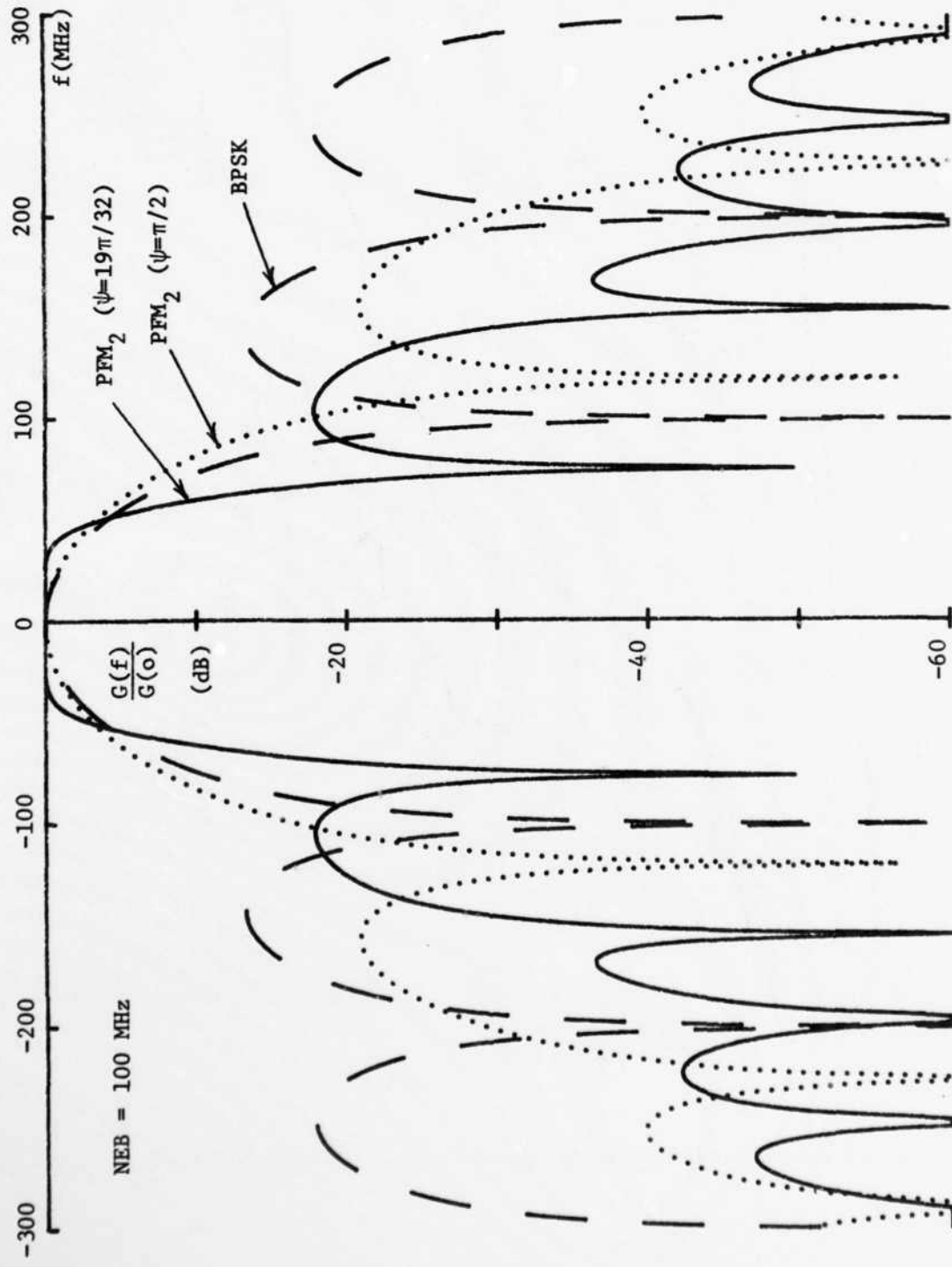


Fig. VII-11. BPSK and PFM₂ relative spectra, equal NEB

AD-A134 850

A CATALOGUE OF SPREADING MODULATION SPECTRA(U)
MASSACHUSETTS INST OF TECH LEXINGTON LINCOLN LAB
E J KELLY 20 SEP 83 TR-596 ESD-TR-83-053

2/2

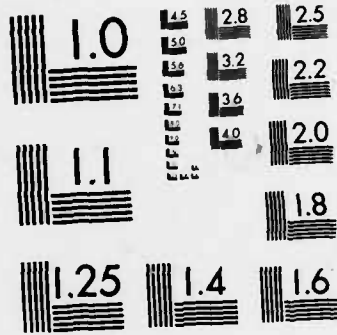
UNCLASSIFIED

F19628-80-C-0002

F/G 17/4

NL





MICROCOPY RESOLUTION TEST CHART
NATIONAL BUREAU OF STANDARDS-1963-A

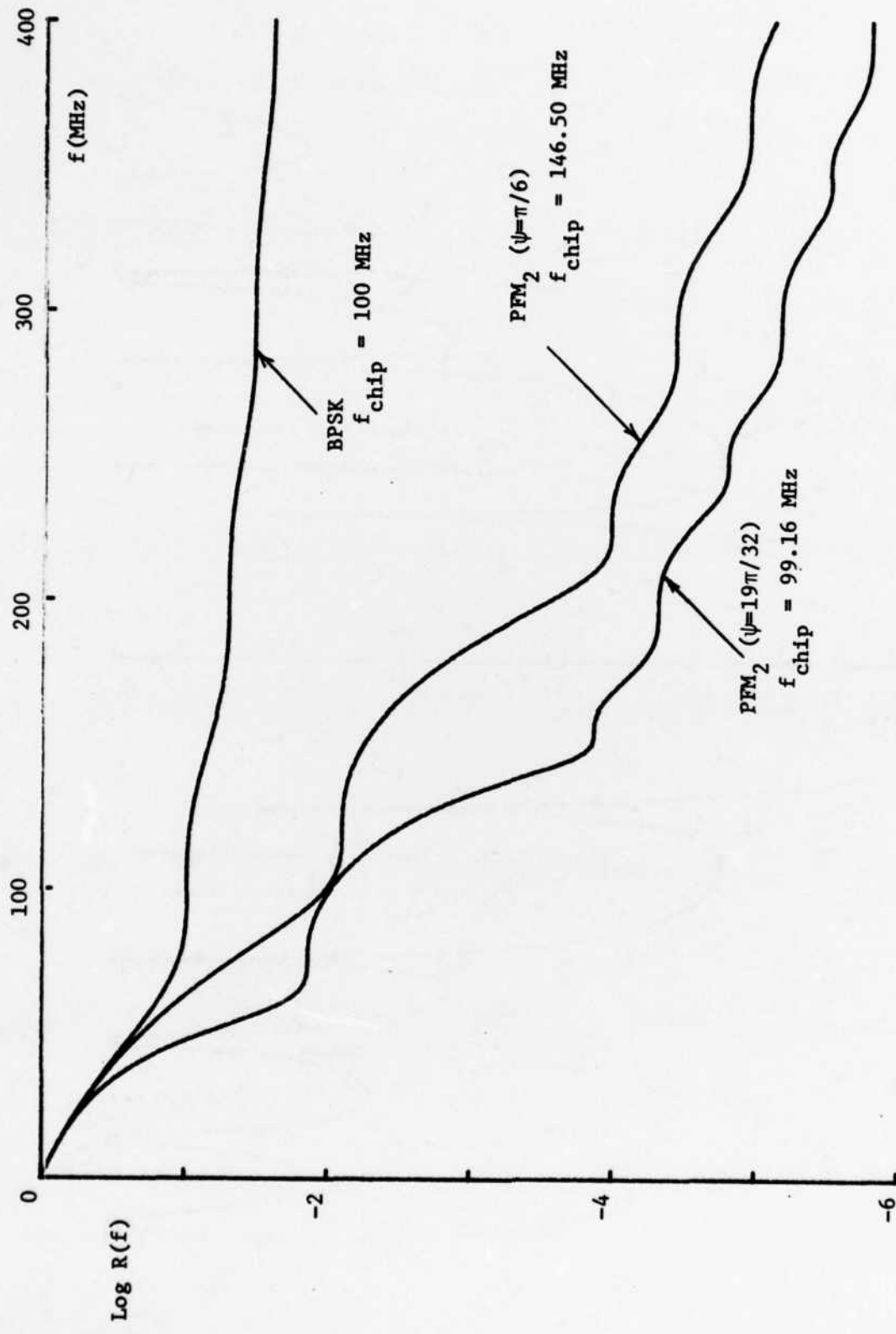


Fig. VII-12. BPSK and PFM₂ cumulative spectra, equal NEB

TR-596(VII-13)

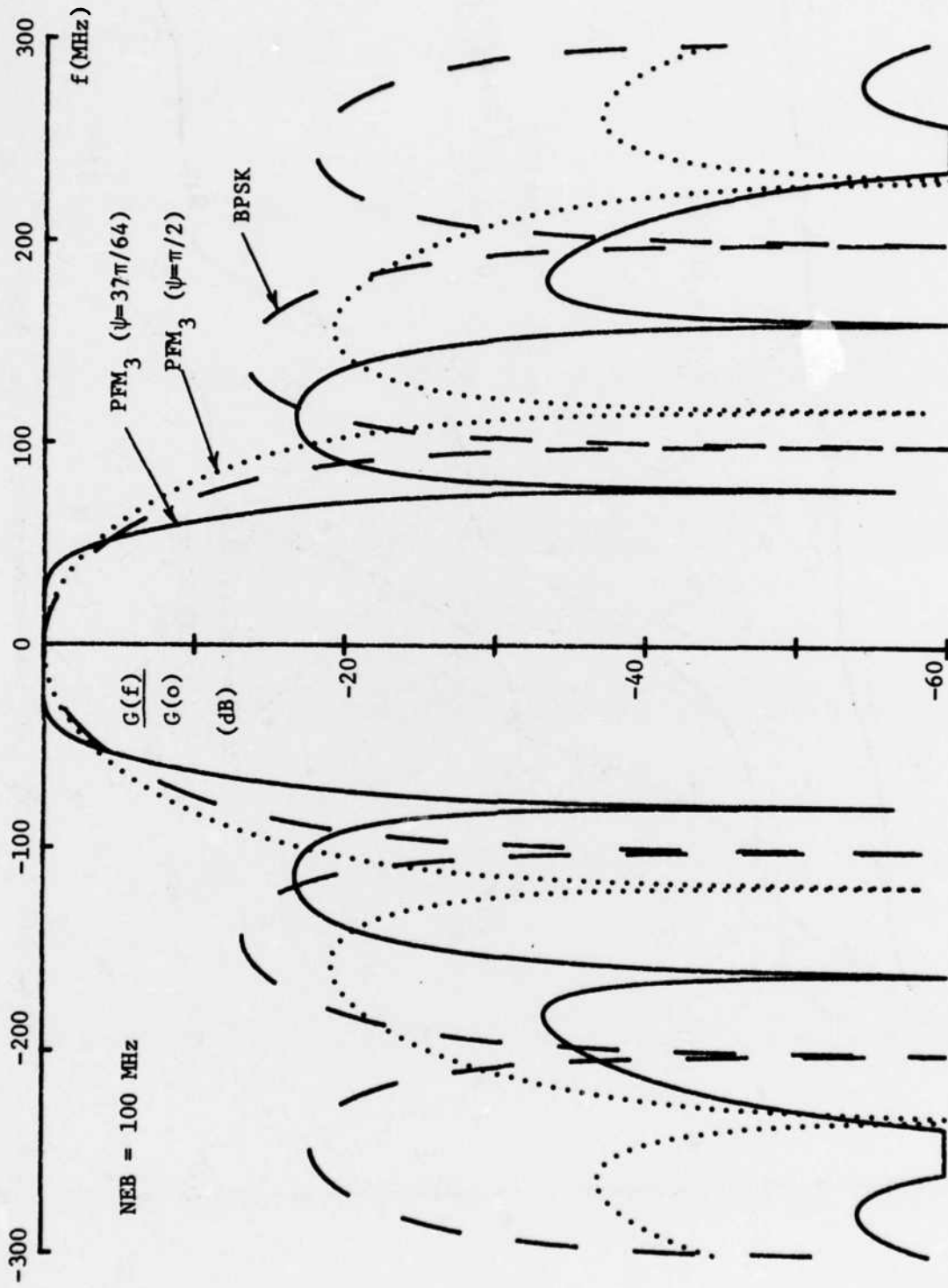


Fig. VII-13. BPSK and PFM₃ relative spectra, equal NEB

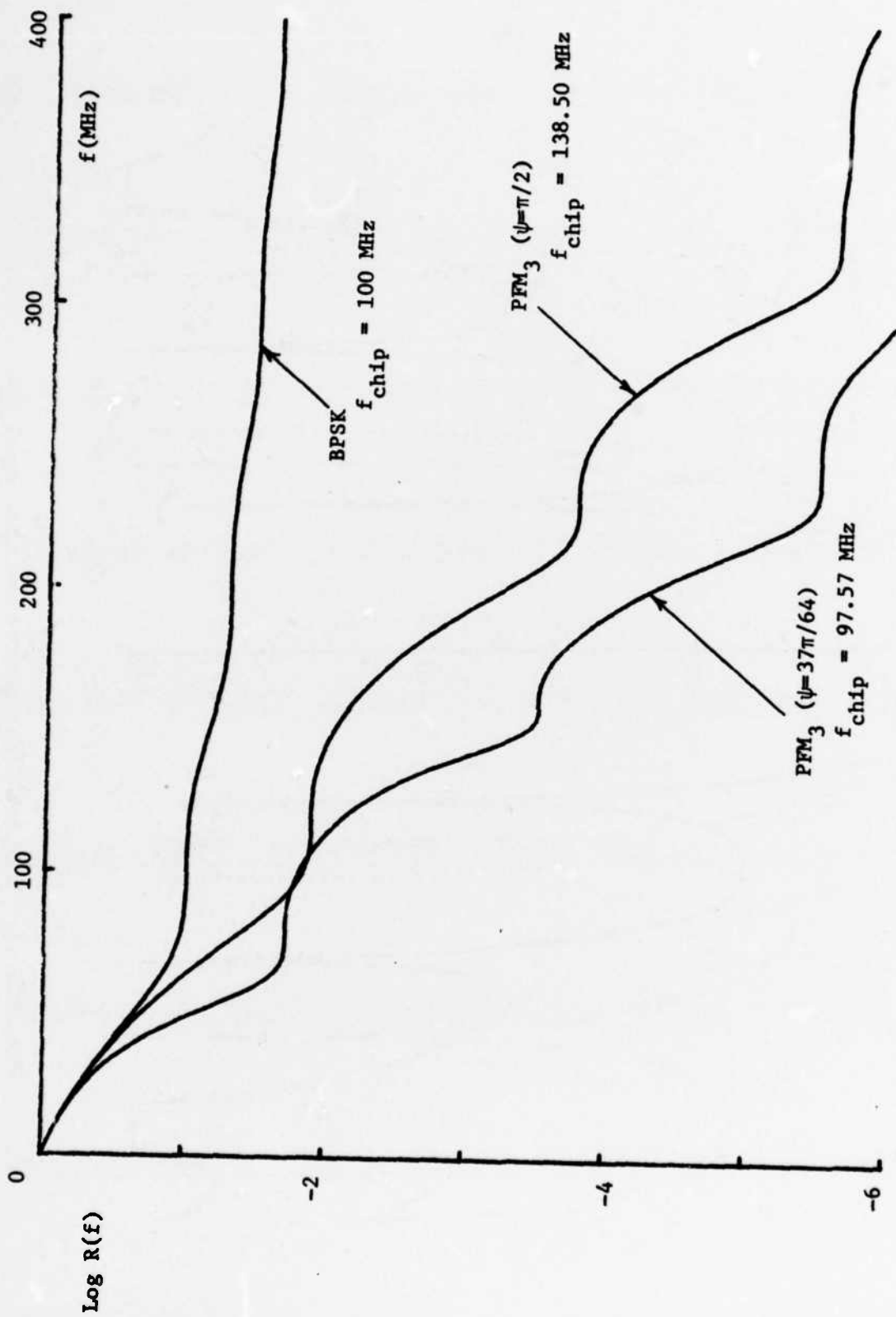


Fig. VII-14. BPSK and PFM₃ cumulative spectra, equal NEB

TR-596(VII-15)

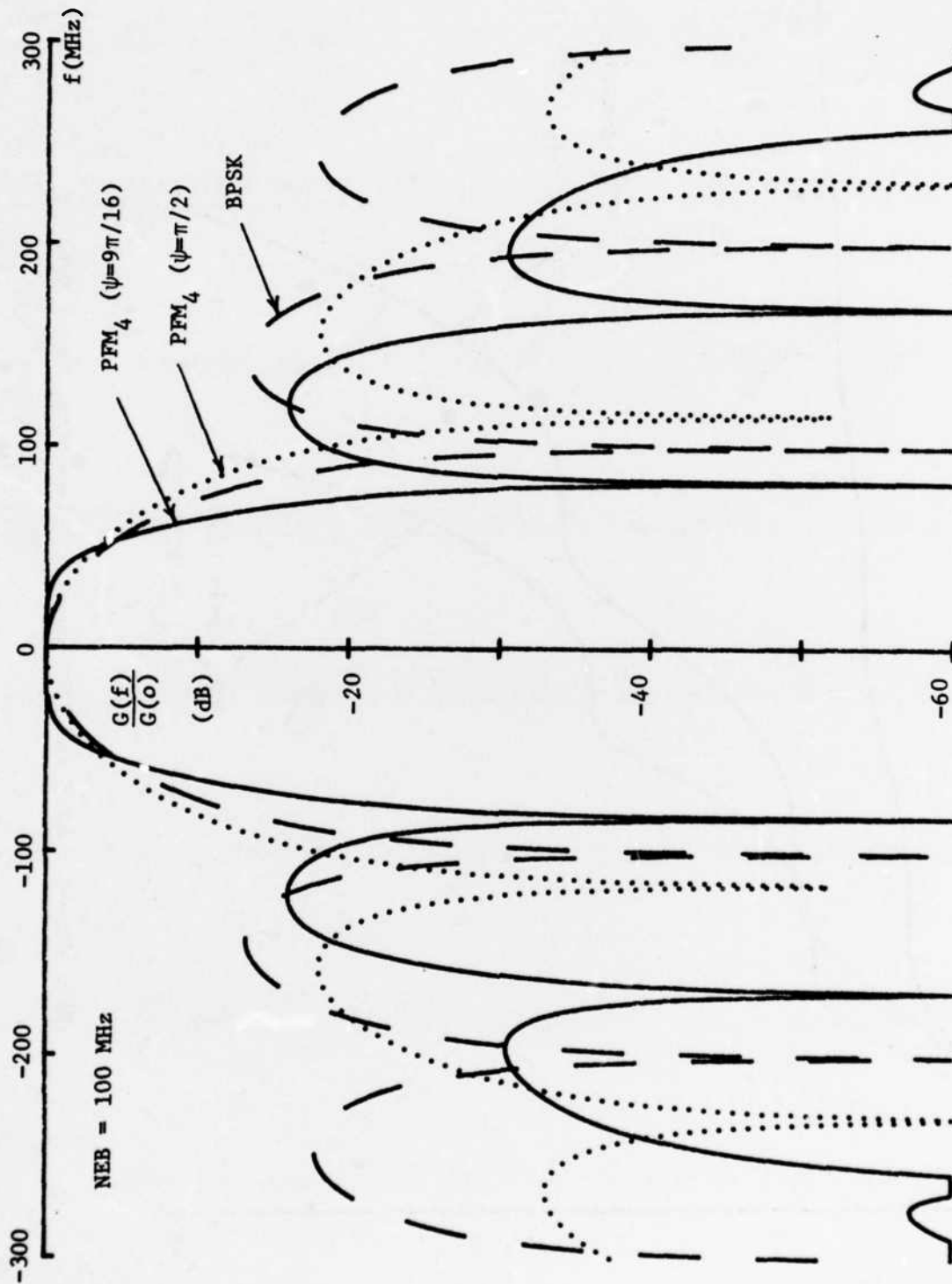


Fig. VII-15. BPSK and PFM₄ relative spectra, equal NEB

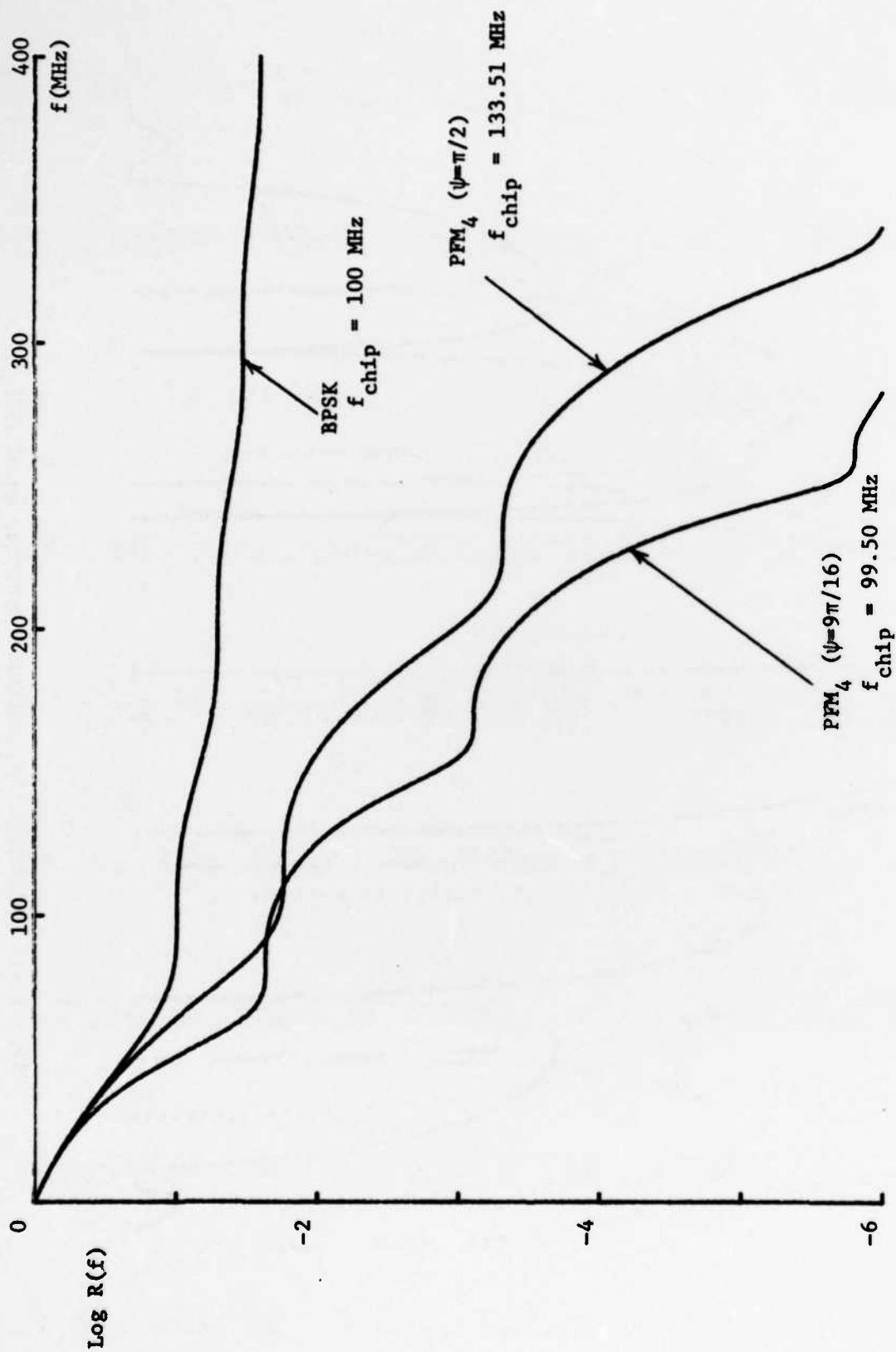


Fig. VII-16. BPSK and PFM₄ cumulative spectra, equal NEB

TR-596(VII-17)

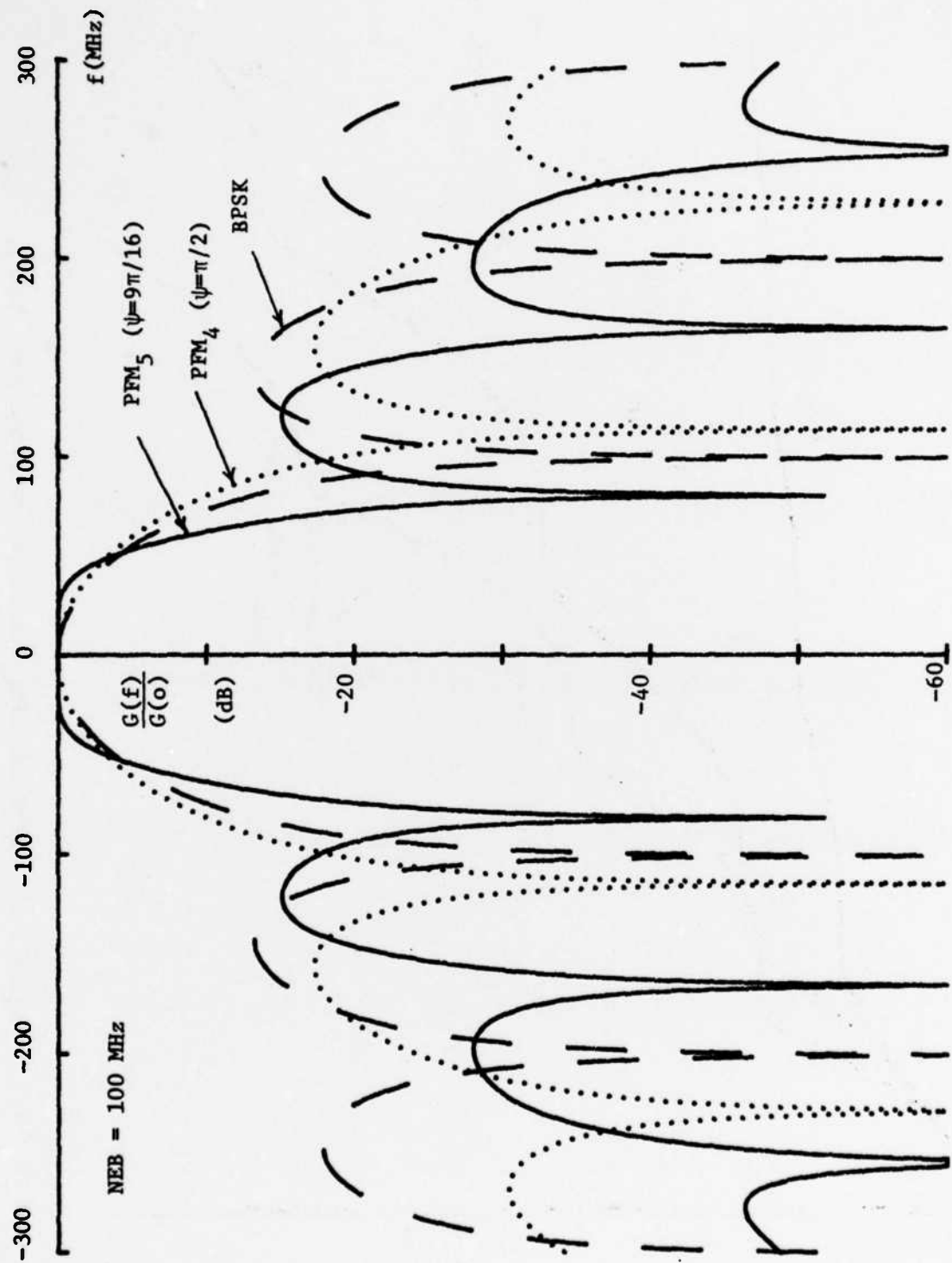


Fig. VII-17. BPSK and PFM₅ relative spectra, equal NEB

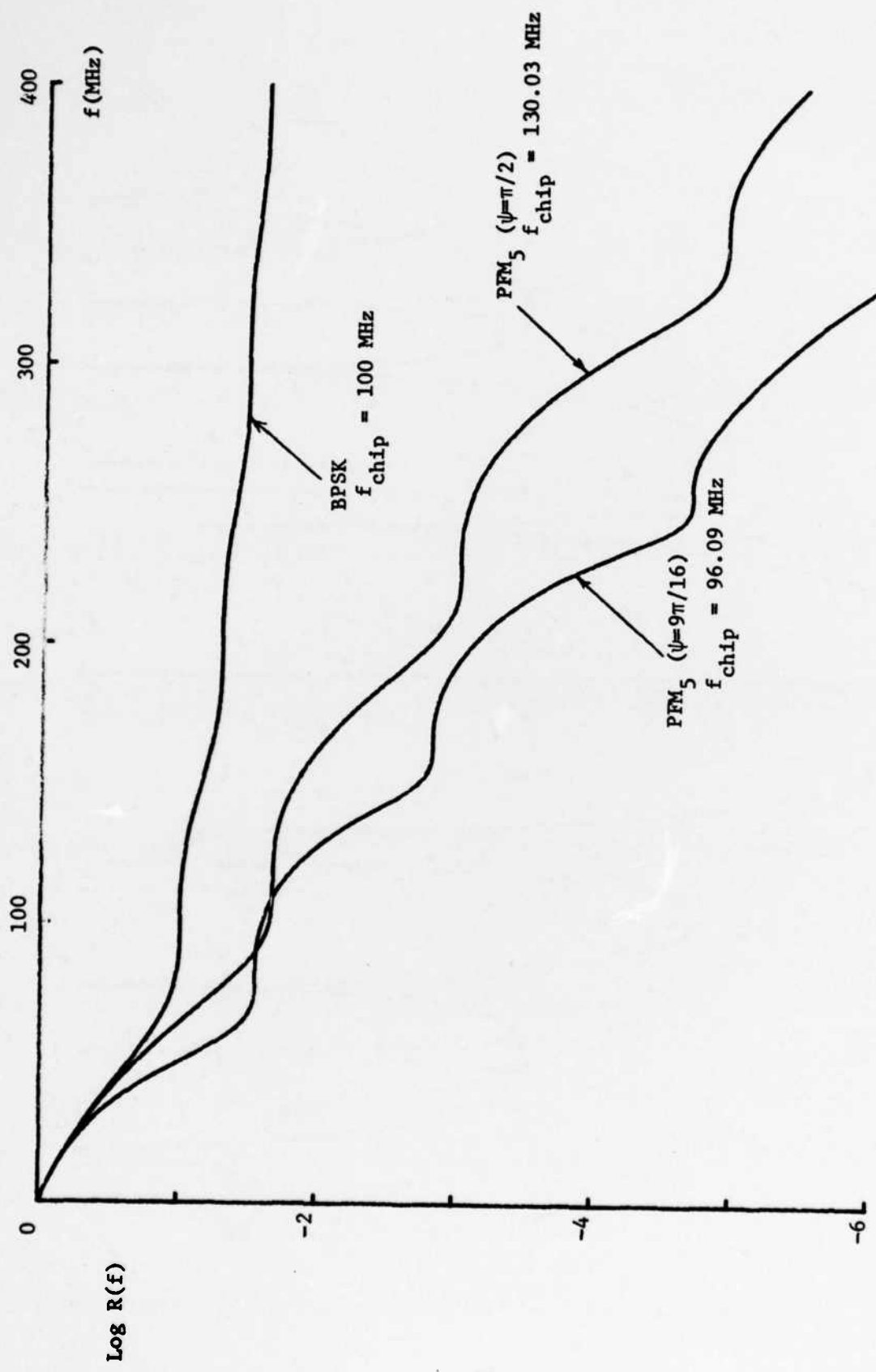


Fig. VII-18. BPSK and PFM₅ cumulative spectra, equal NEB

NEB and BPSK chipping rate is 100 MHz in all these cases, and the corresponding PFM chipping rates are shown on the figures illustrating cumulative spectra. The following table summarizes the different values of NEB/f_{chip} which govern the chipping rates used on these curves.

TABLE VII-1

NEB/ f_{chip} Values

Waveform	ψ -value	NEB/ f_{chip}
BPSK	-	1
PFM ₁	$\pi/2$	0.61685
PFM ₂	$\pi/2$	0.68269
PFM ₃	$\pi/2$	0.72203
PFM ₄	$\pi/2$	0.74901
PFM ₅	$\pi/2$	0.76905
PFM ₁	$5\pi/8$	0.96353
PFM ₂	$19\pi/32$	1.00847
PFM ₃	$37\pi/64$	1.02488
PFM ₄	$9\pi/16$	1.00502
PFM ₅	$9\pi/16$	1.04070

In Table VII-1 the NEB/ f_{chip} values for the PFM waveforms with Table VI-1 ψ -values do not make a smooth sequence, because these ψ -values were essentially eyeball choices, and values of NEB $\cdot\Delta$ near unity are attained in all cases.

VIII. SUMMARY AND CONCLUSIONS

The motivation for the study of spreading modulations was discussed in some detail in Section I. The chief objective is to utilize an instantaneous bandwidth which is much greater than the information rate, and is thus diametrically opposed to the objective of bandwidth conservation in conventional data transmission systems. Spreading is achieved by subdividing information bits into many chips, coded with dummy bits which are known (in effect) to the receiver, but appear random to a potential jammer.

Performance measures for spread-spectrum systems are different from those of ordinary data communications systems, although constant-envelope waveforms with compact spectra are desirable in both cases. Rapid spectral decay outside the principal band is advantageous, and, in the case of spreading modulations, spectral flatness within this band leads to high performance. The spread-spectrum designer wants high noise-equivalent-bandwidth (which determines performance against an optimizing jammer) at the lowest possible chipping rate, while the communicator, considering the same waveform for data transmission, wants to maximize bit rate for a given allowed bandwidth. These issues are discussed in this report in terms of two measures of performance, the so-called spreading efficiency and the chipping factor. In all cases, performance is related to processing gain, which depends strongly on the spectral density of the waveform in question.

A classification system is introduced for spreading modulations, and several familiar examples are illustrated in their appropriate place. This system makes it easy to invent new waveforms, and a number of these are given in the report. A simple method of computation of spectra is developed, based upon a representation theorem which allows all of the waveforms studied to be described in terms of sums of phase-modulated pulses, formally very similar to BPSK. This permits the derivation of spectra of constant-phase waveforms (which is not complicated) to be extended directly to the large class of so-called binary FM waveforms.

Examples of binary FM waveforms, like FSK and SFSK, which have been discussed in the literature, are introduced in Section V, and their spectra illustrated. A general relationship between the spectral properties far from

band center and the smoothness of the frequency modulation pattern characteristic of the waveform is derived. This relation suggests a "graded sequence" of waveforms, with controlled asymptotic properties, and these are introduced in Section VI. A "smoothness index", n , characterizes the members of this family.

Another basic parameter, called ψ , is the magnitude of the total phase change per chip in the binary FM waveforms. Waveforms used for information transmission are usually characterized by the value $\psi=\pi/2$, but we find that spreading performance is often much better when other values, intermediate between $\pi/2$ and π , are used. Each spreading waveform is described by an instantaneous frequency modulation, and ψ is basically a multiplicative factor in this modulation, hence one automatically has a family of waveforms, parametrized by ψ , whenever a frequency modulation pattern is given. This allows generalization of all the familiar modulations, such as SFSK, just as FSK waveforms are generalizations of MSK. Each of the "graded sequence" waveforms, called polynomial FM modulations, is actually a family, with ψ as parameter.

It is shown that the spectral properties of spreading modulations of the binary FM type are largely determined by the values of the two parameters, n and ψ . The actual chipping rate, f_{chip} , of the waveform must be considered a third parameter, which acts as a scale factor on the frequency axis, stretching or compressing the spectrum. When operating within a given allotted frequency band, an optimum choice of chipping rate can be found for any waveform.

A number of tradeoffs appear in the results of this report. Noise-equivalent-bandwidth versus chipping rate, and sidelobe levels versus asymptotic spectral behavior are typical examples. These are discussed at some length, and many of the figures have been designed to illustrate them. Hardware issues are not discussed here, although large variations in implementation difficulty exist among these waveforms. The reasoning is simply that the spectral properties of a waveform are fixed, while the difficulty of using it continually changes with development of the requisite technology.

REFERENCES

- [1]. G. V. Colby, "Development of Techniques for Synchronization of Spread Spectrum Communications," Lincoln Laboratory, M.I.T., (to be published).
- [2]. F. deJager and C. B. Dekker, "Tamed Frequency Modulation, A Novel Method to Achieve Spectrum Economy in Digital Transmission," IEEE Trans. Comm., COM-26, 534 (1978).
- [3]. E. J. Nossen and V. F. Volertas, "Unidirectional Phase Shift Keying," US Patent No. 4, 130,802, Dec. 19, 1978.
- [4]. F. Amoroso, "Pulse and Spectrum Manipulation in the Minimum (Frequency) Shift Keying (MSK) Format," IEEE Trans. Comm., COM-24 , 381 (1976).
- [5]. M. K. Simon, "A Generalization of Minimum-Shift-Keying (MSK)-Type Signalling Based Upon Input Data Symbol Pulse Shaping," IEEE Trans. Comm., COM-24, 845 (1976).

APPENDIX A

MEASURES OF SPREADING PERFORMANCE

We consider a given pulse (or signal segment) which is represented by a transmitted waveform modulation $s(t, b)$, which is T seconds in duration. This waveform is characterized by the bit-sequence $b = b_1 b_2 \dots b_N$ (i.e., a spreading code) and may, for example, be a constant-envelope waveform such as BPSK or FSK. The function $s(t, b)$ represents the complex modulation of some carrier, and we assume it is normalized as follows, independent of the bit-pattern:

$$\int_0^T |s(t, b)|^2 dt = 1$$

The spreading code changes frequently, and is always known to the receiver, but we constrain the jammer to a knowledge only of the spectral density of the family of waveforms (ensemble average over random bit-sequences), as might be obtained by averaging many observed spectra. The jamming waveform is modelled as stationary random noise with unlimited spectral agility (i.e., the jammer is capable of generating noise with arbitrary power spectral density), but finite total power.

The received waveform is modelled as

$$Z(t, b) = A e^{i\delta} s(t, b) + N(t)$$

where $N(t)$ is complex noise with spectral density $G_N(f)$, i.e.,

$$E N^*(t) N(t') = \int_{-\infty}^{\infty} G_N(f) e^{2\pi i f(t'-t)} df .$$

The total noise power is P_N :

$$P_N = \int_{-\infty}^{\infty} G_N(f) df,$$

which includes jamming and receiver noise (also assumed to be finite), and we define the normalized noise spectral density

$$g_N(f) = G_N(f)/P_N ,$$

which obviously integrates to unity.

The average power of the received signal is

$$P_S = A^2/T$$

(averaged over time, not rms), and the input SNR may be taken to be

$$(\text{SNR})_{in} = \frac{P_S}{P_N} = \frac{A^2}{P_N T}$$

We assume that the receiver is synchronized, but does not know carrier phase. It is modelled as a filter whose output at the time of decision is

$$z(b) = \int_{-\infty}^{\infty} h^*(t, b) Z(t, b) dt .$$

The impulse response of this filter depends on the known bit-pattern, and decision is based on the magnitude of z . This filter output contains signal and noise:

$$z(b) = s(b) + n(b)$$

where

$$s(b) = Ae^{i\delta} \int_{-\infty}^{\infty} h^*(t, b) s(t, b) dt$$

and

$$n(b) = \int_{-\infty}^{\infty} h^*(t, b) N(t) dt .$$

The system output SNR is defined in an analogous way:

$$(\text{SNR})_{\text{out}} = \frac{|E s(b)|^2}{E |n(b)|^2} ,$$

where the ensemble average symbolized by E includes the random bits as well as the noise $N(t)$.

In terms of the Fourier transforms

$$S(f, b) = \int_{-\infty}^{\infty} s(t, b) e^{-2\pi i f t} dt$$

and

$$H(f, b) = \int_{-\infty}^{\infty} h(t, b) e^{-2\pi i f t} dt ,$$

we have

$$E s(b) = A e^{i\delta} \int_{-\infty}^{\infty} E\{H^*(f, b) S(f, b)\} df$$

and

$$\begin{aligned} E |n(b)|^2 &= \iint_{-\infty}^{\infty} E\{h(t, b) h^*(t', b)\} E\{N^*(t) N(t')\} dt dt' \\ &= P_N \int_{-\infty}^{\infty} g_N(f) E|H(f, b)|^2 df. \end{aligned}$$

Therefore,

$$(SNR)_{out} = \frac{A^2}{P_N} \cdot \frac{\left| \int_{-\infty}^{\infty} E\{H^*(f, b) S(f, b)\} df \right|^2}{\int_{-\infty}^{\infty} g_N(f) E|H(f, b)|^2 df}$$

To obtain our first performance parameter we now assume that the receiver uses a white-noise filter matched to the transmitted waveform, but truncated outside a symmetrical band of width B . This truncation is our means of recognizing a spectral containment constraint, and it is immaterial whether the band limiting is effected in the transmitter or the receiver. We retain our definition of the input SNR, which uses the unlimited signal waveform, so that the processing gain, defined as

$$PG \equiv \frac{(SNR)_{out}}{(SNR)_{in}},$$

reflects the loss of signal energy due to bandlimiting.

The receiver filter is thus given by

$$H(f, b) = \begin{cases} S(f, b) ; & |f| < B/2 \\ 0 & ; |f| > B/2 \end{cases} ,$$

and therefore

$$\begin{aligned} E\{H^*(f, b) S(f, b)\} &= E|H(f, b)|^2 \\ &= \begin{cases} g_s(f) ; & |f| < B/2 \\ 0 & ; |f| > B/2 \end{cases} \end{aligned}$$

where

$$g_s(f) \equiv E|S(f, b)|^2$$

is the signal power spectral density (ensemble average over bit sequences).

This density is normalized to unity over all frequencies:

$$\int_{-\infty}^{\infty} g_s(f) df = E \int_{-\infty}^{\infty} |s(t, b)|^2 dt = 1 ,$$

by our original convention for the signal waveform.

The processing gain, using this (white-noise) matched filter against the noise spectral density $g_N(f)$, is now found to be

$$PG = T \cdot \frac{\left\{ \int_B g_s(f) df \right\}^2}{\int_B g_N(f) g_s(f) df} ,$$

where the integrals are to be carried out over a symmetrical band of frequencies of width B .

The jammer is now allowed to optimize his spectral density, keeping the total jamming power fixed. His best choice will maximize the denominator in our expression for PG, which occurs when he concentrates all his power at the frequency, f_m at which $g_S(f)$ achieves the peak of its values within the band B. This optimum choice provides a lower bound to the processing gain obtained with the given signal class and receiver design:

$$PG > T \frac{\left\{ \int_B g_S(f) df \right\}^2}{\text{Max}_B g_S(f)} .$$

Now the noise-equivalent-bandwidth of the band-limited signal is defined by the relation

$$(NEB)_B \equiv \frac{\int_B g_S(f) df}{\text{Max}_B g_S(f)} .$$

The corresponding noise-equivalent-bandwidth of the original waveform would be

$$(NEB)_\infty = \frac{\int_{-\infty}^{\infty} g_S(f) df}{\text{Max}_f g_S(f)} = \frac{1}{\text{Max}_f g_S(f)} .$$

In terms of $(NEB)_B$, we have

$$PG > T(NEB)_B \cdot \int_B g_S(f) df .$$

Because of our normalization, the factor

$$F_B \equiv \int_B g_S(f) df$$

is just the fraction of the energy of the original waveform which lies within the band B. Normalizing our processing gain bound to the nominal value TB, we have

$$PG > \eta_0 TB$$

where

$$\eta_0 = \frac{(NEB)_B}{B} F_B < 1 .$$

This parameter provides the desired measure of waveform performance, given that the receiver uses a white-noise matched filter.

Another parameter is obtained if we allow more freedom in the receiver design. Specifically, we let

$$H(f, b) = \begin{cases} C(f) S(f, b) ; & |f| < B/2 \\ 0 & ; |f| > B/2 \end{cases} ,$$

where $C(f)$ is a real positive function of frequency to be chosen presently. This filter may be thought of as a truncated version of a colored-noise filter matched to $S(f, b)$, where the noise spectral density assumed is proportional to $[C(f)]^{-1}$.

The processing gain for a given jammer is now given by

$$PG = T \cdot \frac{\left\{ \int_B C(f) g_S(f) df \right\}^2}{\int_B C^2(f) g_N(f) g_S(f) df}$$

Again the optimum jamming strategy is the use of a line spectrum at f_m , the frequency at which the product $C^2(f) g_S(f)$ is a maximum, within the band B. The corresponding lower bound to the processing gain is

$$PG > T \cdot \frac{\left\{ \int_B C(f) g_S(f) df \right\}^2}{C^2(f_m) g_S(f_m)}$$

$$= T \left\{ \int_B \frac{C(f) \sqrt{g_S(f)}}{C(f_m) \sqrt{g_S(f_m)}} \cdot \sqrt{g_S(f)} df \right\}^2$$

The factor

$$\frac{C(f) \sqrt{g_S(f)}}{C(f_m) \sqrt{g_S(f_m)}}$$

is an arbitrary real positive function within the band, except that it is bounded from above by unity. By choosing this function to be identically unity, we obtain the filter for which the processing gain lower bound is maximized. This "miminax" filter is

$$H(f, b) = \begin{cases} [g_s(f)]^{-1/2} S(f, b) & ; |f| < B/2 \\ 0 & ; |f| > B/2 \end{cases}$$

and the bound obtained is

$$PG > T \left(\int_B \sqrt{g_s(f)} df \right)^2 \equiv \eta TB .$$

This corresponding efficiency parameter is now

$$\eta = \frac{1}{B} \left(\int_B \sqrt{g_s(f)} df \right)^2 .$$

By the Schwarz Inequality, η is never greater than unity, since

$$\left(\int_B \sqrt{g_s(f)} df \right)^2 < \int_B g_s(f) df \cdot \int_B df < B ,$$

in view of the normalization of $g_s(f)$. It is also clear that η would achieve this bound for a signal spectrum which is flat within B and zero elsewhere, which is of course incompatible with the assumption that $s(t, b)$ vanishes outside the interval $[0, T]$.

It is interesting to note that the minimax filter has a flat amplitude characteristic, on the average, and hence the noise power received is independent of the noise distribution within the band B . The noise spectral density can, in fact, be flat:

$$g_N(f) = \begin{cases} 1/B & ; |f| < B/2 \\ 0 & ; |f| > B/2 , \end{cases}$$

without changing the processing gain, which we may call PG_1 :

$$PG_1 \equiv T \left\{ \int_B \sqrt{g_S(f)} df \right\}^2 .$$

If we knew that the noise would be flat, we would use the white-noise band-limited matched filter, say H_2 :

$$H_2(f, b) \equiv \begin{cases} S(f, b) ; & |f| < B/2 \\ 0 & ; |f| > B/2 \end{cases}$$

and obtain the higher processing gain PG_2 :

$$PG_2 = TB \left\{ \int_B g_S(f) df \right\}^2 ,$$

according to the formula derived earlier. PG , cannot exceed PG_2 by the Schwarz Inequality, as just demonstrated above.

However, if we use H_2 and then let the jammer optimize against us, he will pick

$$g_N(f) = \delta(f - f_m) ,$$

where f_m is at the peak of $g_S(f)$ within B , and the processing gain will be reduced to PG_3 :

$$PG_3 = T \frac{1}{\underset{B}{\text{Max}} g_S(f)} \left\{ \int_B g_S(f) df \right\}^2 ,$$

as derived before. Since the minimax/filter optimizes against an optimizing jammer, PG_3 must be less than or equal to PG_1 , and this follows from the inequality

$$\int_B g_S(f) df < \text{Max}_B \sqrt{g_S(f)} \cdot \int_B \sqrt{g_S(f)} df .$$

With the minimax filter the jammer can do no better than with white noise, but the receiver does not use the white-noise matched filter. All these distinctions disappear for the "ideal signal", whose spectral density is flat within the allotted band and negligible elsewhere. In this limit,

$$PG_1 = PG_2 = PG_3 = TB.$$

When we compare spreading modulations, the chipping rate is a parameter for each case, hence it is natural to consider efficiency as a function of chip rate for each waveform, such as BPSK, MSK etc. This comparison is facilitated by introducing the dimensionless variable, $\theta \equiv 2\pi f\Delta$, in place of frequency, where Δ is the chip duration (i.e., $\Delta^{-1} = f_c$ is the chipping rate), and the dimensionless parameter

$$x \equiv B\Delta = B/f_c .$$

We define

$$g(\theta) \equiv \frac{1}{\Delta} g_S(f) ,$$

so that

$$\frac{1}{2\pi} \int_{-\infty}^{\infty} g(\theta) d\theta = 1.$$

This quantity, $g(\theta)$, is the same as the normalized spectral density used in the main text. The matched-filter efficiency parameter, η_0 , is expressed in terms of $g(\theta)$ by the formula

$$\eta_0 = \frac{\left\{ \int_B g_S(f) df \right\}^2}{B \text{ Max}_{|f| < B/2} g_S(f)}$$

$$= \frac{\left\{ \int_{-\pi x}^{\pi x} g(\theta) \frac{d\theta}{2\pi} \right\}^2}{x \text{ Max}_{|\theta| < \pi x} g(\theta)},$$

or

$$\eta_0(x) = \frac{4}{x} \frac{\left\{ \int_0^{\pi x} g(\theta) \frac{d\theta}{2\pi} \right\}^2}{\text{Max}_{0 < \theta < \pi x} g(\theta)}$$

In the last step we have assumed that $g_S(f)$ is symmetrical. For each type of spreading modulation, $g(\theta)$ is a unique function of θ , and the effect of variation of chip rate for a given bandwidth, B , is represented by the dependence of η_0 on the dimensionless parameter x .

The minimax efficiency parameter, η , is also expressible in the simple form

$$\eta(x) = \frac{4}{x} \left\{ \int_0^{\pi x} \sqrt{g(\theta)} \frac{d\theta}{2\pi} \right\} .$$

Figure A.1a provides a comparison of BPSK, MSK and FSK for the special value $\psi = 1.9905$, using the matched filter measure of efficiency. Figure A.1b is a similar comparison using the minimax filter. Note that the minimax filter provides more processing gain against the optimizing jammer in all cases, but that the difference is slight for the special FSK. The difference would vanish altogether for an ideal spectrum, flat within a band and zero elsewhere. In Fig. A.2a FSK waveforms are compared with ψ as a parameter, using the matched filter efficiency criterion. Figure A.2b is a similar plot using the minimax filter efficiency. The optimum efficiency occurs for the values $\psi = 2.2$ (minimax) and $\psi = 2.0$ (matched filter), but the maxima are broad in both cases.

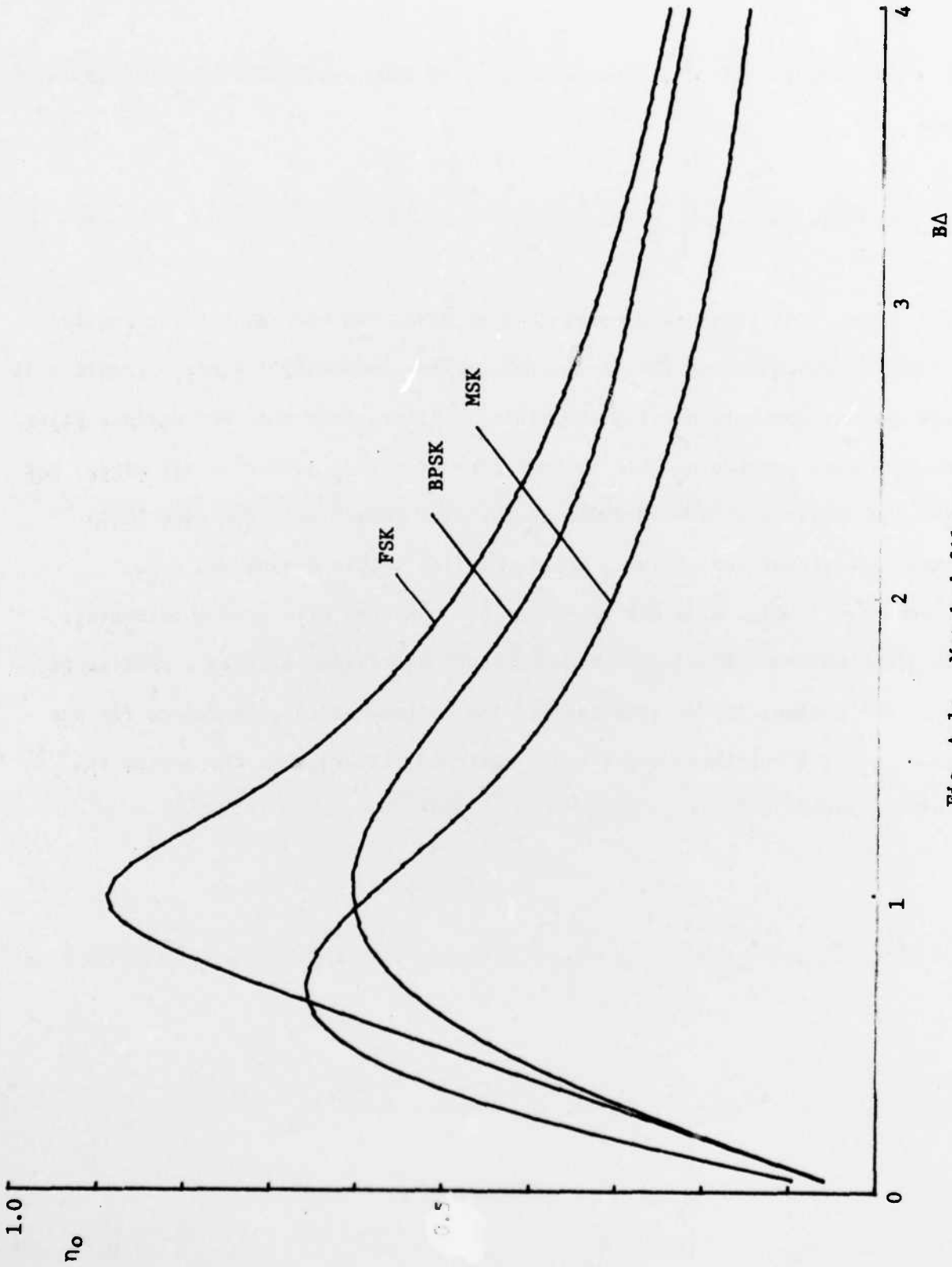
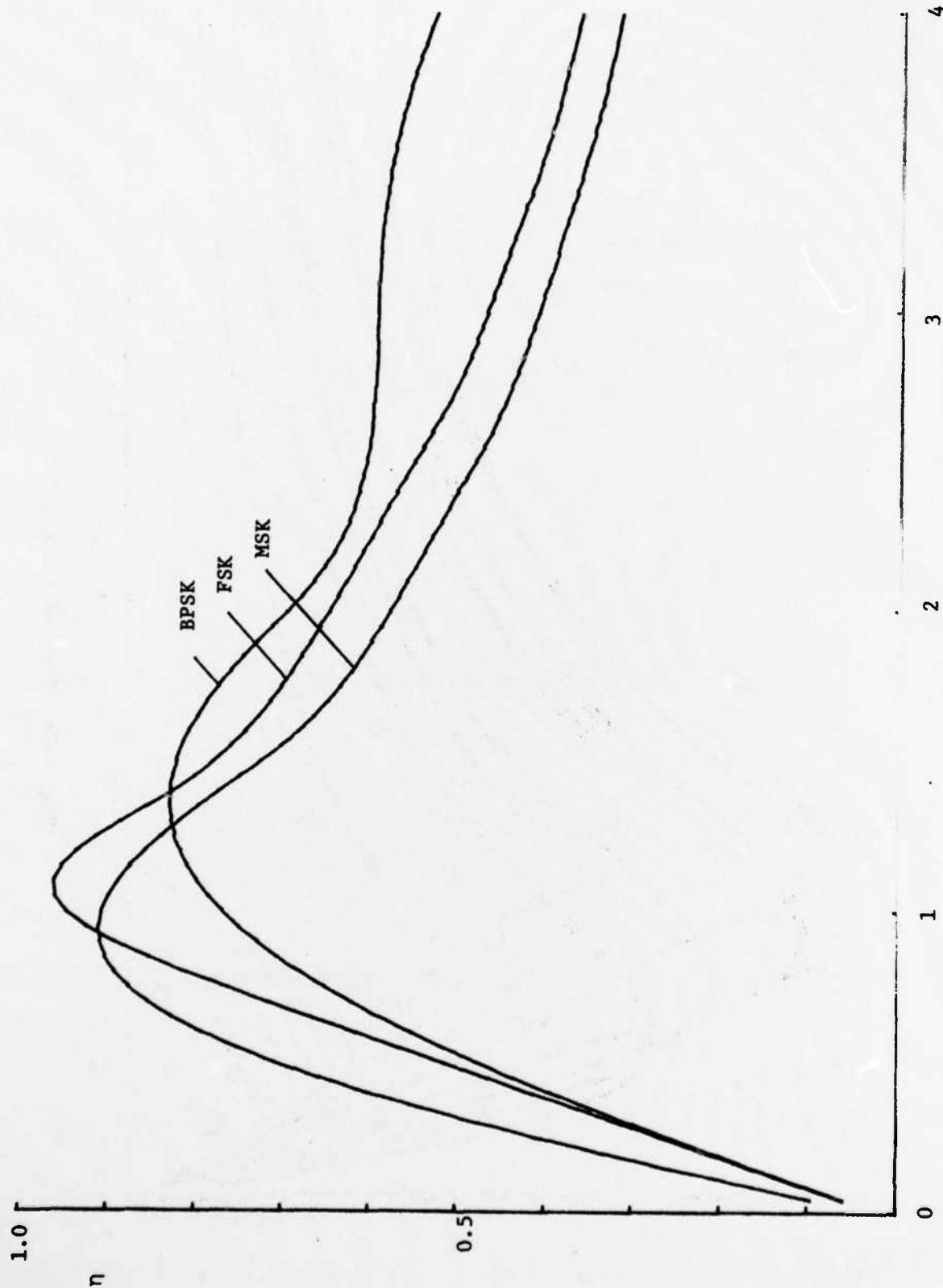


Fig. A-1a. Matched filter.

TR-596(A-1a)

TR-596(A-1b)



$B\Delta$

Fig. A-1b. Minimax filter.

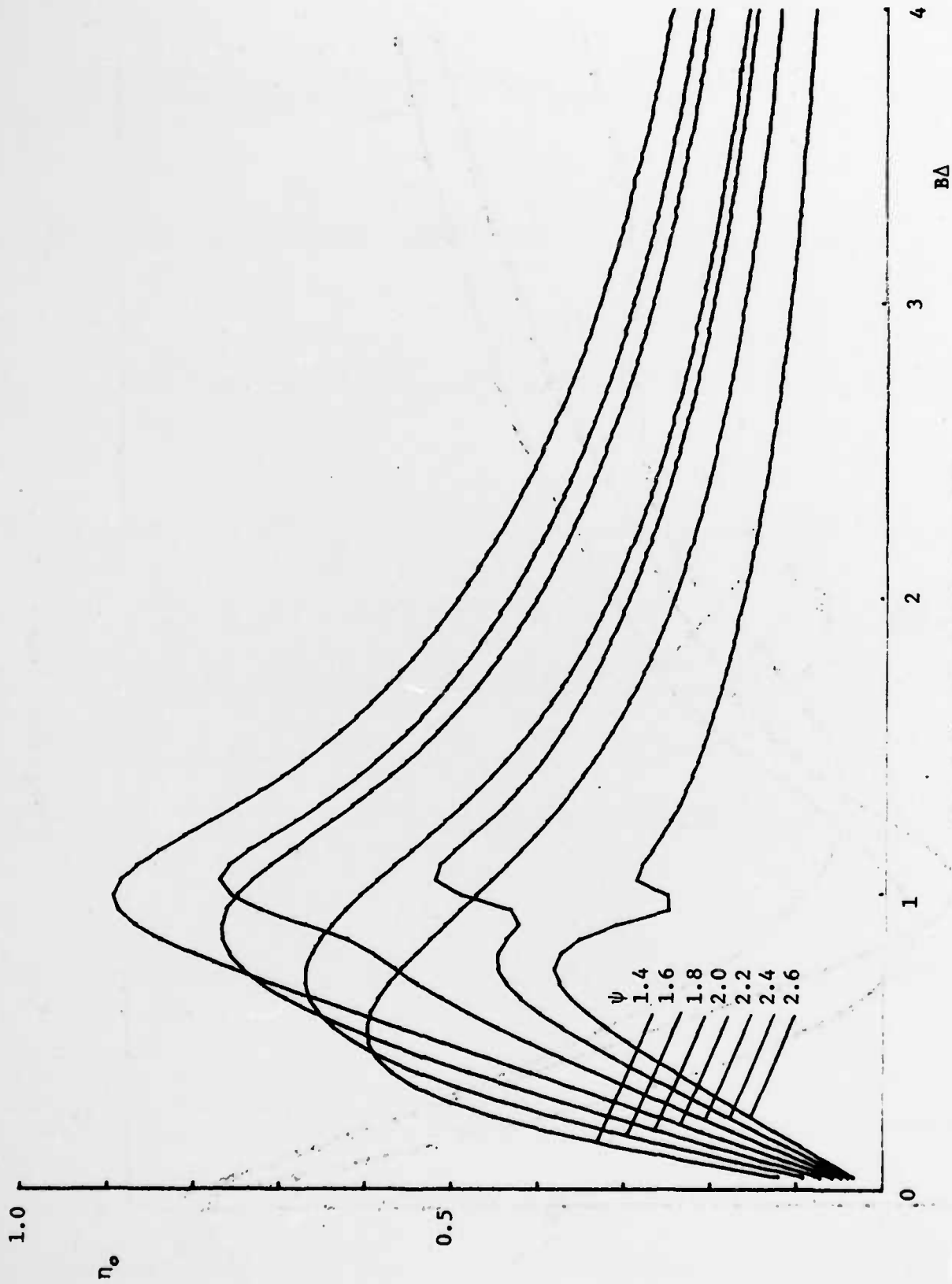


Fig. A-2a. Matched filter; FSK.

TR-596(A-2a)

TR-596(A-2b)

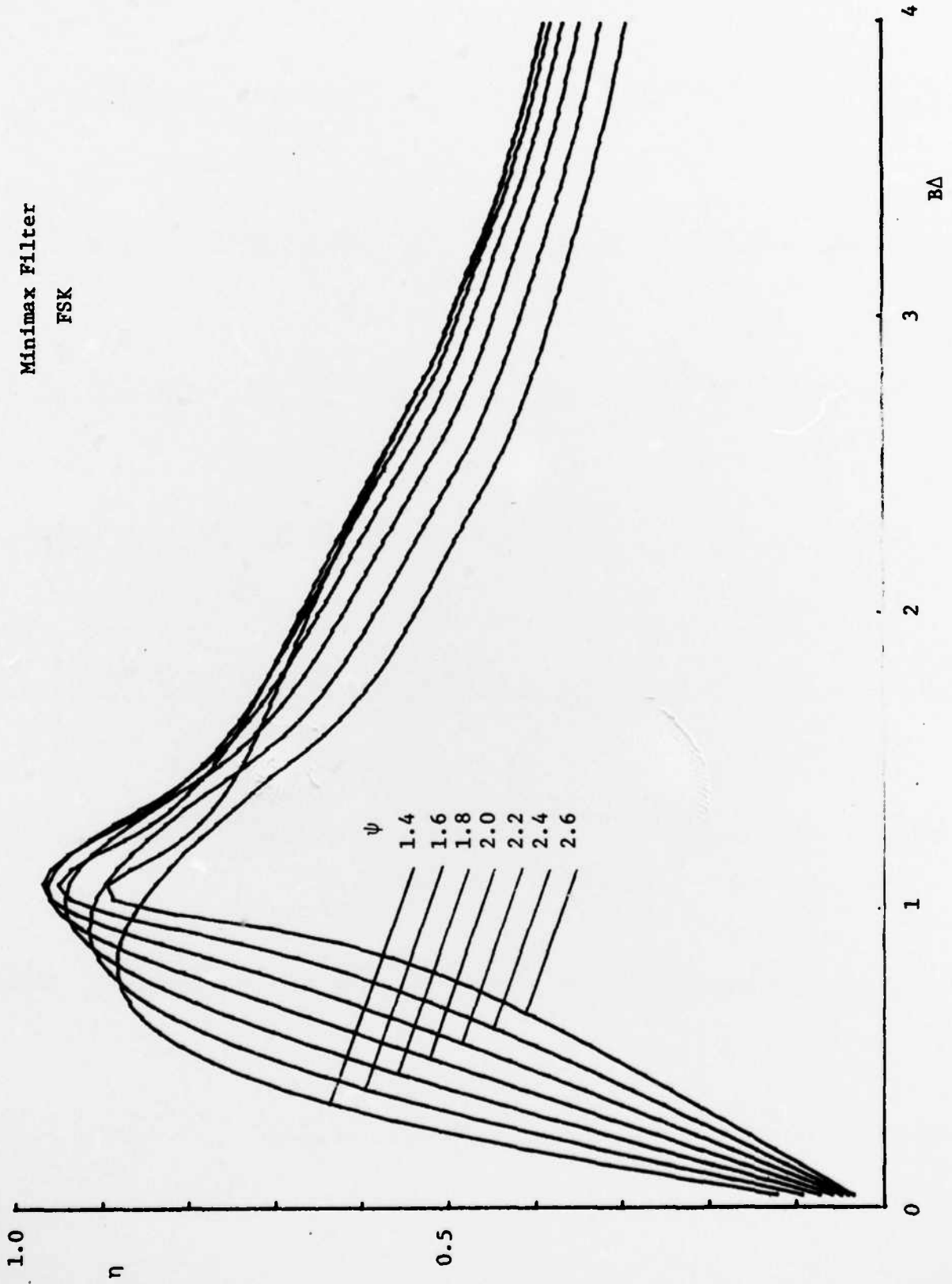


Fig. A-2b. Minimax filter; FSK.

UNCLASSIFIED

SECURITY CLASSIFICATION OF THIS PAGE (When Data Entered)

REPORT DOCUMENTATION PAGE		READ INSTRUCTIONS BEFORE COMPLETING FORM
1. REPORT NUMBER ESD-TR-83-053	2. GOVT ACCESSION NO. AD-A134850	3. RECIPIENT'S CATALOG NUMBER
4. TITLE (and Subtitle) A Catalogue of Spreading Modulation Spectra		5. TYPE OF REPORT & PERIOD COVERED Technical Report
		6. PERFORMING ORG. REPORT NUMBER Technical Report 596
7. AUTHOR(s) Edward J. Kelly		8. CONTRACT OR GRANT NUMBER(s) F19628-80-C-0002
9. PERFORMING ORGANIZATION NAME AND ADDRESS Lincoln Laboratory, M.I.T. P.O. Box 73 Lexington, MA 02173-0073		10. PROGRAM ELEMENT, PROJECT, TASK AREA & WORK UNIT NUMBERS
11. CONTROLLING OFFICE NAME AND ADDRESS Air Force Systems Command, USAF Andrews AFB Washington, DC 20331		12. REPORT DATE 20 September 1983
		13. NUMBER OF PAGES 126
14. MONITORING AGENCY NAME & ADDRESS (if different from Controlling Office) Electronic Systems Division Hanscom AFB, MA 01731		15. SECURITY CLASS. (of this report) Unclassified
		15a. DECLASSIFICATION/DOWNGRADING SCHEDULE
16. DISTRIBUTION STATEMENT (of this Report) Approved for public release; distribution unlimited.		
17. DISTRIBUTION STATEMENT (of the abstract entered in Block 20, if different from Report)		
18. SUPPLEMENTARY NOTES None		
19. KEY WORDS (Continue on reverse side if necessary and identify by block number) spreading modulation spectral properties system performance waveform parameters		
20. ABSTRACT (Continue on reverse side if necessary and identify by block number) Spreading modulation waveforms are discussed in general terms, and a classification system is described. Several well-known examples are given, and a new, standard set of spreading modulations is introduced. Spectra of all the waveforms are given, and spectral properties are discussed in relation to system performance. It is shown that these properties are essentially determined by three waveform parameters, for a large class of spreading modulations.		

END

FILMED

12-83

DTIC